1966

Simply supported non-prismatic folded plates

Claude Derrell Johnson
Iowa State University

JOHNSON, Claude Derrell, 1938-
SIMPLY SUPPORTED NON-PRISMATIC FOLDED PLATES.

Iowa State University of Science and Technology, Ph.D., 1966
Engineering, civil

SIMPLY SUPPORTED NON-PRISMATIC FOLDED PLATES

by

Claude Derrell Johnson

A Dissertation Submitted to the

Graduate Faculty in Partial Fulfillment of

The Requirements for the Degree of

DOCTOR OF PHILOSOPHY

Major Subject: Structural Engineering

Approved:

Signature was redacted for privacy.

In Charge of Major Work

Signature was redacted for privacy.

Head of Major Department

Signature was redacted for privacy.

Dean of Graduate College

Iowa State University
Of Science and Technology
Ames, Iowa

1966

TABLE OF CONTENTS

I. INTRODUCTION

Folded plate structures have become quite popular in the United States in recent years. They have been used most extensively in reinforced concrete roof construction to bridge long spans and provide more column free floor space. These structures have been constructed in many different geometrical shapes to form interesting architectural designs. The basic principles of folded plates are not limited to roof design. These principles have also been applied in the design of floor systems, staircases, bins and foundations.

The largest majority of folded plate roofs have been designed prismatic, where the plate elements are rectangular in shape and constant in thickness. An extensive amount of analytical and experimental research has also been conducted on the behavior of prismatic folded plates. The main contributions prior to 1963 have been summarized in a report by the A.S.C.E. Task Committee on Folded Plate Construction (1). More recent investigations have been conducted by Beaufaut and Gray (2,3), Graham (10), Powell (12) and Scordelis and Gerasimenko (13).

Recently, the trends in architectural design have been to generalize the shape of folded plates by making the plate elements non-prismatic, as shown for example in Fig. 1. By combining triangular, trapezoidal and rectangular plates in a variety of folded patterns, many other geometrical shapes can be formed.

Several non-prismatic folded plate structures have been constructed in the past decade. A prestressed concrete roof similar to the structure shown in Fig. 1 has been reported by Benito (4). Other applications in the form of cantilever roof structures used for office buildings, airplane hangers and grandstands have been discussed by Del Pozo et al. (7) and Whitney et al. (19,20). Non-prismatic plate elements have also been combined in radially symmetric patterns to form roofs for auditoriums and family dwellings. Structures of this type have been described by Faerber (8), Welch (18) and Whitney et al. (20).

Only a limited amount of information has been reported on the design of these structures. In most cases, however, the structural design has been based on model studies or approximate theories. In order to give the architect and structural engineer more flexibility in the design of folded plates, there is a definite need for general methods of analysis which can be applied to non-prismatic folded plates. An introductory study has been conducted at the University of California by Yamahara (21) to investigate some possible approaches to the analysis of these structures.

The main purpose of this investigation is to develop a theory that can be used to analyse simply supported non-prismatic folded plates. The predicted results obtained by applying this theory are compared to the measured results of an experimental investigation that was conducted on two non-prismatic folded plates. This theory can also be used to analyse prismatic folded plates. Solutions obtained by the proposed theory are compared to known solutions for prismatic folded plates to further test

the theory. In addition, a study was conducted to investigate the structural behavior of non-prismatic folded plates and to compare their behavior to that of prismatic folded plates. This study also includes an investigation to determine if simplified theories which are applied in the design of some prismatic structures can also be applied to non-prismatic folded plates.

II. ANALYSIS OF NON-PRISMATIC FOLDED PLATES

One of the primary objectives of this study is to formulate a method of analysis that can be used to predict the behavior of non-prismatic folded plates. In this investigation, the term "non-prismatic" refers to variations in the depth of plate elements with respect to the longitudinal span of the structure. In many respects, the theory is similar to "Ordinary Folded Plate Theory" used in the analysis of prismatic folded plates. When the plate elements in a structure are non-prismatic, the common assumptions of similar loading and normal curve distributions used in Ordinary Folded Plate Theory no longer apply. The theory developed in this investigation generalizes Ordinary Folded Plate Theory to account for the conditions of non-similar loading and the effects of non-prismatic plate elements. As a result, prismatic folded plates can also be analysed as a special case using this theory.

The theory only applies for the analysis of "long non-prismatic folded plates" where the ratio of the length of the plates relative to their widest depth is greater than two. On the basis of this criterion, the main structural behavior is controlled by flexure in the longitudinal direction and one-way slab action in the transverse direction. This restriction is actually not a serious one since folded plates are usually used to bridge long spans in order to provide more column free floor space.

The theory will be presented in three phases in order to separate the general approach to the analysis from the detailed formulation. In this chapter, the basic principles of folded plate behavior will be presented. This will be followed by a discussion of the method of analysis used for non-prismatic folded plates. In Chapter III, various parts of the theory will be formulated and the derivation of equations will be presented. The theory will be presented in a form that can be readily programmed for a digital computer since the analysis of non-prismatic folded plates is only practical when a digital computer is employed. Three computer programs were written for this investigation. A discussion of these programs and the main flow charts will be presented in Chapter IV.

A. Basic Folded Plate Behavior

The type of folded plate structures considered in this investigation consist of a folded combination of plate elements of constant thickness spanning between two supporting end diaphragms as shown in Fig. 2. In general, the plate elements may take the shape of triangles, trapezoids or rectangles. Continuity is maintained along the intersections of the plate elements.

The basic structural behavior of a folded plate can be described by composite action of two basic structural systems: the "slab structure" and the "plate structure". These systems are illustrated on a typical cross-section shown in Fig. 3. In the basic slab structure, it is assumed

that continuity is maintained perpendicular to all the joints. The plate structure, however, consists of articulated joints. These two basic systems are inter-related in that the deflections at the joints of the slab structure must conform to those of the plate structure.

Loads applied to the surface of the structure are assumed to be transferred to the longitudinal joints by the continuous transverse "slab action" of the slab structure. These loads form a set of basic joint loads, distributed along the length of the joints which are then applied to the articulated plate structure. The joint loads are resolved into the plane of the plates to form a set of plate loads which are distributed along the length of each plate element. These plate loads are then carried to the supporting end diaphragms by the longitudinal flexural action of the plates, which is commonly referred to as the "plate action" of the structure.

B. Method of Analysis

The analysis of a folded plate structure can be divided into two parts: the "primary analysis" and the "correction analysis". The primary analysis consists of analysing the structure for the applied loading condition on the basis of the assumption that the relative joint displacements at any transverse cross-section do not occur. In order to satisfy this assumption, the longitudinal joints of the structure are temporarily restrained against relative vertical displacements. Relative joint displacements do occur, however, and a correction analysis

is required to account for the additional stresses, moments and deflections that are introduced as a result of these joint displacements. The final solution is then obtained by superimposing the results of the primary analysis and the correction analysis.

1. Primary analysis

The method of analysis presented in this study can be generally described as a method of nodal analysis. A number of equally spaced nodal sections are initially defined along the length of the structure as shown in Fig. 4. The point which defines the intersection of a nodal section and a longitudinal joint will be referred to as a "node". In the primary analysis, a condition of unyielding supports is temporarily applied along the length of the ridges and valleys of the slab structure to provide restraint against relative joint displacements. These supports are shown on a typical cross-section in Fig. 5. It is then assumed that the surface loads between the joints of the structure are transferred to the longitudinal joints by a continuous one-way slab action in the transverse direction. An independent transverse bending analysis on the basis of a unit width of slab is required at each nodal section to determine the primary transverse bending moments, $TM^{p}_{no,j}$[1] and the primary joint reactions, $AR^{p}_{no,j}$, at each joint.

The transverse bending analysis at each nodal section can be conducted by any common method used for analysing continuous beams. In

---

[1]The notation used in this dissertation is defined in Appendix A.

this investigation a general matrix formulation on the basis of a basic stiffness method was used. This method is very general and can be readily programmed for a digital computer. When the proper stiffness matrix is used, the analysis can be carried out on the basis of the horizontal projection of a transverse nodal section. A detailed formulation of the stiffness method used in this investigation is presented in the next chapter.

The primary joint reactions, $AR^{p}_{no,j}$, obtained at each nodal section, when reversed, form a set of joint loads, $RI^{p}_{no,j}$, which must be carried by the plate structure. When a sufficient number of nodal sections are considered, the distribution of the joint loading applied to each joint can be defined over its entire length as shown in Fig. 6. On the basis of the assumption that the plate structure is articulated at the joints, these joint loads are then resolved into plate loads, $PI_{no,j,k}$, which act in the plane of the plates at each nodal section, as shown in Fig. 7. The total plate load intensity, $PL_{no,i}$, at each nodal section is then determined by the sum of the intensisites which contributes to a given plate from each adjacent joint. The distribution of plate load will then be defined over the length of each plate as shown in Fig. 8a.

When each plate is assumed to act independently, the longitudinal plate load bending moments, $MO_{no,i}$, can be determined at each nodal section. The distribution of plate loads between nodal sections can be defined in terms of a second degree parabola which will simplify to the case of a linear or uniform distribution of load, if the plate loads are

distributed in this manner. On the basis of this assumption, the distributed plate load can be expressed in terms of a set of statically equivalent concentrated plate loads, $PC_{no,i}$, acting at each nodal section as shown in Fig. 8b. The plate load bending moments, $MO_{no,i}$, are then determined at each nodal section by statics.

As a result of the plate load moments, longitudinal stresses are developed in each plate. In general, the stresses which are developed in two adjacent plates along their common edge will not be equal because it has been assumed that each plate acts as an independent beam. A condition of strain compatibility must exist along this common edge and in an elastic structure, this condition implies that the stresses must also be compatible. As a result, a distribution of unit shearing forces, q_j, must exist along the edges of the plate, as shown in Fig. 9, in order to satisfy this compatibility requirement.

In the next chapter, a "Modified Three Shear Equation" will be derived. This equation expresses the state of stress compatibility along the joints in terms of the known plate load bending moments, $MO_{no,i}$ and the unknown shear forces, $T_{no,j}$. This equation has been formulated for the general condition of matching the stresses along the common edge of two non-prismatic plate elements. When the angles of taper of the plates, α_i, are taken to be zero, the Modified Three Shear Equation simplifies to the Ordinary Three Shear Equation which is used for matching stresses in prismatic folded plates.

In the analysis of prismatic folded plate structures, the basic assumptions of similar loading and normal curves are usually employed. With these assumptions, the condition of matching stresses can be satisfied by an analysis at any typical cross-section because the longitudinal distribution of the stress functions are all the same. Unfortunately, this approach cannot be taken in the analysis of non-prismatic folded plates since each cross-section is different from an adjacent cross-section and the conditions of normal curves and similar loading do not apply. In addition, when the Modified Three Shear Equation is written at a particular node, no, the unknown shear forces at the two neighboring nodes, no-1 and no+1, on the same joint are involved. Theoretically then, the Modified Three Shear Equation must be satisfied at an infinite number of nodes along all joints at once. This condition is impossible to satisfy, but sufficient accuracy can be obtained by satisfying the compatibility of stresses at a finite number of nodal points within the structure. This approach is basically the same as the approach used for solving boundary value problems by finite difference methods. The problem of matching stresses may then be solved by formulating a set of (nn × nij) simultaneous equations which result from writing the Modified Three Shear Equation at all interior nodes of the structure. Here, the notation (nn × nij) refers to the number of nodal sections times the number of interior joints. The unknown shear forces, $T_{no,j}$, are then determined at each interior node by solving this set of simultaneous equations. Once the shear forces are known, the

primary longitudinal stresses, $\bar{f}^{p}_{no,i,j}$, can be determined at each node of the structure.

It should be noted that for a structure which contains 4 interior joints where 15 nodal sections are considered, the solution of 60 simultaneous equations is required. This number of equations should leave little doubt that the aid of a digital computer is needed to carry out this analysis.

As a result of the stresses developed in each plate element, the plates deflect in their own plane. If the plates are temporarily considered to be disconnected, the curvature, $\phi_{no,i}$, at each nodal section of each plate may be determined in terms of the known longitudinal stresses, $\bar{f}^{p}_{no,i,j}$. The distribution of curvature along the neutral axis of each plate can then be defined by considering a sufficient number of nodal sections as shown in Fig. 10b. On the basis of the assumption that the distribution of curvature between nodal sections varies as a second degree parabola, the deflected shape of the structure can be determined by the use of Moment-Area Principles and numerical integration. Basically, the deflected shape of the structure can be defined by a set of concentrated angle changes $\bar{\phi}_{no,i}$, applied at each nodal section as shown in Fig. 10c. These concentrated angle changes can be determined by a numerical integration of the curvature diagram. The plate deflections, $\delta_{no,i}$, are then obtained by considering the basic geometry of the deflected curve and the boundary conditions.

In the preceding deflection analysis, each plate is considered to act independently. However, the final deflected position of the common joint between two plates must define a single deflected shape. By applying a basic Williot Diagram at each node where the plate deflections are known, the vertical joint deflections, $\delta v_{no,j}$, can be determined as shown in Fig. 11.

The primary analysis which does not account for the effects of relative joint displacements is complete at this stage. As shown in Fig. 11, relative joint displacements do occur in the plate structure. Consequently, the deflected shape of the slab structure must be made to conform to the deflected shape of the plate structure. In order to satisfy this compatibility requirement, a new set of transverse moments and vertical holding forces are introduced at the joints.

In some structures, the magnitudes of the relative joint displacements may be quite small. Whenever this is the case, the analysis may be terminated at the end of the primary analysis and the primary stresses, $\bar{f}^{p}_{no,i,j}$, transverse moments, $TM^{p}_{no,j}$, and deflections $\delta v^{p}_{no,j}$, can be taken as an accurate prediction of the final results. This condition seldom applies in the analysis of non-prismatic folded plates where the effects of relative joint displacements are usually quite large.

2. Correction analysis

The first step in applying the correction analysis is to determine the transverse moments and holding forces that are introduced into the

slab structure as it is deformed along the longitudinal joints to conform to the deflected shape of the plate structure. This part of the correction analysis is defined as the secondary analysis. A set of fixed end moments which result from the relative translations of the edges of the plates, shown in Fig. 11, can be determined at each nodal section. An independent transverse bending analysis is then carried out at each nodal section of the one-way continuous slab structure to determine the secondary transverse bending moments, $TM^{s}_{no,j}$. Each transverse bending analysis is conducted on the basis of the same assumptions used in the primary analysis. The slab structure is assumed to be supported along the joints by a system of unyielding supports. As a result of this assumption, a system of secondary holding forces, $AR^{s}_{no,j}$, are developed at each interior node. This set of holding forces defines a distribution along each joint. It should be noted that the total system of holding forces form a self-equilibrating force system on the slab structure and no additional load is introduced to the plate structure. This conclusion can be made by considering that the fixed end moments at this stage are a direct result of relative joint displacements.

This system of secondary holding forces cannot exist because relative joint displacements are not prevented in the actual structure. A method of analysis must be formulated to remove their effect so that the stresses, moments and deformations of the structure can be determined where relative joint displacements are allowed to occur.

Two procedures were used to account for the effects of relative joint displacements. Both methods are commonly used in the analysis of prismatic folded plates. In this study, they have been extended to cover the more general case of the analysis of non-prismatic folded plates. The methods investigated are known as the "Iteration Method" and the "Particular Load Method". The basic principles involved in applying these methods to the analysis of non-prismatic folded plates will be discussed in the remainder of this chapter.

In the Iteration Method, the effects of the secondary holding forces are removed by reversing their action and by reapplying them to the plate structure as a new set of joint loads. As described in the primary analysis, these joint loads, $RI_{no,j}$, can then be resolved into the plane of the plates to form a new distribution of plate loads. The remaining portion of the analysis follows the form presented in the primary analysis. A new set of stresses is then determined on the basis of the assumptions that relative joint displacements do not occur. However, these stresses introduce a new set of relative joint displacements and another correction analysis is required to make the deflected shape of the slab structure conform to the deflected shape of the plate structure. The entire procedure is then repeated and each correction analysis introduces a new correction analysis. The iteration procedure is continued until the correction moments introduced at any cycle of iteration are small at each node. The results of the primary analysis and the results of each cycle

of iteration are then added to determine the final stresses, transverse moments and deflections.

In each correction analysis, the condition of unyielding supports is introduced in the transverse bending analysis. Consequently, the structure that is analysed is always stiffer than the actual structure. This condition generally causes the stresses and moments to be over-predicted in some areas of the structure and with each cycle of iteration, the stresses and moments are reversed in sign. As a result, the iteration solution may tend to oscillate around the true solution and in some cases may even diverge. In general, the convergence of the Iteration Method depends on the relative rigidities of the plate structure and the slab structure. In non-prismatic folded plates, these factors are influenced greatly by the shape of the plate elements. Further comments on applying the Iteration Method to the analysis of non-prismatic folded plates will be included in Chapter V.

The principles of the Particular Load Method have been applied to the correction analysis for prismatic folded plates by Yitzhaki (22). In applying these concepts to the analysis of prismatic folded plates, the conditions of similar loadings and normal curve distributions are assumed to be satisfied. These conditions seldom exist in the case of non-prismatic folded plate structures. Therefore, the principles of the Particular Load Method are extended in this investigation to cover the more general case of non-prismatic folded plates with non-similar loading.

The Particular Load Method displays a distinct advantage over the Iteration Method because the problem of correcting for the effects of relative joint displacements can be solved in the form of complete solution. This eliminates the uncertainties of oscillation and divergence that may be encountered in applying the Iteration Method. The over-all objective of the Particular Load Method is to remove the effects of the secondary holding forces. This can be accomplished by expressing the distributions of the secondary holding forces in terms of a linear combination of particular loading systems. In general, a particular loading system is a known loading condition for which a unique set of transverse moments, longitudinal stresses and deflections can be determined. Since the secondary holding forces are expressed in terms of a linear combination of a number of particular loading systems, the stresses resulting from their effect alone can be determined also by a linear combination of the stresses of each particular loading system. The transverse bending moments and the vertical joint deflections can be obtained in the same manner. A complete solution, which accounts for the effects of relative joint displacements, is then obtained by adding these results to those of the primary and secondary analysis.

A particular loading can be formed by initially applying a known loading condition to the plate structure. A set of complementary holding forces which is required to bend the slab structure to conform to the deflected shape of the plate structure is then determined. The combination of the applied load and the resulting complementary holding forces then

constitute a particular loading system for which the stresses, transverse moments and deflections of the structure are known.

The intensity of the secondary holding forces, $AR^{s}_{no,j}$, have been determined at each interior node of the structure in the secondary analysis. On the basis of the assumption that the distribution of these forces along a joint varies as a second degree parabola between nodes, it is possible to establish a set of (nn × nij) statically equivalent concentrated holding forces, $RC^{s}_{no,j}$, one applied at each interior node. In order to remove the effects of these concentrated forces a total of (nn × nij) particular loading systems will be required.

Any type of applied loading condition can be used to initiate a system of particular loading. The only basic requirement on all particular loading systems is that they are linearly independent. Therefore, each applied loading used to initiate a particular loading system should be independent of all the other applied loadings. In this investigation, a particular loading system is formed by first applying a known concentrated force $K^{r}_{no,j}$, at a particular interior node of the plate structure. The structure is then analysed for this loading condition by the same procedure as described for the primary analysis to determine the stresses and deflections introduced into the plate structure. A set of transverse moments and complementary holding forces, $FI^{r}_{no,j}$, are introduced to make the deflected shape of the slab structure conform to the deflected shape of the plate structure. The analysis procedure at this stage is the same as described for the secondary analysis. The distribution of the

complementary holding forces $FI^{r}_{no,j}$, along each joint can also be expressed in terms of a set statically equivalent concentrated forces, $FC^{r}_{no,j}$, by assuming that the distribution between nodes varies as a second degree parabola. The combination of the applied load, $K^{r}_{no,j}$, and all the complementary holding forces, $FC^{r}_{no,j}$, form a particular loading system for which a unique set of stresses, moments and deflections associated with this loading system are known. A complete particular loading system will then consist of a total of (nn × nij) concentrated nodal forces, $F^{r}_{no,j}$. By initially applying a single concentrated force at all the other interior nodes, a total of (nn × nij) particular loading systems can be formed in a similar manner.

The secondary holding forces are then expressed in terms of a linear combination of these particular loading systems by writing a set of (nn × nij) linear simultaneous equations. Each equation is obtained by expressing the secondary holding force, $AR^{s}_{no,j}$, at a particular interior node of the structure in terms of a linear combination of the concentrated nodal forces at that same node, $F^{r}_{no,j}$, of all the particular loading systems. A similar equation is written at each interior node to obtain the total set. By solving this set of equations, the coefficients, β_1, $\beta_2 \cdots \beta_r, \cdots \beta_{nn \times nij}$ can be determined which express the proportion of each particular loading system that is required to remove the effects of the secondary holding forces.

The stresses, moments and deflections resulting from removing the effects of the secondary holding forces are then determined by a linear

combination of the appropriate results of each particular loading system. These results combined with those of the primary and secondary analysis form the final stresses, moments and deflections. The analysis of the structure is now complete and the effects of relative joint displacements have been taken into account.

III. FORMULATION OF THE THEORY

In a complete analysis of a non-prismatic folded plate many phases of the analysis are continually repeated. Each phase also involves certain basic operations that are usually performed at all nodes in the structure. A formulation of these operations is presented in this chapter. The basic assumptions used in the theory are summarized and a discussion on the range of their validity is presented before the theory is formulated.

A. Basic Assumptions

The following assumptions are used in the analysis of non-prismatic folded plates:

1. The material is homogeneous and linear elastic.
2. The structure is monolithic.
3. The structural behavior in the transverse direction is governed by a continuous one-way slab action.
4. The plate elements act as beams spanning between end diaphragms. The basic flexure formula applies in the analysis of the longitudinal stresses where the distribution is assumed to be linear over the depth of a plate.
5. The plate deflections in the plane of a plate are controlled by bending and are assumed to occur perpendicular to the neutral axis of the plate. Shear deformations are neglected.

III. FORMULATION OF THE THEORY

In a complete analysis of a non-prismatic folded plate many phases of the analysis are continually repeated. Each phase also involves certain basic operations that are usually performed at all nodes in the structure. A formulation of these operations is presented in this chapter. The basic assumptions used in the theory are summarized and a discussion on the range of their validity is presented before the theory is formulated.

A. Basic Assumptions

The following assumptions are used in the analysis of non-prismatic folded plates:

1. The material is homogeneous and linear elastic.
2. The structure is monolithic.
3. The structural behavior in the transverse direction is governed by a continuous one-way slab action.
4. The plate elements act as beams spanning between end diaphragms. The basic flexure formula applies in the analysis of the longitudinal stresses where the distribution is assumed to be linear over the depth of a plate.
5. The plate deflections in the plane of a plate are controlled by bending and are assumed to occur perpendicular to the neutral axis of the plate. Shear deformations are neglected.

6. The supporting end diaphragms are considered to offer infinite stiffness within the plane of the diaphragms and are assumed to be perfectly flexible in a direction normal to their own planes.
7. The degree of taper of the plate elements is limited to a range in which the flexure formula yields a satisfactory prediction of the stresses.
8. The plate elements are assumed to be in the shape of isosceles trapezoids, isosceles triangles or rectangles.
9. The plane of a transverse nodal section is parallel to the supporting end diaphragms of the structure.
10. All distributions of load and curvature vary according to the curve of a second degree parabola between nodal sections. This assumption reduces to a linear variation or uniform variation whenever the intensities specify such a distribution.

The first six assumptions stated above are the same as those used in Ordinary Folded Plate Theory for the analysis of prismatic structures. Some of the remaining assumptions which mainly pertain to the degree of taper of the non-prismatic plates require some discussion on the range of their validity.

In the proposed theory, the longitudinal stresses in the plate elements are computed on the basis of the basic flexure formula. The validity of applying the flexure formula to the bending analysis of tapered plates has been discussed by Timoshenko (15,16). A comparison of the

flexure formula to the mathematical solution of the bending of a wedge shows that stresses predicted by the flexure formula are nearly exact if the angle of taper, α_i, is less than 5°. The flexure formula is shown to under-predict the stresses at the edges of the plate by 3.0%, 5.3% and 9.4% as the angle of taper, α_i, increases to 10°, 15° and 20° respectively. It should be noted, that the angle of taper, α_i, only defines half of the full angle of taper as shown in Fig. 9. These predictions show that no serious limitation is placed on the theory as a result of using the flexure formula, since it is doubtful that structures of this type would be designed with taper angles, α_i, larger than 15° for aesthetic reasons. When the plate elements have larger tapers, the structural behavior will be closer to that of pyramid structures. The behavior of this type of a structure is not considered in this study. Many simplified theories for analysis of pyramid structures have been presented by Born (5,6).

As stated in the assumptions, the plate elements are assumed to be in the form of isosceles trapezoids, isosceles triangles or rectangles. In a general non-prismatic folded plate, this assumption may be slightly violated. For example, it can be shown by geometry that if one longitudinal edge of a trapezoidal plate element is in the horizontal plane and the two parallel sides are parallel to the vertical end diaphragms, the requirements of an isosceles trapezoid can only be met if the plate slopes at 45° to the horizontal. When the bottom edge is inclined to the horizontal, the conditions of an isosceles trapezoid

will be satisfied by some other plate slope. The basic geometry of a non-prismatic folded plate is in general very complex. In order to determine a specific geometrical form in which all the plates are truly isosceles trapezoids or triangles, a set of complicated geometrical relationships must be satisfied. In such a case, the structural configuration which results may not be desirable. In the analysis of the structures considered in this investigation, certain geometrical approximations were used. In cases where the plate elements did not take the exact shape of an isosceles trapezoid, the average length of the edges of all plates was used to define a common edge length. In addition, the neutral axis was defined from the mid-depth at each end of the plate as shown in Fig. 12. It was then assumed that the elements formed isosceles trapezoids by the geometrical approximations also shown in Fig. 12. These approximations will introduce a negligible amount of error within the range of taper angles which are valid for stress predictions by the flexure formula.

Another basic assumption is that the structural action in the transverse direction is controlled by one-way slab action. This same assumption is used in Ordinary Folded Plate Theory for the analysis of prismatic folded plates. In both cases, the assumption is violated mainly in localized regions near the supports where two-way slab action actually occurs. It is generally considered that one-way slab analysis can be applied to rectangular plates if the length to depth ratio is

greater than 2. On the basis of this criterion the amount of load transferred in the longitudinal direction is usually negligible.

One-way slab analysis tends to over-predict the transverse moments especially near the widest end of tapered plates. In other regions where the plates are narrower, except at the supports, this assumption should be much more valid. Compared to the assumptions used for prismatic elements, it would seem quite conservative if the ratio of the length to the widest depth of tapered plates is restricted to values larger than 2. If this criterion is used, the angle of taper, α_i, for a triangular plate would be limited to approximately 14°. The angle of taper for trapezoidal plates should be somewhat smaller because of the added plate width. It should be noted that the flexure formula predicts the stresses within 5% if the angle of taper, α_i, is limited to 14°. In general, the combination of the lower limit on the length to maximum depth ratio and the maximum angle of taper will depend on the accuracy that is desired.

The assumptions that are used in the analysis of non-prismatic folded plates are within the same range of validity as those used in Ordinary Folded Plate Theory. Folded plate structures of this type are usually referred to as "long folded plates".

B. Sign Conventions

In many parts of the formulation, the typical non-prismatic folded plate shown in Fig. 2 will be used as a reference structure. The notation,

co-ordinate systems and sign conventions which define the geometry of this structure are given in Figs. 12, 13, 14 and 15. Particular reference should be made to the node-joint notation given in Fig. 13. The sign conventions used for forces, moments and deflections are designated in the positive sense on all the figures presented in this chapter. Several of the most basic sign conventions are defined below:

1. Surface loads and joint loads are positive when directed downward.
2. Reactions and holding forces are positive when directed upward.
3. Plate loads are positive when directed toward the preceding joint.
4. End-action shears are positive when directed upward.
5. End-action moments and plate load moments are positive if counterclockwise.
6. Translational displacements are positive when directed upward.
7. Rotational displacements are positive in a counterclockwise direction.
8. Plate deflections in the plane of a plate are positive when directed toward the preceding joint.
9. Vertical joint deflections are defined positive when directed downward.
10. The longitudinal stresses and strains are considered to be positive when tensile.

C. Transverse Bending Analysis

One of the most frequently repeated steps in the analysis of a non-prismatic folded plate is the transverse bending analysis. At any phase of the analysis, the transverse bending moments and joint reactions are computed on the basis of the assumption that the structure acts as a continuous one-way slab at every nodal section. In the first stage of the primary analysis, it is assumed that surface loads are transferred to the longitudinal joints by one-way slab action. A transverse bending analysis is also required to account for the effects of relative joint displacements. In this phase, the secondary transverse moments and holding forces are introduced when the deflected shape of the slab structure is forced to conform to the deflected shape of the plate structure. In addition, a complete transverse bending analysis is required to determine the moments and complementary holding forces for each particular loading system. A complete transverse analysis at any given phase requires an independent analysis at each nodal section because the geometry of each cross-section is different. In a structure that contains 4 interior joints and 15 nodal sections, as many as 930 independent transverse bending analyses are performed. It is evident from these considerations that the transverse slab analysis must be formulated in general terms and in an orderly manner.

A general matrix formulation based on a basic stiffness method was used in this investigation. This choice was made because a stiffness method is normally more suitable for computer programming. In this method,

the choice of the basic restrained structure is limited to one possibility and the analysis involves only localized effects. These advantages are not generally true in applying a basic flexibility method where a number of choices of redundants are usually possible and the effects may not be localized.

The stiffness method used in this investigation is basically the same as the method presented by Gere and Weaver (9) for the analysis of continuous beams. Modifications have been made to the basic stiffness matrices so that a general cross-sectional shape can be analysed on the basis of the horizontal projection. This method will be presented only in sufficient detail to illustrate the basic formulation approach. A more detailed presentation on the concepts is given in Gere and Weaver (9).

The typical transverse nodal section shown in Fig. 16 will be used for specific reference in the discussion to follow. In this discussion, the cross-sections of the basic plate elements will be referred to as "members" and the moments and shears that are developed at the ends of the members will be generally referred to as "end-actions". It will be assumed that the support conditions at the joints supply full restraint in the vertical direction, but allow free translation in the horizontal direction. The only displacement components that will be considered are vertical translation and rotation in the plane of the structure.

1. Stiffness method

In a basic stiffness method, the unknown forces such as shears, end moments and reactions can be expressed in terms of the fixed end-actions resulting from the loading and the end-actions caused by the joint displacements. A stiffness matrix is generated and defined by the end-actions that are developed as a result of applying separate unit displacements of translation and rotation to each joint of the basic restrained structure, shown in Fig. 17. When load is applied to the restrained structure a set of fixed end-actions and reactions are determined which satisfy the condition of compatibility of displacements, but violate the condition of equilibrium at the joints. The unknown displacements of the structure are then determined on the basis that joint equilibrium must be restored. In the structural systems being considered, the kinematic degrees of freedom can be expressed as follows:

$$n = 2nj - nr$$

where n = number of degrees of freedom,

nj = number of joints, and

nr = number of restraints.

The following matrix equations are used to formulate the stiffness method at a specific nodal section, no.

$$\{AD\}_{no} = [S]_{no} \{D\}_{no} \tag{1}$$

where $\{AD\}_{no}$ = the column vector of end-actions (shears and moments) corresponding to the degrees of freedom of the system,

$[S]_{no}$ = the stiffness matrix corresponding to the degrees of freedom,

$\{D\}_{no}$ = the column vector of unknown displacements corresponding to the degrees of freedom, and

no = the subscript indicating that these matrices are for nodal section no.

The unknown displacements can be determined by solving Eq. 1,

$$\{D\}_{no} = [S]_{no}^{-1} \{AD\}_{no} \tag{2}$$

The final reactions and end-actions may then be determined from the following matrix equations:

$$\{AR\}_{no} = \{ARL\}_{no} + [SRD]_{no} \{D\}_{no} \tag{3}$$

$$\{AM\}_{no,i} = \{AML\}_{no,i} + [SM]_{no,i} \{DM\}_{no,i} \tag{4}$$

where $\{AR\}_{no}$ = the column vector of unknown reactions,

$\{ARL\}_{no}$ = the column vector of reactions in the restrained structure resulting from the applied load, corresponding to the unknown reactions,

$[SRD]_{no}$ = the stiffness matrix of end-actions corresponding to the support restraints which are caused by unit displacements corresponding to the degrees of freedom,

$\{AM\}_{no,i}$ = the column vector of unknown end-actions for the member i,

$\{AML\}_{no,i}$ = the column vector of fixed end-actions for the member i,

$[SM]_{no,i}$ = the basic member stiffness matrix for member i, and

$\{DM\}_{no,i}$ = the column vector of displacements corresponding to the ends of the member i.

The stiffness method used in this investigation was formulated in terms of an over-all joint stiffness matrix which is generated to include all possible joint displacements, those corresponding to the degrees of freedom of the system and those corresponding to the restrained portions. This approach differs from the usual one in which the stiffness matrix is formulated in terms of the degrees of freedom only. The advantage of using this approach exists in the fact that the stiffness matrix can be formulated in general terms without reference to the actual joint restraint conditions and it can be partitioned later according to the actual degrees of freedom and restrained portions of the structure. This approach is particularly advantageous when the analysis is programmed for a digital

computer. A formulation on the basis of an over-all joint stiffness matrix requires that the structure is subjected to loads acting only at the joints. This condition is usually not satisfied by the actual applied loading condition where distributed load may act on the members. To account for this condition, loads which act on the members are replaced by statically equivalent joint loads, AE. The total combined joint loading, AC, is then obtained by adding the actual joint loads, AJ, to the equivalent joint loads, AE. The equivalent joint loadings are formed from the fixed end-actions which result when the surface loads are applied to the restrained structure.

2. Formulation of the over-all joint stiffness matrix

A generalized notation system used to refer to the joints and members at a typical nodal section is shown in Fig. 18a. In this figure, the horizontal projection is used in lieu of the actual cross-section. The numbers on the top refer to the members while those on the bottom refer to the joints. It should be noted that the index of joint j is numerically equal to the index of member i, while the index of joint k is equal to i+1.

All possible joint displacements for a general cross-section are shown in vector symbols in Fig. 18b. These displacements are numbered in a sequence of translation, then rotation, proceeding from left to right. The rotational displacement vector follows the standard right hand rule. The four possible end-displacements for a member, i, are

given in Fig. 18c. The notation for the member end-displacements are related to the notation for the joint displacements by the following expressions:

$$j1 = 2i - 1$$

$$j2 = 2i$$

$$k1 = 2i + 1$$

$$k2 = 2i + 2$$

The over-all joint stiffness matrix, $[SJ]_{no}$, is formed from the contributions of the individual member stiffness matrices, $[SM]_{no,i}$. In order to analyse a general shape of cross-section as shown in Fig. 16 on the basis of the horizontal projection, and to determine the final joint reactions in the vertical direction, the member stiffness matrices must be formulated in a specific manner. The stiffness coefficients which correspond to translation are determined on the basis of unit displacements in the vertical direction rather than perpendicular to the members. When this approach is used, all end-action shears must also be defined in the vertical direction. The member stiffness matrix for a typical sloping member is formulated by considering the end-actions which result from applying all four unit displacement components separately as shown in Fig. 19. The resulting member stiffness matrix is given by the following relationship:

$$[SM]_{no,i} = \begin{bmatrix} \frac{+12EI_{no,i}}{d_{no,i}h^2_{no,i}} & \frac{+6EI_{no,i}}{d_{no,i}h_{no,i}} & \frac{-12EI_{no,i}}{d_{no,i}h^2_{no,i}} & \frac{+6EI_{no,i}}{d_{no,i}h_{no,i}} \\ \frac{+6EI_{no,i}}{d_{no,i}h_{no,i}} & \frac{+4EI_{no,i}}{d_{no,i}} & \frac{-6EI_{no,i}}{d_{no,i}h_{no,i}} & \frac{+2EI_{no,i}}{d_{no,i}} \\ \frac{-12EI_{no,i}}{d_{no,i}h^2_{no,i}} & \frac{-6EI_{no,i}}{d_{no,i}h_{no,i}} & \frac{+12EI_{no,i}}{d_{no,i}h^2_{no,i}} & \frac{-6EI_{no,i}}{d_{no,i}h_{no,i}} \\ \frac{+6EI_{no,i}}{d_{no,i}h_{no,i}} & \frac{+2EI_{no,i}}{d_{no,i}} & \frac{-6EI_{no,i}}{d_{no,i}h_{no,i}} & \frac{+4EI_{no,i}}{d_{no,i}} \end{bmatrix} \quad (5)$$

where E = the modulus of elasticity of the material

$I_{no,i}$ = the moment of interia of a unit width of slab for member (plate) i at nodal section no,

$d_{no,i}$ = the depth of the member i at nodal section no, and

$h_{no,i}$ = the horizontal projection of the depth $d_{no,i}$.

The over-all joint stiffness matrix is then formed by considering the stiffness coefficients of each member stiffness matrix contributing to a single joint. As shown in Fig. 20, the joint stiffness matrix coefficient can be obtained by adding the contributions of the member stiffness matrices. The joint stiffness coefficients, shown in Fig. 20a, which result from a unit vertical displacement at joint j are given by the following equations:

$$
\begin{aligned}
(SJ)_{no,j1,j1} &= (SM_{33})_{no,i-1} + (SM_{11})_{no,i} \\
(SJ)_{no,j2,j1} &= (SM_{43})_{no,i-1} + (SM_{21})_{no,i} \\
(SJ)_{no,k1,j1} &= (SM_{31})_{no,i} \\
(SJ)_{no,k2,j1} &= (SM_{41})_{no,i}
\end{aligned} \tag{6}
$$

The notation used in these equations is defined in the following typical examples:

$(SJ)_{no,j2,j1}$ = the joint stiffness coefficient in the direction j2 caused by a unit displacement in the direction j1, at nodal section no.

$(SM_{43})_{no,i-1}$ = the coefficient at the 4th row and 3rd column of the member stiffness matrix for member i-1, at nodal section no.

All the other stiffness coefficients at joints j and k caused by the other three unit displacements are given in Fig. 20.

By a thorough examination of the joint stiffness coefficients, it can be seen that the member stiffness coefficients contribute to the joint stiffness coefficients in a regular pattern. The basic groupings of the member stiffness matrices for the typical cross-section shown in Fig. 21a are illustrated in the joint stiffness matrix representation shown in Fig. 21b. In this matrix, all the possible joint displacements shown in Fig. 21a have been considered. The individual cross-hatched blocks represent the individual member stiffness matrices and all elements outside the cross-hatched section are zero. The over-lapping portion of the blocks

represents the coefficients of the joint stiffness matrix which are composed of elements from both of the adjacent member stiffness matrices. It should be noted that the matrix is 12x12 since two displacement conditions are possible at each joint.

The over-all joint stiffness matrix at this stage has been formulated in terms of all possible joint displacements. In order to obtain the final solution to the problem, however, the stiffness matrix corresponding to the degrees of freedom of the system and that corresponding to the restrained portion of the structure must be known. These matrices can be obtained by rearranging and partitioning the basis joint stiffness matrix in Fig. 21b.

The rearranged joint stiffness matrix for the structure shown in Fig. 16 is given in Fig. 22b. To obtain this matrix, the rows and columns of the original joint stiffness matrix, shown in Fig. 21b, are switched so that the stiffness coefficients which pertain to the actual degrees of freedom are placed in the first eight rows and columns of the matrix in Fig. 22b. At the same time, the stiffness coefficients which pertain to the restrained displacements are placed in the last four rows and columns of the matrix in Fig. 22b. The numbers shown at the bottom and to the right of the matrix in Fig. 21b indicate the new positions of the elements in the matrix in Fig. 22b. When the joint stiffness matrix is rearranged in this manner, it is equivalent to generating the matrix according to the numbering system for the displacements shown in Fig. 22a. In this new numbering system, the displacements which correspond to the actual degrees of freedom of the structure shown in Fig. 16 have been numbered in sequence from left to right in order of translation, then rotation at each

joint. The remaining restrained displacements are then numbered in sequence in the same manner. The rearranged joint stiffness matrix is partitioned in the manner designated by the dotted lines in Fig. 22b. The individual submatrices in each partitioned portion consist of

$$[SJ]_{no} = \left[\begin{array}{c|c} S & SDR \\ \hline SRD & SRR \end{array}\right] \tag{7}$$

where the submatrices in this equation are defined as:

$[S]_{no}$ = the stiffness matrix corresponding to the degrees of freedom of the system (8x8 for the example structure),

$[SRD]_{no}$ = the stiffness matrix corresponding to the support restraints,

$[SDR]_{no} = [SRD]^{T}_{no}$ = the matrix of actions corresponding to the degrees of freedom and caused by unit displacements corresponding to the joint restraints, and

$[SRR]_{no}$ = the matrix of actions corresponding to the support restraints caused by unit displacements corresponding to the same set of restraints.

The submatrices $[SDR]_{no}$ and $[SRR]_{no}$ may be used in the analysis of structures in which displacements such as support settlements are specified. The support conditions for the structure in Fig. 16 are assumed to be fully restrained in the vertical direction; therefore, these two

submatrices are not required. The submatrices $[S]_{no}$ and $[SRD]_{no}$ of the partitioned joint stiffness matrix are required for the solution of the basic stiffness analysis and will be used in the solution of Eqs. 1, 2, 3 and 4.

The operations of rearranging the joint stiffness can be programmed for the digital computer by specifying a joint restraint list for the structure. The joint restraint list simply designates the particular displacement components that are restrained in the actual structure and those that are free to displace. A restraint condition can be designated by the index 1 and a condition of no restraint by the index 0. When the rearranged joint stiffness matrix is generated in the computer with the aid of the joint restraint list, the matrices $[SDR]_{no}$ and $[SRR]_{no}$ are not formed because they are not required in the analysis. A detailed explanation of programming the computer to perform these operations with the aid of the joint restraint list is given in Gere and Weaver (9).

3. Fixed end-actions

Before a final solution can be obtained, the matrices corresponding to the loading conditions on the structure must be determined. In the case of the primary analysis, the fixed end-actions are caused by the applied surface loading, while in the correction analysis, fixed end-actions are introduced by the effects of relative joint translations. The basic applied loading that was considered is shown in Fig. 23 where the distribution of live load, w_{LLi}, is based on the horizontal projection. The distribution of dead load, w_{DLi}, must be modified to account for the slope of the plate elements in the longitudinal direction of the structure. The dead load per unit width of slab is then given by the

equation

$$w_{DLi} = \frac{\gamma' \, t_i \, Lna_i}{L} \tag{8}$$

where γ' = the unit weight of the slab material,

t_i = the thickness of the plate i,

Lna_i = the length of the neutral axis of the plate i, and

L = the span of the structure between the end diaphragms.

The resultant load on the member, $W_{Tno,i}$ shown in Fig. 23, is given by the expression

$$W_{Tno,i} = w_{LLi} \, h_{no,i} + w_{DLi} \, d_{no,i} \tag{9}$$

The fixed end-actions for the primary analysis, designated in Fig. 23, are then determined on the basis of the horizontal projection of the cross-section by the following expressions:

$$\begin{aligned} AML_{no,i,1} &= \frac{W_{Tno,i}}{2} \\ AML_{no,i,2} &= \frac{W_{Tno,i} \, h_{no,i}}{12} \\ AML_{no,i,3} &= \frac{W_{Tno,i}}{2} \\ AML_{no,i,4} &= -\frac{W_{Tno,i} \, h_{no,i}}{12} \end{aligned} \tag{10}$$

where

$AML_{no,i,1}$ = the fixed end shear at the left end of member i at nodal section no,

$AML_{no,i,2}$ = the fixed end moment at the left end of member i at nodal section no,

$AML_{no,i,3}$ = the fixed end shear at the right end of member i

at nodal section no, and

$AML_{no,i,4}$ = the fixed moment at the right end of member i at nodal section no.

Other loading conditions applied to the structure would of course produce other fixed end-actions.

In the correction analysis phase of the problem, fixed end-actions are caused by relative joint displacements. The fixed end-actions resulting from translation of the joints may be expressed in terms of the vertical deflections of the joints, $\delta v_{no,j}$, or the displacements perpendicular to the member, $\Delta_{no,i}$. In either case, the shearing forces must be determined in the vertical direction to correspond with the derivation of the stiffness matrix and so that the final joint reactions will be in the vertical direction. The fixed end-actions shown in Fig. 24, expressed in terms of the relative displacements perpendicular to the member, $\Delta_{no,i}$, are given by the equations:

$$
\begin{aligned}
AML_{no,i,1} &= \frac{-12\, E\, I_{no,i}\, \Delta_{no,i}}{d_{no,i}^2\, h_{no,i}} \\
AML_{no,i,2} &= \frac{-6\, E\, I_{no,i}\, \Delta_{no,i}}{d_{no,i}^2} \\
AML_{no,i,3} &= \frac{+12\, E\, I_{no,i}\, \Delta_{no,i}}{d_{no,i}^2\, h_{no,i}} \\
AML_{no,i,4} &= \frac{-6\, E\, I_{no,i}\, \Delta_{no,i}}{d_{no,i}^2}
\end{aligned}
\qquad (11)
$$

4. Equivalent and combined joint loads

The fixed end-actions given above must now be used to form a set of

equivalent joint loads. The end-actions are applied to the joints as shown in Fig. 25 and the equivalent joint loads, $AE_{no,j}$, are determined by writing two equations of equilibrium at each joint. The equivalent joint loads at joints j and k, shown in Fig. 25, are given by the following expressions:

$$\begin{aligned} AE_{no,2j-1} &= - AML_{no,i-1,3} - AML_{no,i,1} \\ AE_{no,2j} &= - AML_{no,i-1,4} - AML_{no,i,2} \\ AE_{no,2k-1} &= - AML_{no,i,3} - AML_{no,i+1,1} \\ AE_{no,2k} &= - AML_{no,i,4} - AML_{no,i+1,2} \end{aligned} \tag{12}$$

and the column vector of all equivalent joint loads, $\{AE\}_{no}$, takes the form

$$AE_{no} = \begin{vmatrix} AE_{no,1} \\ \cdot \\ \cdot \\ \cdot \\ AE_{no,2j-1} \\ AE_{no,2j} \\ AE_{no,2k-1} \\ AE_{no,2k} \\ \cdot \\ \cdot \\ \cdot \\ AE_{no,2m+2} \end{vmatrix} \tag{13}$$

The joint notation for the equivalent joint loads is the same as the notation used to designate the joint displacements shown in Fig. 18b. The subscript m denotes the last member in a nodal section.

In the case of the primary analysis, the structure may also be subjected to actual joint loadings. In this case, the total combined joint

load vector, $\{AC\}_{no}$, is formed by adding the actual joint load vector, $\{AJ\}_{no}$, to the equivalent joint load vector given by the matrix equation

$$\{AC\}_{no} = \{AJ\}_{no} + \{AE\}_{no} \tag{14}$$

When the structure is being analysed for the effects of relative joint displacements, all elements of the joint load vector, $\{AJ\}_{no}$, are set equal to zero.

The combined joint load vector must now be rearranged in the order of the numbering system given in Fig. 22a where the loads corresponding to the degrees of freedom portion are listed first, followed by those that correspond to the joint restraints. This operation may also be accomplished in the computer with the aid of the joint restraint list. The rearranged vector $\{AC\}_{no}$ is then partitioned as shown below:

$$\{AC\}_{no} = \begin{bmatrix} AD \\ \hline - ARL \end{bmatrix}_{no} \tag{15}$$

5. Joint reactions and transverse bending moments

The submatrices in Eq. 15 are now used to complete the solution to the transverse bending analysis. Joint displacements corresponding to the degrees of freedom are determined by the relationship:

$$\{D\}_{no} = [S]_{no}^{-1} \{AD\}_{no} \tag{2}$$

where $\{AD\}_{no}$ is the upper submatrix of vector $\{AC\}_{no}$.

The support reactions may also be determined by the following matrix equation:

$$\{AR\}_{no} = \{ARL\}_{no} + [SRD]_{no} \{D\}_{no} \tag{3}$$

The joint reactions, given in vector $\{AR\}_{no}$ are then rearranged in the order of the original numbering system shown in Fig. 21a. This may also be accomplished by the aid of the joint restraint list in the computer.

Before the final end-actions such as the transverse moments and shears can be determined, an over-all joint displacement vector $\{DJ\}_{no}$ must be formulated. The elements of $\{D\}_{no}$ are positioned in $\{DJ\}_{no}$ according to the original numbering system given in Fig. 21a. All the other displacements in the vector $\{DJ\}_{no}$ which correspond to the restraints are set equal to zero. The joint displacement vector now consists of the displacements which correspond to the ends of each consecutive member as shown below:

$$\{DJ\}_{no} = \begin{bmatrix} D_{no,1} \\ D_{no,2} \\ D_{no,3} \\ D_{no,4} \\ D_{no,5} \\ D_{no,6} \\ \vdots \\ D_{no,2j-1} \\ D_{no,2j} \\ D_{no,2k-1} \\ D_{no,2k} \\ \vdots \\ D_{no,2m+2} \end{bmatrix} \begin{matrix} \\ \\ \\ \\ \\ \\ \\ \\ \\ \\ \\ \\ \end{matrix} \begin{matrix} \\ \longrightarrow \{DM\}_{no,1} \\ \\ \\ \longrightarrow \{DM\}_{no,2} \\ \\ \\ \\ \\ \longrightarrow \{DM\}_{no,i} \\ \\ \\ \\ \end{matrix} \tag{16}$$

The end-actions for each individual member are then determined from Eq. 4,

$$\{AM\}_{no,i} = \{AML\}_{no,i} + [SM]_{no,i} \{DM\}_{no,i} \tag{4}$$

and the transverse bending analysis is complete. It should be noted that the elements of $\{AM\}_{no,i}$ correspond to the shears and transverse bending moments at the ends of the member i at nodal section no. The relationship between the notation used to define the transverse moments on the members and that used to define the transverse moments at the joints is shown in Fig. 26.

This method of analysis may appear to be quite long and involved. It should be emphasized, however, that an independent analysis must be performed at each nodal section to obtain a complete transverse bending analysis at any stage of the problem. When this method is programmed for the digital computer, these repetitive computations can be performed in short order. By the aid of the joint restraint list, the transverse support conditions can also be varied. In this study, the conditions of free and simply supported outer longitudinal edges were considered. Conditions of joint symmetry may also be used by specifying in the joint restraint list an additional rotational restraint at the interior joint of symmetry.

In the analysis of a particular structure, the joint stiffness matrices for each nodal section can be formulated at the beginning of the analysis because they depend only upon the properties of the cross-section. The stiffness matrix corresponding to the degrees of freedom portion of the structure, $[S]_{no}$, at each nodal section, is then inverted and stored in the computer along with the original stiffness matrix corresponding to the restrained portion $[SRD]_{no}$. At any stage where a

complete transverse bending analysis is required, a new set of fixed end-actions at each nodal section are introduced and the analysis may be performed by recalling these stored matrices. It may be noted that for the typical structure shown in Fig. 4, an 8x8 matrix must be inverted for each nodal section.

D. Plate Analysis

1. Resolution of joint loads

During the primary analysis and in each cycle of the Iteration Method, the joint reactions, $AR_{no,j}$, are applied to the plate structure to form the intensities of joint loading, $RI_{no,j}$. These joint loads are then resolved into the plane of the plates at each node to form the plate load intensities, $PI_{no,j,k}$. This same operation is performed in the correction analysis by the Particular Load Method. In this case, the concentrated nodal force, $K^{r}_{no,j}$, which is applied at a specific interior node of the structure to initiate a particular loading system, is resolved into the plane of the adjacent plates.

The plate loads which are obtained from the resolution of forces on the articulated plate structure, shown in Fig. 27, are given by the following expressions:

$$PI_{no,j,k} = \frac{-RI_{no,j} \cos \theta_{i-1}}{\sin \gamma_{i-1,i}} \qquad (17)$$

$$PI_{no,k,j} = \frac{+RI_{no,k} \cos \theta_{i+1}}{\sin \gamma_{i,i+1}} \qquad (18)$$

where θ_{i-1} = the slope of the plate i-1 with respect to the horizontal,

θ_{i+1} = the slope of the plate i+1 with respect to the horizontal,

$\gamma_{i-1,i}$ = the deflection angle between plates i-1 and i, and

$\gamma_{i,i+1}$ = the deflection angle between plates i and i+1.

The total plate load intensity, $PL_{no,i}$ is then determined from the contributions of the two adjacent joint loads

$$PL_{no,i} = PI_{no,j,k} + PI_{no,k,j} \tag{19}$$

2. Plate load bending moments

In the case of the primary analysis and the Iteration Method, the plate load intensities are determined at each nodal section of each plate. It is then assumed that each plate acts independently and that the distribution of plate load between nodal sections varies as a second degree parabola. The distributed load along the neutral axis is expressed in terms of a number of statically equivalent concentrated forces, $PC_{no,i}$, which are applied at each nodal section as shown in Fig. 8. These concentrated plate loads can be determined by the following equation:

$$PC_{no,i} = \frac{\ell na_i}{12} [PL_{no-1,i} + 10\ PL_{no,i} + PL_{no+1,i}] \tag{20}$$

where ℓna_i = the length between nodal sections along the neutral axis of plate i.

It should be noted that the plate load intensities, $PL_{o,i}$, and $PL'_{o,i}$, in Fig. 8, can be obtained by a linear or parabolic extrapolation of the interior plate loading.

On the basis of statics, the modified reaction at the left support,

$R\ell_i$, shown in Fig. 8 is given by the equation,

$$R\ell_i = \frac{1}{Lna_i}\left[PC_{1,i}(Lna_i - \ell na_i) + PC_{2,i}(Lna_i - 2\ell na_i) + \ldots \right. \quad (21)$$

$$\left. + PC_{nn,1}\,(Lna_i - (nn)\times \ell na_i)\right] .$$

The plate load bending moments, $MO_{no,i}$, at the nodal sections are also determined by statics and are given by the following equations:

$$\begin{aligned} MO_{1,i} &= R\ell_i\ (\ell na_i) \\ MO_{2,i} &= R\ell_i\ (2\ell na_i) - PC_{1,i}(\ell na_i) \\ MO_{3,i} &= R\ell_i\ (3\ell na_i) - PC_{1,i}(2\ell na_i) - PC_{2,i}(\ell na_i) \end{aligned} \quad (22)$$

etc.

3. Derivation of the Modified Three Shear Equation

In the plate load bending analysis, each plate is assumed to act as an independent beam. Consequently, the stresses developed at the common edge of two adjacent plates are not equal. A condition of strain compatibility must be satisfied along each joint which infers that the stresses parallel to the common edge must also be equal. This condition of stress compatibility is given by the following relationship:

$$f_{i,j} = f_{i+1,j} \quad (23)$$

where $f_{i,j}$ = the stress parallel to the joint j in plate i along joint j, and

$f_{i+1,j}$ = the stress parallel to the joint j in plate i+1 along joint j.

In order to satisfy this compatibility requirement a distribution of unit shearing forces q_j must be introduced along the common joint as shown in Fig. 28. The longitudinal stresses parallel to the joint

can be expressed in terms of the stresses parallel to the neutral axis and the unit shearing forces by considering the equilibrium of forces on two elemental plate sections shown in Fig. 29. The expressions for these stresses are:

$$f_{i,j} = \frac{\bar{f}_{i,j}}{\cos^2\alpha_i} - \frac{2q_j \tan\alpha_i}{t_i} \tag{24}$$

$$f_{i+1,j} = \frac{\bar{f}_{i+1,j}}{\cos^2\alpha_{i+1}} + \frac{2q_j \tan\alpha_{i+1}}{t_{i+1}} \tag{25}$$

where $\bar{f}_{i,j}$ = the longitudinal stress parallel to the neutral axis in plate i at joint j, and

$\bar{f}_{i+1,j}$ = the longitudinal stress parallel to the neutral axis in plate i+1 at joint j.

By substituting Eqs. 24 and 25 into Eq. 23 the condition of matching stresses is given by the following relationship:

$$\frac{\bar{f}_{i+1,j}}{\cos^2\alpha_{i+1}} - \frac{\bar{f}_{i,j}}{\cos^2\alpha_i} + 2q_j \left(\frac{\tan\alpha_i}{t_i} + \frac{\tan\alpha_{i+1}}{t_{i+1}}\right) = 0 \tag{26}$$

The stresses parallel to the neutral axis at a specific nodal section no can be expressed in terms of the plate load bending moments, $MO_{no,i}$, and the unknown shear forces, $T_{no,j}$, shown in Fig. 28. The stress developed parallel to the neutral axis of plate i at joint j is given by the equation:

$$\bar{f}_{no,i,j} = -\frac{MO_{no,i}}{Z_{no,i}} + \frac{(T_{no,j} - T_{no,j-1})\cos\alpha_i}{A_{no,i}} + \frac{(T_{no,j} + T_{no,j-i})d_{no,i}\cos\alpha_i}{2\,Z_{no,i}} \tag{27}$$

where it is assumed that tensile stresses are positive and

$A_{no,i}$ = the cross-sectional area of plate i at nodal section no, and

$Z_{no,i}$ = the section modulus of plate i at nodal section no.

Similarly, the stress parallel to the neutral axis of plate i+1 at joint j is given by the following equation:

$$\bar{f}_{no,i+1,j} = +\frac{MO_{no,i+1}}{Z_{no,i+1}} + \frac{(T_{no,j+1} - T_{no,j})\cos\alpha_{i+1}}{A_{no,i+1}} - \frac{(T_{no,j+1} + T_{no,j})\,d_{no,i+1}\cos\alpha_{i+1}}{2\,Z_{no,i+1}} \tag{28}$$

The relationship between the unit shear force, q_j and the total shear force, T_j, is given by the equation:

$$q_j = \frac{dT_j}{dx} \tag{29}$$

where the variable x defines the length along the joint j.

The equation for the unit shear force $q_{no,j}$, at a specific nodal section, no, can be expressed in numerical form in terms of the shear forces at the two neighboring nodes, no+1 and no-1 along the same joint. This is accomplished by writing Eq. 29 in terms of the central finite difference expression for the first derivative, given by the equation:

$$q_{no,j} = \frac{T_{no+1,j} - T_{no-i,j}}{2\ell e} \tag{30}$$

where ℓe = the edge length of the plates between nodal sections.

When Eqs. 27, 28 and 30 are substituted into the condition of matching stresses, Eq. 26, the final expression to be known as the Modified Three Shear Equation is obtained. This expression is given by the following relationship:

$$\begin{aligned}
&\left[\frac{2}{A_{no,i+1}\cos\alpha_{i+1}}\right]T_{no,j+1} + \left[4\left(\frac{1}{A_{no,i}\cos\alpha_i} + \frac{1}{A_{no,i+1}\cos\alpha_{i+1}}\right)\right]T_{no,j} \\
&+ \left[\frac{2}{A_{no,i}\cos\alpha_i}\right]T_{no,j-1} + \left[\frac{-1}{\ell e}\left(\frac{\tan\alpha_i}{t_i} + \frac{\tan\alpha_{i+1}}{t_{i+1}}\right)\right]T_{no+1,j} \\
&+ \left[\frac{1}{\ell e}\left(\frac{\tan\alpha_i}{t_i} + \frac{\tan\alpha_{i+1}}{t_{i+1}}\right)\right]T_{no-1,j} = \frac{MO_{no,i}}{Z_{no,i}\cos^2\alpha_i} \\
&+ \frac{MO_{no,i+1}}{Z_{no,i+1}\cos^2\alpha_{i+1}}
\end{aligned} \tag{31}$$

or, in terms of a set of coefficients and a constant:

$$\begin{aligned}
&(AA_{no,j+1})T_{no,j+1} + (AA_{no,j})T_{no,j} + (AA_{no,j-1})T_{no,j-1} \\
&+ (AA_{no+1,j})T_{no+1,j} + (AA_{no-1,j})T_{no-1,j} = C_{no,j}
\end{aligned} \tag{32}$$

where the coefficients are defined as:

$$AA_{no,j+1} = + \frac{2}{A_{no,i+1}\cos\alpha_{i+1}}$$

$$AA_{no,j} = + 4\left(\frac{1}{A_{no,i}\cos\alpha_i} + \frac{1}{A_{no,i+1}\cos\alpha_{i+1}}\right)$$

$$AA_{no,j-1} = \frac{+ 2}{A_{no,i}\cos\alpha_i}$$

$$AA_{no+1,j} = -\frac{1}{\ell e}\left(\frac{\tan\alpha_i}{t_i} + \frac{\tan\alpha_{i+1}}{t_{i+1}}\right)$$

$$AA_{no-i,j} = +\frac{1}{\ell e}\left(\frac{\tan\alpha_i}{t_i} + \frac{\tan\alpha_{i+1}}{t_{i+1}}\right)$$

and the constant on the right hand side of the equation is given by:

$$C_{no,j} = \frac{MO_{no,i}}{Z_{no,i}\cos^2\alpha_i} + \frac{MO_{no,i+1}}{Z_{no,i+1}\cos^2\alpha_{i+1}}$$

The Modified Three Shear Equation is generally valid for matching stresses at the common edge of the two tapered plate elements. For prismatic cases the angles of taper α_i and α_{i+1} are zero, and the "Modified Three Shear Equation" reduces to the "Ordinary Three Shear Equation" which is valid at all sections and is given by the expression:

$$\left[\frac{2}{A_{i+1}}\right]T_{j+1} + \left[4\left(\frac{1}{A_i} + \frac{1}{A_{i+1}}\right)\right]T_j + \left[\frac{2}{A_i}\right]T_{j-1} = \frac{MO_i}{Z_i} + \frac{MO_{i+1}}{Z_{i+1}} \qquad (33)$$

4. Matrix formulation of the Modified Three Shear Equations

In order to match the stresses at every section along each joint, the Modified Three Shear Equation must be written at an infinite number of nodes. It is impractical if not impossible to satisfy this requirement. However, the problem can be solved with sufficient accuracy by matching the stresses at a finite number of nodal points. This is basically the same approach that is used in the solution of boundary value problems by finite difference methods.

The unknowns involved in writing the Modified Three Shear Equation at a particular node are the shear forces at three joints on the same nodal section and the shear forces at the two adjacent nodes along the

same joint. At a particular node, the coefficients $AA_{no,j}$, defined in Eq. 32, are known constants and the constant $C_{no,j}$ is defined in terms of the known plate load bending moments, $MO_{no,i}$ and the plate geometry. If the Modified Three Shear Equation is written at all interior nodes of the structure the unknown shear forces at the boundaries will be included. The boundary condition of zero shear exists at each joint along the end diaphragms since it is assumed that these diaphragms serve as simple supports. When the outer longitudinal edges of the structure are free or simply supported, the boundary condition of zero shear also exists at all nodes along the outer edges. It should be noted that this same boundary condition would also be specified at an interior joint of symmetry.

By writing the Modified Three Shear Equation at all interior nodes taking into account the specified boundary conditions, a set of (nn×nij) linear simulaneous equations can be formulated and solved to determine the unknown shear forces. In order to solve this set of equations on the digital computer, the notation system must be orderly. The equations are formulated according to the new notation system for the shear forces T' and the co-ordinate system shown in Fig. 30. The Modified Three Shear Equation is written first at all interior nodes of the first nodal section proceeding in the direction of the positive z axis. The remaining equations are then written at all the other nodal sections in the same manner, proceeding in the direction of the positive x axis. The resulting matrix equation written in standard matrix notation takes the form:

$$\begin{bmatrix} AA_{11} & AA_{12} & AA_{13} \cdots & AA_{1,nn \times nij} \\ AA_{21} & AA_{22} & AA_{13} \cdots & AA_{2,nn \times nij} \\ \vdots & \vdots & \vdots & \vdots \\ AA_{nn \times nij,1} \cdots & & & AA_{nn \times nij,nn \times nij} \end{bmatrix} \begin{bmatrix} T'_1 \\ T'_2 \\ T'_3 \\ \vdots \\ T'_{nn \times nij} \end{bmatrix} = \begin{bmatrix} C_1 \\ C_2 \\ C_3 \\ \vdots \\ C_{nn \times nij} \end{bmatrix} \tag{34}$$

which may be written as,

$$[AA]\ \{T'\} = \{C\} \tag{35}$$

The shear forces at all interior nodes are then determined by solving Eq. 35, resulting in the following expression:

$$\{T'\} = [AA]^{-1}\ \{C\} \tag{36}$$

The vector $\{T'\}$ is then rearranged according to the actual node-joint notation shown in Fig. 30 to give the vector $\{T\}_{no,j}$. The relationship between these two shear force vectors is given below:

$$\begin{bmatrix} T_{1,2} \\ T_{1,3} \\ \vdots \\ T_{1,nj-1} \\ T_{2,2} \\ T_{2,3} \\ \vdots \\ T_{nn,nj-1} \end{bmatrix} = \begin{bmatrix} T'_1 \\ T'_2 \\ \vdots \\ T'_{nij} \\ T'_{nij+1} \\ T'_{nij+2} \\ \vdots \\ T'_{nn \times nij} \end{bmatrix} \tag{37}$$

After the shear force vector $\{T\}_{no,j}$ has been formed, the matched longitudinal stresses, $\bar{f}_{no,i,j}$, at the edges of the plates, parallel to the neutral axis, are determined by substituting the proper shearing forces from the vector $\{T\}_{no,j}$ into Eq. 27 or 28.

As a specific example of formulating these equations, consider the typical structure shown in Fig. 31a where only three nodal sections have been used. The matrix [AA] is given in Fig. 31b where each row of the matrix represents the coefficients of the Modified Three Shear Equation, Eq. 32, written at a specific interior node of the structure. The order in which these equations are written is designated by the node-joint numbering system on the left hand side of the matrix. The coefficients in the matrix are numbered in standard matrix form.

As shown in Fig. 31b, the matrix [AA] is banded about the main diagonal and contains two diagonal lines of elements positioned slightly

away from the main diagonal. These diagonal lines are a result of the inter-relationship of the shears at nodes no+1 and no-1 when the Modified Three Shear Equation is written at node no. It is interesting to note that when the structure is prismatic or if the effect of taper is neglected, the matrix reduces to the coefficients shown in the three larger blocks in Fig. 31b. Each of these blocks would then represent the coefficients of the Ordinary Three Shear Equation if it were written at all joints of a particular nodal section. In the case of a prismatic structure, only one of these individual submatrices shown in the larger blocks needs to be inverted and this inverted matrix could then be used for the analysis at all nodal sections. On the other hand, if the plate taper in a non-prismatic structure is neglected, an approximation of the matched stresses can be determined by satisfying the Ordinary Three Shear Equation at all the joints in each nodal section separately. This fact may be useful if it is desired to reduce the computer time required for matrix inversion. The error involved in this approximation should be quite small if the taper angles are not too large.

E. Deflection Analysis

1. Plate deflections

After the stresses have been matched at the joints, the deflections of the structure resulting from these stresses are computed. The plate deflections, $\delta_{no,i}$, are computed first on the basis of the assumption that

the plate structure is temporarily disconnected at the joints. Before these deflections can be computed, the distribution of curvature over the length of the neutral axis of each plate must be determined.

The curvature, $\phi_{no,i}$, at any nodal section of a plate is determined from the strain distribution at the section, shown in Fig. 10a. The expression for the curvature is given by the relationship:

$$\phi_{no,i} = \frac{\bar{\varepsilon}_{no,i,j-1} - \bar{\varepsilon}_{no,i,j}}{d_{no,i}} \tag{38}$$

where $\bar{\varepsilon}_{no,i,j-1}$ = the strain parallel to the neutral axis of plate i at joint j-1 for nodal section no, and

$\bar{\varepsilon}_{no,i,j}$ = the strain parallel to the neutral axis of plate i at joint j for nodal section no.

In an elastic structure, stresses are proportional to strains; therefore, the curvature may be expressed in terms of the known stresses by the following equation:

$$\phi_{no,i} = \frac{\bar{f}_{no,i,j-1} - \bar{f}_{no,i,j}}{(E)(d_{no,i})} \tag{39}$$

The curvature distribution is then determined by computing the curvature at each nodal section of a plate and by assuming that the distribution between nodal sections varies as a second degree parabola. Once the curvature distribution has been defined, the deflections in the plane of each plate can be evaluated on the basis of Moment-Area Principles. The

operations involved in computing the plate deflections, $\delta_{no,i}$, are completely analogous to those used to compute the plate load bending moments, $MO_{no,i}$. The basis of the analogy exists between the differential equation of bending deflection

$$\frac{d^2\xi}{d\eta^2} = \phi$$

and the statics equation

$$\frac{d^2(MO)}{d\eta^2} = PL$$

where η and ξ are the co-ordinates parallel and perpendicular to the neutral axis of a plate respectively as shown in Fig. 12. The following analogy can be established between the variables of the two problems:

Deflections	Statics
$\phi_{no,i}$	$PL_{no,i}$
$\bar{\phi}_{no,i}$	$PC_{no,i}$
$\theta\ell_i$	$R\ell_i$
$\delta_{no,i}$	$MO_{no,i}$

The notation which is used in the deflection problem is defined in Fig. 10. This analogy proves to be quite useful when a digital computer is used to perform the computations because the same program can be used to determine $MO_{no,i}$ and $\delta_{no,i}$.

The basic computations needed to determine the plate deflections will be explained briefly with reference to Fig. 10 and the equations associated with the computations of the plate load bending moments. A set of concentrated angle changes, $\bar{\phi}_{no,i}$, can be defined at each nodal section by a numerical integration of the curvature diagram. These angle changes are determined by using the analogies specified above and Eq. 20. By assuming that the slope at the left support is zero, as shown in Fig. 10c, the deflection, δR_i, at the right support is determined by summing the incremental deflections at the right support caused by each concentrated angle change. The boundary condition at the right support requires that the deflection, δR_i, must equal zero, which results in the requirement of rotating the deflected curve by a concentrated angle, $\theta \ell_i$, about the left support. The evaluation of $\theta \ell_i$ is directly analogous to the evaluation of the left reaction, $R\ell_i$ given by Eq. 21. The deflections, $\delta_{no,i}$, at each nodal section are then computed from the basic geometry of the deflected curve which is directly analogous to determining the plate load bending moments, $MO_{no,i}$, at each nodal section, given by Eq. 22.

This method of analysis defines the exact deflection at each nodal section of the plate if the curvature distribution is exact. The accuracy of the computed deflections is then a function of the numerical accuracy of the curvature distribution assumed between nodal sections and the accuracy of the intensities of curvature at each nodal section.

2. Williot geometry

In the preceding analysis, the plate deflections were computed by assuming that each plate acts independently. As a result, the deflections of two adjacent plates do not define the same deflected position of the common joint, as shown in Fig. 11. The final deflected positions of the joints are then determined in terms of the plate deflections, by applying a basic Williot diagram at each node along each joint. The vertical joint deflection, $\delta v_{no,j}$, is determined from the Williot geometry shown in Fig. 32 and is given by the equation:

$$\delta v_{no,j} = \frac{\delta_{no,i-1} \cos \theta_i}{\sin \gamma_{i-1,i}} - \frac{\delta_{no,i} \cos \theta_{i-1}}{\sin \gamma_{i-1,i}} \tag{40}$$

The relative displacement perpendicular to the plate, $\Delta_{no,i}$, shown in Fig. 32, is also computed on the basis of the Williot geometry and is given by the following equation:

$$\Delta_{no,i} = \delta_{no,i-1} \csc \gamma_{i-1,i} - \delta_{no,i} (\cot \gamma_{i-1,i} + \cot \gamma_{i,i+1}) + \delta_{no,i+1} \csc \gamma_{i,i+1} \tag{41}$$

3. Relative joint displacements

In many parts of the complete analysis of a non-prismatic folded plate, the stresses introduced into the plate structure are computed on the basis of the assumption that relative joint displacement do not occur. The deflections which are computed on the basis of these stresses show

that relative joint displacements do occur, as shown in Fig. 11. The deflected shape of the slab structure is then forced to conform to the deflected shape of the plate structure. As a result, a set of transverse moments and complementary holding forces are introduced into the slab structure at each nodal section. A complete transverse bending analysis of the structure is required to determine the transverse moments and holding forces that are introduced. The fixed end-actions used in this analysis are computed on the basis of the relative displacements perpendicular to the plates given in Eq. 41. These fixed end-actions have been defined in Eq. 11 and are shown in Fig. 24.

F. Iteration Method

In order to complete the correction analysis, the secondary holding forces which result from neglecting the effects of relative joint displacements in the primary analysis must be removed. In the case of the Iteration Method, these secondary holding forces are reapplied to the joints of the plate structure to form a new set of joint loads. Once these new joint loads have been defined, the entire analysis procedure is repeated. The basic steps involved in the Iteration Method are summarized below with reference to the formulation presented in the preceding sections of this chapter.

Step 1. Compute the primary transverse moments and primary joint reactions at each nodal section by carrying out a complete

transverse bending analysis for the applied loading as described in Section III.C.

Step 2. Apply the joint reactions or holding forces to the plate structure as a set of joint load intensities.

Step 3. Resolve the joint loads into the plane of the plates at each nodal section as described in Section III.D.1.

Step 4. Compute plate loads and plate load bending moments at each nodal section of each plate as described in Section III.D.2.

Step 5. Compute the longitudinal stresses and match them at each node by applying the Modified Three Shear Equation as described in Section III.D.4.

Step 6. Compute plate deflections and relative joint displacements as described in Section III.E.

Step 7. Compute the fixed end-actions caused by relative joint displacements for all the plates at each nodal section as described in Section III.C.3.

Step 8. Compute a new set of transverse moments and holding force intensities at each node as described in Section III.C.

Step 9. Determine the accumulated transverse moments, longitudinal stresses and vertical deflections computed up to this stage of the analysis at each node.

Step 10. Compare the transverse moments resulting from the effects of joint displacements in this iteration cycle to the

accumulated transverse moments at each node respectively, to see if another iteration cycle is required.

Step 11. Repeat Steps 2 through 10 if another cycle of iteration is required.

G. Particular Load Method

The general principles of the Particular Load Method and the manner in which they can be applied in the analysis of non-prismatic folded plates have been discussed in Chapter II. In this section, the details of formulating this method are presented.

1. Concentrated secondary holding forces

The first step in applying the Particular Load Method is to express the distribution of secondary holding forces, $AR^{s}_{no,j}$, shown in Fig. 33 in terms of a statically equivalent set of concentrated holding forces. These concentrated holding forces, $RC^{s}_{no,j}$, are determined by the same procedures used to determine the concentrated plate loads. If the distribution of secondary holding forces is assumed to vary as a second degree parabola between nodal sections, the resulting concentrated holding force at each interior node can be obtained from the following expression:

$$RC^{s}_{no,j} = \frac{\ell e}{12} [AR^{s}_{no-1,j} + 10\ AR^{s}_{no,j} + AR^{s}_{no+1,j}] \qquad (42)$$

It should be noted that when the holding forces are computed in this manner, small portions of the distributed loads near the supports are

neglected, as shown in Fig. 33. When a sufficient number of nodal sections are considered, this effect will be negligible. In order to remove the effects of the secondary holding forces, a linear combination of (nn × nij) particular loading systems is required.

2. Particular loading systems

Each particular loading system must be formed separately and each must be independent. A particular loading system is initiated by first applying a known concentrated nodal force, $K^{r}_{no,j}$, to an interior node of the plate structure. A complete analysis of the structure subjected to this concentrated load must then be conducted to determine the complementary loading which results. The steps involved in forming a particular loading system are outlined below with reference to the formulation presented in the preceding sections of this chapter.

Step 1. Apply a concentrated nodal force, $K^{r}_{no,j}$, at a particular interior node of the structure.

Step 2. Resolve the concentrated nodal force into two concentrated plate loads acting in the planes of the two adjacent plates. Equation 17 or 18 may be used for this calculation.

Step 3. Compute the plate load bending moments, $MO_{no,j}$, in the two adjacent plates at each nodal section resulting from the effect of the concentrated plate loads. An analysis similar to that described in Section III.D.2 must be performed.

Step 4. Match the stresses at all interior nodes by using the Modified Three Shear Equation and by applying the procedure outlined in Section III.D.4. It should be noted that plate load stresses will only exist at the nodal sections of the two plates being considered; however, the condition of matching stresses will introduce stresses, $\bar{f}^{r}_{no,i,j}$, at all nodal sections of all plates in the structure.

Step 5. Compute the plate deflections at all nodal sections for each plate as described in Section III.E.1.

Step 6. Compute the vertical joint displacements, $\delta v^{r}_{no,j}$ and the relative displacements perpendicular to the plates, $\Delta_{no,i}$, at each nodal section using the equations given in Section III.E.2.

Step 7. Compute the fixed end-actions at each nodal section of each plate resulting from relative joint displacements by using Eq. 11.

Step 8. Run a complete transverse bending analysis as described in Section III.C. to determine the transverse moments, $TM^{r}_{no,j}$, and the complementary holding force intensities, $FI^{r}_{no,j}$, introduced by the requirement that deflected shape of the slab and plate structure must conform.

Step 9. Express the distribution of complementary holding forces along each joint in terms of a set of statically equivalent

concentrated holding forces, $FC^{r}_{no,j}$, one at each interior node. Equation 42 is used for these computations.

Step 10. Combine the applied load, $K^{r}_{no,j}$, with all the complementary holding forces, $FC^{r}_{no,j}$, to form a complete particular loading system. This system consists of a total of (nn × nij) concentrated forces, $F^{r}_{no,j}$.

By applying a known concentrated force, $K^{r}_{no,j}$, at each interior node of the structure in turn and by carrying out the steps described above for each case, a complete set of (nn × nij) particular loading systems can be established.

3. Matrix formulation of the Particular Load Method

In the Particular Load Method, an appropriate linear combination of these particular loading systems is then used to remove the effects of the secondary holding forces, $RC^{s}_{no,j}$. The corresponding mathematical expression is a set of linear simultaneous equations shown in matrix form in Fig. 34. In this set of equations, the unknowns β_1, β_2, β_3.... β_r.... $\beta_{nn \times nij}$ represent portions of the particular loading systems, 1,2,3....r...(nn × nij), required to eliminate the effect of the secondary holding forces. The elements of the coefficient matrix are subscripted according to the "node-interior joint" notation, while the superscript indicates the index number for a particular loading system. The method of formulating this matrix equation is illustrated in Fig. 35 where a plan view of the typical non-prismatic folded plate is shown to contain

only three nodal sections. Each equation in the set represents the linear sum of concentrated nodal forces of all the particular loading systems at one node equated to the negative effect of the concentrated secondary holding force at that node. The equations are first written for all the interior joints in the first nodal section, proceeding in the direction of the positive z axis. The remaining equations are then written at the other nodal sections in the same manner, proceeding in the direction of the positive x axis.

The elements of the matrix shown in Fig. 34 must be renumbered in the standard matrix form in order to solve the problem on the digital computer. Once this has been accomplished the matrix equation in Fig. 34 can be represented by the following equation:

$$[F]\ \{\beta\} = \{R\} \tag{43}$$

The unknowns β_r are then determined by solving Eq. 43:

$$\{\beta\} = [F]^{-1}\ \{R\} \tag{44}$$

After the coefficients, β_r, have been determined, the final results can be obtained as described in the following section.

4. Final results

A complete set of stresses, $\bar{f}^{r}_{no,i,j}$, transverse moments, $TM^{r}_{no,j}$ and deflections, $\delta v^{r}_{no,j}$, are known for each particular loading system. The resulting stresses, moments and deflections introduced by removing the

effects of the secondary holding forces can then be determined by the following linear sums:

$$\begin{aligned}
\bar{f}^{c}_{no,i,j} &= \beta_1 \bar{f}^{1}_{no,i,j} + \beta_2 \bar{f}^{2}_{no,i,j} + \ldots\ldots \beta_{nn \times nij} \bar{f}^{nn \times nij}_{no,i,j} \\
TM^{c}_{no,j} &= \beta_1 TM^{1}_{no,j} + \beta_2 TM^{2}_{no,j} + \ldots\ldots \beta_{nn \times nij} TM^{nn \times nij}_{no,j} \\
\delta v^{c}_{no,j} &= \beta_1 \delta v^{1}_{no,j} + \beta_2 \delta v^{2}_{no,j} + \ldots\ldots \beta_{nn \times nij} \delta v^{nn \times nij}_{no,j}
\end{aligned} \tag{45}$$

where the superscript c refers to the results of the correction analysis not including the secondary transverse moments. These expressions are valid at each node of the structure.

The final solution to the non-prismatic folded plate analysis is obtained by superimposing the results of the primary analysis and the correction analysis:

$$\begin{aligned}
\bar{f}^{f}_{no,i,j} &= \bar{f}^{p}_{no,i,j} + \bar{f}^{c}_{no,i,j} \\
TM^{f}_{no,j} &= TM^{p}_{no,j} + TM^{s}_{no,j} + TM^{c}_{no,j} \\
\delta v^{f}_{no,j} &= \delta v^{p}_{no,j} + \delta v^{c}_{no,j}
\end{aligned} \tag{46}$$

where the superscript f refers to the final results.

IV. COMPUTER PROGRAMS

An examination of the theory makes it quite evident that the only practical means of analysing non-prismatic folded plates is with the aid of a digital computer. The theory has been presented in a form which can be programmed in any standard computer language. In this investigation, programs were written in Fortran IV using single precision variables and the analysis was carried out on an IBM 360 Model 50 digital computer available at the Iowa State University Computational Center. A computer program was written for both the Iteration Method and the Particular Load Method. Each program consisted of approximately 750 Fortran statements. Thus, a number of trial runs were required before the programs were completely de-bugged. A description of these programs is presented in this chapter along with the basic flow charts of each program. In addition, a small program was written for analysing the elements of a non-prismatic folded plates by Beam Theory. A brief discussion of this program is also presented at the end of this chapter.

A. Programs for the Iteration Method and the Particular Load Method

All computations in the Iteration Method and the Particular Load Method were carried out on the computer. These computations included generating all the matrices and solving them. The basic input data for these programs consisted of the geometry of the structure, the properties of the material and the loading conditions. The final output

data consisted of the calculated stresses, transverse moments, shear forces and deflections. These programs were designed to analyse simply supported non-prismatic folded plates only.

1. Basic input data

The geometry of the structure and the material properties were specified by the following input data:

1. Number of plates, m
2. Number of joints, nj
3. Number of restraints, nr
4. Number of nodes, nn
5. Joint restraint list
6. Span of the structure, L
7. Length of the neutral axis of each plate, Lna_i
8. Edge length of all plates, Le
9. Thickness of each plate, t_i
10. Slope angle of the first plate, θ_1
11. Deflection angles between all the plates, $\gamma_{i,i+1}$
12. Modulus of elasticity of the material, E.

A joint restraint list was used to designate the support conditions for the transverse bending analysis. Two restraint conditions were specified for each joint, one for vertical displacement and the other for rotational displacement. In the joint restraint list, a restrained

displacement was designated by the index, 1, while a condition of no restraint was designated by the index 0.

2. Loading conditions

The proposed method of analysis is not restricted to the cases of similar loading; therefore, many types of loading can be considered. The programs are designed so that surface loads can be specified in three ways:

1. Load can be defined in the form of a uniform intensity for each plate.
2. The intensities of load uniform in the transverse direction can be specified separately at each nodal section of each plate.
3. The fixed end-actions for each plate at each nodal section can be specified separately instead of the previous two forms of loading.

When the surface loads are defined in the form of intensities, it is assumed that the distribution is uniform in the transverse direction. The fixed end-actions, given in Eq. 10, are then calculated by a routine which is built into the programs. The intensities of load can consist of live load based on the horizontal projection or dead load distributed over the surface of the structure as shown in Fig. 23. Joint loads are also specified in the form of intensities common to all nodes along a particular joint.

If the load intensity is specified at each nodal section separately, the distribution of loading in the longitudinal direction can be varied. The only requirement in this case is that the intensities must be specified at a sufficient number of nodal sections to properly define the longitudinal distribution. It is also possible to consider other distributions of load in the transverse direction. These distributions are defined in terms of the fixed end-actions which are read directly into the computer. Concentrated loads and concentrated line loads are also considered in this manner.

3. Output data

The computed results were written out at the end of the primary analysis and at the end of the complete analysis. In the case of the primary solution, the output data consisted of

1. Primary longitudinal stresses at each node, $\bar{f}^{p}_{no,i,j}$.
2. Primary transverse moments at each node, $TM^{p}_{no,j}$.

At the end of the analysis, the final output data consisted of

1. Final longitudinal stresses at each node, $\bar{f}^{f}_{no,i,j}$.
2. Final transverse moments at each node, $TM^{f}_{no,j}$.
3. Final shear forces at each node, $T^{f}_{no,j}$.
4. Final vertical joint deflections at each node, $\delta v^{f}_{no,j}$.

4. Flow charts

The computer programs for the Iteration Method and the Particular Load Method will be presented in the form of flow charts. These flow

charts do not contain the detailed operations of the programs. Instead, they present the logical steps required to organize each method of analysis. The actual details of the program follow closely to the formulation presented in Chapter III and specific reference is made to this formulation in each flow chart. These basic flow charts also serve as a summary for the entire method of analysis.

The operations that are performed at the beginning of each computer program are exactly the same. These operations are present in a common flow chart shown in Fig. 36. The flow charts for the Iteration Method and the Particular Load Method are presented in Figs. 37 and 38 respectively. In each case, the flow charts are presented on one or more pages. The flow of operations is clearly indicated by a system of matching numbers. The numbering system also indicates where the common flow chart in Fig. 36 enters the program for each method of analysis.

In the common flow chart, the joint stiffness matrix and the coefficient matrix for the Modified Three Shear Equations are generated. These matrices are then inverted by a subroutine for matrix inversion called MATINV and the inverted matrices are stored for use throughout the main programs. The loading combinations which are possible are also indicated. A series of load indexes must be read into the computer to designate the branching system that is to be followed. These are also used to specify the number of nodal sections of each plate that are loaded. Load data is then read into the computer for only the loaded parts of the structure.

The operations in the flow charts for the Iteration Method and the Particular Load Method are closely related to the formulation presented in Chapter III; therefore, these flow charts will not be discussed in detail. The only point that may need clarification is related to the subroutine MODEFL. A common subroutine called MODEFL was formulated to perform the calculations for both the plate load bending moments and the plate deflections. As stated in the theory, these operations are completely analogous.

5. Size of the structure

A limited number of consecutive plates can be considered using the present computer programs. The main limitation is in the storage capacity of the computer. The problem of round-off error may be encountered in the matrix inversion computations if the matrices get too large. This problem can be partially solved by using double precision variables instead of single precision variables. However, this programming technique requires twice as much storage capacity. The programs written for this study were dimensioned to use nearly the full core storage capacity of the IBM 360 Model 50. On the basis of this limitation, structures in which $(nn \times nij) \leq 60$ can be analysed using the present computer programs. A few combinations that can be considered are listed below:

1. When the structure is symmetrical about an interior joint, the symmetrical part of the structure can consist of

(a) 4 plates, 4 interior joints and 15 nodal sections, or

(b) 8 plates, 8 interior joints and 7 nodal sections.

2. When the structure is not symmetrical about an interior joint, the full structure can consist of

(a) 7 plates, 6 interior joints and 10 nodal sections, or

(b) 9 plates, 8 interior joints and 7 nodal sections.

Other combinations within the range of (nn × nij) $\leq$ 60 are of course possible.

6. Computation time

The source programs for both the Iteration Method and the Particular Load Method are compiled on the IBM 360 Model 50 in approximately 1 minute.

The computation time required to perform an analysis by the Iteration Method depends on the convergence of the solution. This effect will be discussed further in the next chapter where the method was used to analyse a few non-prismatic folded plates. Since convergence problems may be encountered, it is impossible to estimate the computational time for a complete solution; however, it is possible to state a few examples of the time requirements to complete one cycle of iteration. In the case of a structure that contains 9 joints and 15 nodal sections, one cycle of iteration can be completed in approximately 1 minute if joint symmetry is used. For the same structure in which 7 nodal sections are considered instead of 15, an iteration cycle can be completed in 25 seconds.

It is much easier to estimate the time requirements of a complete solution by the Particular Load Method because in this method a solution is obtained in a complete form. In a structure which contains 9 joints and 15 nodal sections the analysis can be completed in 2 3/4 minutes if conditions of joint symmetry are used. The analysis of a structure which contains 7 joints and 7 nodal sections, where joint symmetry is used, can be completed in 40 seconds. In this case, it takes longer to compile the program than to analyse the problem.

These computation times are given mainly to illustrate the speed in which non-prismatic folded plates can be analysed with the proposed methods of analysis. It should be noted, however, that the stated time requirements only apply to the IBM 360 Model 50 which is presently one of the fastest machines on the commercial market.

B. Program for Beam Theory

In certain types of prismatic folded plates, Beam Theory can be used to predict the stress distribution in interior plate elements. A program was written in this investigation to apply Beam Theory to the elements of non-prismatic folded plates. This program was designed to calculate the longitudinal stresses at any number of nodal sections along a plate. These computations can be performed by hand, but even Beam Theory involves numerous calculations when applied to non-prismatic folded plates.

Each nodal section of a non-prismatic folded plate is different; therefore, the moment of inertia must be computed at each nodal section.

When the structure is analysed for distributed load, the bending moment calculations become quite tedious. In this case, the longitudinal distributions of dead load and live load must be computed separately and the resulting distributions are not necessarily linear over the length of the structure.

A computer program was written to carry out these repetitive calculations. This program was used to analyse some example non-prismatic folded plates so that the stresses predicted by Beam Theory could be compared to those predicted by the Particular Load Method of the proposed theory.

V. VERIFICATION OF THE PROPOSED THEORY

A literature review has shown that no analytical or experimental information has been published on the type of non-prismatic folded plates considered in this investigation. In order to establish a basis for the proposed theory, three comparative studies were conducted. The first two studies consisted of comparing the predicted results of the proposed theory with those obtained by applying Ordinary Folded Plate Theory in the analysis of a prismatic folded plate. In the first case, a similar loading condition was considered. This type of loading will seldom exist for non-prismatic folded plates; therefore, the second analysis was conducted for a case of non-similar loading. The final study consisted of comparing the predictions of the proposed theory with the measured results of an experimental study which was conducted on two non-prismatic folded plate models.

All the theoretical results which will be presented in this chapter were determined on the basis of the Particular Load Method. A discussion will also be included on the results that were obtained by applying the Iteration Method. In addition, a study will be presented to show how the accuracy of a solution is affected by the number of nodal sections that are considered in an analysis.

A. Similar Loading on Prismatic Folded Plates

One of the basic assumptions used in Ordinary Folded Plate Theory in the analysis of prismatic folded plates is that the longitudinal

distributions of the loads applied to the individual plates in a structure are similar in form. With this assumption, the functions which represent the distributions of load and moment are common to all plates and can be factored out in the analysis. Thus, the primary analysis by Ordinary Folded Plate Theory only needs to be carried out at one typical cross-section of the structure. A full distribution of dead load and live load over the entire surface of a prismatic folded plate produces a uniform distribution of joint loads on the plate structure. This is an example of a similar loading.

The joint displacements which result from a uniform distribution of plate loads in the primary analysis are distributed in the form of a fourth degree parabola. It is usually assumed, however, that the deflected shape of the structure varies in the form of a sine curve. It has been shown by Yitzhaki and Reiss (23), that the deflected shape of a beam structure is almost the same whether it is subjected to a uniform distribution of load, a concentrated load at midspan or a normal curve loading. Therefore, the correction analysis of a simply supported folded plate can be simplified by assuming a sine curve deflected shape. If this assumption is used, the secondary holding forces will also be distributed in the form of a sine curve. Consequently, the entire correction analysis can also be carried out at just one cross-section since the sine curve function will be common to all distributions of load, moment and deflection. The final distributions of stress, moment and deflections are then determined by superimposing the distributions

obtained in the primary analysis and the correction analysis for these respective quantities.

The prismatic folded plate shown in Fig. 39 which has been analysed on the basis of Ordinary Folded Plate Theory by Simpson (14) and Traum (17) was chosen as an example for comparing the theories. The condition of similar loading in this case consists of a uniform distribution of dead load over the surface of each plate. In this study, the problem was analysed on the basis of the Particular Load Method of the proposed theory using seven nodal sections.

The results of the analysis by both theories are given in Table 1 in terms of the longitudinal stresses and transverse moments at midspan. A comparison of these results shows that the predictions by both theories are practically identical. In addition to this comparison, the distributions of the longitudinal stresses and transverse moments along each joint of the structure are shown in Figs. 41 and 42 respectively. Both theories also predict almost identical distributions.

B. Non-Similar Loading on Prismatic Folded Plates

Ordinary Folded Plate Theory can also be applied to analyse prismatic folded plates with conditions of non-similar loading. In this case, the load on the structure must be partitioned into a number of similar loading cases and the structure is then analysed for each case separately. The final solution is obtained by superimposing the results of each similar loading analysis.

One of the main advantages of the proposed theory is that any non-similar loading condition can be considered in a single analysis of a structure. This has to be true if the theory is to apply in the analysis of non-prismatic folded plates. The same structure that was considered in the last section of this chapter was also analysed for a condition of non-similar loading. As shown in Fig. 40 the non-similar loading case consisted of a full distribution of dead load over the surface of the plates plus a partial distribution of live load. The structure was analysed by Ordinary Folded Plate Theory for the conditions of dead load and live load separately because each separate case constitutes a condition of similar loading. The solution for the dead load portion has already been presented in Table 1. An additional analysis on the basis of Ordinary Folded Plate Theory was conducted for the partial live load condition. These two solutions were then superimposed to obtain a complete solution by Ordinary Folded Plate Theory.

The structure was also analysed by the Particular Load Method of the proposed theory where the given non-similar loading was treated in a single analysis of the structure. This analysis was performed on the basis of 15 nodal sections.

The longitudinal stresses and transverse moments predicted by both theories for the midspan cross-section are given in Table 2. A comparison of these results shows that the predictions by both theories are almost identical. The distributions of stress and transverse moment along the length of each joint are also compared in Figs. 43 and

44 respectively. These two theories also predict almost identical distributions for this non-similar loading case. It should be noted that both theories will be slightly in error in predicting the distributions of the transverse moments at the quarter points of the span along joints 3 and 4 where a discontinuity in the load exists. An analysis based on two-way slab action would probably show a slightly smoother distribution in the regions of these discontinuities.

C. Experimental Study of Non-Prismatic Folded Plates

The proposed theory has been verified for the analysis of prismatic folded plates. In addition, it has been shown that conditions of non-similar loading can be considered in a single analysis of a structure. This condition is definitely a prerequisite if the theory is to be applied to analyse non-prismatic folded plates. In order to test the accuracy of the proposed theory in the analysis of non-prismatic folded plates, an experimental study was conducted on two alumninum model structures.

The longitudinal stresses, vertical deflections and transverse moments at various locations throughout the models were determined experimentally and these results were compared to those obtained by applying the proposed theory. Actually, the model study was initiated before the theory had been finalized. This step was taken in order to gain some insight into the behavior of non-prismatic folded plates. The results of this study will be presented after the details of the experimental study have been discussed.

1. Design and fabrication of the models

Two non-prismatic folded plate models were designed to have the geometry conditions shown in Fig. 45. Photographs of these model structures are shown in Figs. 47 and 48. These models were not designed to represent a scaled version of any particular prototype structure.

In the design of the models, all geometrical parameters were held constant except the amount of taper and the shape of the plate elements. Both models were cut from the same sheet of 1100-H14 aluminum which had a thickness of 0.063 in. The folds in the models were then made on a large sheet metal bending brake with the aid of a template to insure that the fold angles were accurate. The supporting end diaphragms were cut from the same type of material having a thickness of 0.190 in. These diaphragms were then attached to the folded surfaces of the models by small sheet metal screws as shown in Fig. 47. The plate elements of Model 1 were tapered from 8 in. at one end to zero at the other. Model 2 consisted of plate elements which were tapered from a depth of 6 in. to 2 in. Consequently, the midspan cross-sections of both models were the same. The plates in both models were sloped at 40° to the horizontal.

2. Test apparatus and instrumentation

An adequate support system for the test apparatus, was supplied by two large concrete blocks. These blocks were held in position at the top by a welded angle frame which also provided a base for the support

system of the models. A photograph of the test apparatus is shown in Fig. 46.

The models were tested on a simply supported span of 24 in. As shown in Fig. 47, relatively free rotation was provided at one end of the model by a 3/4 in. steel roller which was grooved to fit the end diaphragm and rested on the steel support frame. At the other end, free translation was provided by two small rollers placed between the steel support frame and a plate which was attached to the end diaphragm.

The loading apparatus for the models was provided by a number of small cans each filled with steel shot. As shown in Fig. 47, the load was transferred by a system of hangers to three continuous wooden loading blocks which applied a uniformly distributed line load along the parallel ridges of the models. To insure a more uniform distribution of load, the loading blocks were grooved to fit the top ridges of the models and the grooves were lined with a layer of foam rubber. This loading apparatus proved to be quite flexible because static load could be applied in a number of equal load increments. The test results in this study will be presented on the basis of one load increment which consists of a line load of 2.334 lbs./in. applied along the inner ridges of the models as shown in Fig. 49. This magnitude of line load is based on the horizontal projection of a ridge.

Deflection measurements were taken at seven locations along the joints with Ames dials which measured to 0.0005 in. per dial division. As shown in Fig. 48, these dials were attached to a deflection frame which

was welded to the steel support frame. A rigid base was provided for the deflection apparatus by the concrete supports. The Ames dials were pulled so that the dials loaded against the dial mechanisms at all times. A fine piece of steel wire provided the pulling mechanism. The deflection apparatus was arranged in this manner so that measurements on the order of 0.003 in. per load increment could be made accurrately with a minimum amount of error.

Both model structures were instrumented with rectangular rosette strain gages which were placed at selected locations on the plate surfaces shown in Figs. 50 and 51. In most cases, the individual gages in each rosette were orientated to measure strains parallel, perpendicular and at 45° to the ridges and valleys of the models. A different type of strain gage was used on each model. In the case of Model 1, Baldwin Type FAR-50-12-(45)-S13 foil rosettes were placed at matching locations on the top and bottom surfaces of the plates. The rectangular rosettes used on Model 2 were formed from three individual Baldwin Type AF-7-S6 paper backed strain gages which were arranged in a rectangular rosette pattern. These gages were only placed on the top surface of Model 2. Strain measurements were made with a Baldwin Type N SR-4 Strain Indicator.

A few problems were encountered in making the electrical connections to the foil rosettes used on Model 1. The original gages were not supplied with lead wires; therefore, a total of six small lead wires had to be attached directly to the small tab areas provided on each gage. The electrical connections were made with a highly conductive form of liquid

silver solder. In general, this method of attaching the lead wires proved to be quite successful; however, the procedure was very time consuming. A few faulty connections were found during the actual testing operation. These were later repaired with hot solder joints.

In order to avoid the problems which were encountered in making the electrical connections on Model 1, a different type of strain gage was used for Model 2. The strain gages used on Model 2 were single directional paper backed gages which were supplied with lead wires. No difficulty was encountered in the application or wiring of these gages.

The strain measurements from the first tests conducted on Model 1 indicated that the effects of transverse bending were quite small. It was decided that very little additional information could be obtained by applying strain gages to both surfaces of Model 2; therefore, strain gages were only placed on the top surface.

3. Testing procedures

It would have been most desirable to conduct the model tests in a room where temperature and humidity was controlled, but this facility was not available. Some difficulty was initially encountered in eliminating drift in the strain gage readings caused by the effects of temperature variation. The strain gages used on Model 1 were actually self-temperature compensating gages, however, a temperature compensating strain gage was also provided in the Wheatstone Bridge circuit. Providing

temperature compensation for the strain gages, does not completely eliminate the effect of temperature variations from the experimental results. In a highly indeterminate structure such as a folded plate, changes in temperature will introduce strains into the structure itself. These strains cannot be eliminated from the strain gage reading unless the effects of temperature variations are eliminated by some means.

During the initial phase of the testing program for Model 1, a number of complete tests were run. The model was loaded in four equal increments of load. After each load increment had been applied, deflection measurements were taken and strain gage readings were recorded for all the rosettes on the model. A complete test of this type was conducted in approximately two hours. During this time, it was found that temperature variations of as much as 5°F would occur. As a result, it was very difficult to reproduce the initial strain gage readings at the end of a test. In order to eliminate the effects of drift caused by temperature variation, the remaining tests were conducted in the late evening when the variation in temperature was less. In addition, the testing procedure was also changed to shorten the time required to complete a test to 10 or 15 minutes by running separate tests for only a few rosettes at a time. In each of these tests, strain and deflection measurements were taken after each load increment had been applied. This procedure proved to be quite tedious, but the effects of temperature variations were eliminated and the initial strain gage

readings could be reproduced by this method of testing. The test procedure used for Model 2 was quite similar; however, it was found that the strain gages on this model were much more stable.

4. Evaluation of the test data

Graphs were first plotted relating the measured strain increments to the load increments for each individual strain gage. In all cases, the data defined a linear variation between load and strain. The mean strain gage reading per load increment was obtained from each of these graphs. The strain gage data for Model 1 was then corrected to account for the transverse sensitivity of the gages. This procedure was not used for Model 2 because in this case, the rosettes were arranged from single direction gages and the information on the transverse sensitivity of these gages was not available.

The longitudinal stresses predicted by the proposed theory are calculated in a direction parallel to the neutral axis of the plates. In order to determine the measured stresses in this direction, the strain gage data measured from the rosettes was used to determine the measured strains directed parallel and perpendicular to the neutral axis. When the magnitudes and the directions of three strain measurements ε_1, ε_2 and ε_3 are known at a point, the normal strains, ε_η and ε_ξ and the shearing strain, $\gamma_{\eta\xi}$, in any other orientation can be determined from the following equations (11):

$$\varepsilon_1 = \frac{\varepsilon_\eta + \varepsilon_\xi}{2} + \frac{\varepsilon_\eta - \varepsilon_\xi}{2} \cos 2\Phi_1 + \frac{\gamma_{\eta\xi}}{2} \sin 2\Phi_1$$

$$\varepsilon_2 = \frac{\varepsilon_\eta + \varepsilon_\xi}{2} + \frac{\varepsilon_\eta - \varepsilon_\xi}{2} \cos 2\Phi_2 + \frac{\gamma_{\eta\xi}}{2} \sin 2\Phi_2 \qquad (47)$$

$$\varepsilon_3 = \frac{\varepsilon_\eta + \varepsilon_\xi}{2} \quad \frac{\varepsilon_\eta - \varepsilon_\xi}{2} \cos 2\Phi_3 + \frac{\gamma_{\eta\xi}}{2} \sin 2\Phi_3$$

The values of ε_1, ε_2 and ε_3 in the case of the experimental results correspond to the strain gage measurements parallel, perpendicular and at 45° to the ridges or valleys of the model, respectively. The angles Φ_1, Φ_2 and Φ_3 correspond to the above strains and can be taken as the orientation of these strains with respect to the neutral axis of a plate. By solving Eqs. 47, the normal strains, ε_η and ε_ξ, which are parallel and perpendicular to the neutral axis respectively can be determined. The magnitude of the stresses parallel and perpendicular to the neutral axis are then determined on the basis of Hooke's Law, given by the following equations:

$$\sigma_\eta = \frac{E}{1-\mu^2} (\varepsilon_\eta + \mu\varepsilon_\xi) \qquad (48)$$

$$\sigma_\xi = \frac{E}{1-\mu^2} (\varepsilon_\xi + \mu\varepsilon_\eta) \qquad (49)$$

where σ_η = the stress parallel to the neutral axis of a plate,

σ_ξ = the stress perpendicular to the neutral axis of a plate, and

μ = the value of Poisson's ratio for the material.

Two direct tension tests were conducted to determine the modulus of elasticity, E, of the material. The measured value was found to be 10.4×10^6 psi. The standard value of Poisson's ratio for aluminum, $\mu = 0.33$, was used in evaluating the test results.

In the case of Model 1, the experimental values of the longitudinal stresses were evaluated on the basis of the average of the strain measurements at the top and bottom surfaces of the plates. The longitudinal stresses in Model 2 were determined on the basis of the strains measured at the top surfaces of the plates only. The experimental stresses per load increment at all the strain gage locations in both models are presented in Table 3.

In general, the deflection measurements were quite small. The largest value of deflection recorded per load increment for Model 1 was in the order of 0.007 in. and the largest value for Model 2 was in the order of 0.004 in. Deflection measurements were recorded during six complete loading tests of Model 1 and eight loading tests of Model 2. Measurements were taken after each load increment had been applied in each test. The results of the average deflections per load increment are given in Table 4. The locations of the deflection dials in Model 1 and Model 2 are given in Figs. 50 and 51 respectively. These test results represent the average of a number of different sets of test data and in each case, the average for a number of load increments. The deflection measurements recorded for the first increment of load were

not included in the averages because this loading increment was used to seat the models.

5. Comparisons of the experimental and theoretical results

The model structures were analysed by the Particular Load Method of the proposed theory on the basis of 15 nodal sections. The output data from the computer gave the predicted values of the longitudinal stresses and transverse moments at all the nodes in the structure. These results were then used to determine the stresses and transverse moments at the strain gage locations shown in Figs. 50 and 51. The stresses at these interior plate locations were determined on the basis of a linear distribution of stress. A linear variation of transverse moments was also used to determine moments at interior locations of the plates. This variation was used because the models were not subjected to transverse plate loads.

A comparison of the theoretical and experimental longitudinal stresses for both Models is given in Table 3. The percentages of error that are noted are based on the deviation of the theoretical results from the experimental values.

The longitudinal stresses predicted by the theory for Model 1 are generally in good agreement with the experimental results. In most cases, the error is less than 14%. Some larger errors are indicated at gage locations 3, 10 and 15. It should be noted that at these locations the magnitudes of stress are quite small. Consequently, larger

percentages of error are indicated at these locations for approximately the same magnitudes of variation between the theoretical and experimental results that are observed at other gage locations. The only significant error is indicated at the location of gage 1 which is in the vicinity of a pointed plate element. In this region, the strain gradient is very large. As a result, the strains measured from the three gages in the rosette will not define the strains at a point (11). The experimental value of longitudinal stress was therefore calculated only on the basis of the measured strain in the direction of the neutral axis. It is very possible that this evaluation does not give a true indication of the stress at this location.

The theoretical stresses predicted in the region of pointed plate elements are definitely influenced by the point effect. On the basis of Eq. 27, it can be shown that this point effect introduces a singularity condition and the theoretical stresses approach infinity. In the actual model, however, the material would be stressed into the inelastic range in this localized region. This effect would then cause a redistribution of stresses to other parts of the structure in the vicinity of the point which would also have a sizeable influence on the stresses at the location of gage 1. Unfortunately, the effects of inelastic redistribution cannot be taken into account in a theory that is based on elastic behavior. Nevertheless, the theory tends to over-predict the stresses at this gage location.

A comparison of the measured and predicted values of the longitudinal stresses in Model 2 is also given in Table 3. In this case, the test results and theoretical predictions are also in good agreement with most variations falling well within 14%. A much larger error is indicated at the location of gage 6; however, the stress at this location is quite small so that this error is not really significant.

In general, the theory tends to over-predict the experimental stresses for Model 1. This trend should be expected because the theory does not account for some of the restraint conditions that actually exist in the models. For example, it is assumed that the end diaphragms offer no resistance to movement perpendicular to the plane of the diaphragms. However, in the models, the diaphragms actually offer a considerable resistance to movement in this direction. A study of the results for Model 2 indicates that the theoretical stresses are generally smaller than the experimental stresses. This observation is not surprising because the experimental stresses for this model were not evaluated on the basis of the average of the strains at the top and bottom surfaces of the plates. The measured strains at the top surface of Model 1 were also generally larger than the average strains at the same general locations where the theory is shown to under-predict the experimental stresses in Model 2.

Deflection measurements were taken at seven locations in each model structure. In Table 4, the predicted results of the theory are compared to the measured values of these deflections. As indicated by the results,

the deflections predicted by the theory are in good agreement with the measured values. A maximum deviation of 13% is indicated for the results of Model 1 while the predicted results for Model 2 are well within 10% of the measured values.

In regions near the pointed portions of the plate elements in Model 1, the transverse moments were larger than in other regions of the structure. The measured differences of strains at gage locations 1, 2, 12, 15 were evaluated to determine the transverse bending moments. The surface strains which are parallel and perpendicular to the neutral axis were determined from Eq. 47 by a separate evaluation of the strain gage data for the top and bottom rosettes. The stresses perpendicular to the neutral axis were then determined from Eq. 49 and the measured transverse moments were calculated on the basis of the flexure formula. This procedure was not used at the location of gage 1 because the measured rosette strains at this location do not give a good indication of the strains at a point.

The theoretical and experimental results for the transverse moments are given in Table 5. The difference between the measured and predicted values are slightly larger than those indicated in the other comparisons that have been made in this study. However, this comparison serves to show that the larger transverse moments predicted by the theory in the regions of the points do exist. The experimental results shown in Table 5 are actually under-estimated, because an accurate evaluation of the

surface strains should be made by taking into account the thickness of the strain gage and the adhesive (10). This experimental error can be quite important in evaluating the transverse moments because the plates are very thin. In order to make this correction a number of special tests would be required to determine the average thickness of the gages and the adhesive. This did not seem to be warranted in view of the small amount of test data that is compared.

D. Rate of Convergence of the Iteration Method

In any iterative procedure, it is very important that the solution converges. The model structures used in the experimental study were also analysed by means of the computer program developed for the Iteration Method to determine whether convergence would be a problem. When the Iteration Method was applied in an analysis of Model 1 using 15 nodal sections, the solution began to oscillate and the analysis was terminated after 10 cycles of iteration. This problem was not encountered when the Iteration Method of analysis was applied to Model 2. In this case, the solution converged after only one cycle of iteration. These results definitely indicate that the degree of taper of the plates influences the rate of convergence of the Iteration Method.

A study was conducted to further determine when the Iteration Method can be applied to the analysis of non-prismatic folded plates. This study consisted of analysing theoretical structures of the same cross-sectional shape as the model structures shown in Fig. 45 except that different plate

tapers were considered. It was found that as long as the plates did not taper to a point, as in Model 1, solutions by the Iteration Method would converge. For example, a solution was obtained in three cycles of iteration when the plates tapered from 7 1/2 in. at one end to 1/2 in. at the other. The pointed effect of the plate elements in Model 1 introduces a singularity condition which will cause problems in most any method of analysis.

Unfortunately, the degree of taper of the plates is not the only factor which affects the rate of convergence of the Iteration Method. Whenever the effects of relative joint displacements are large, the correction analysis portion of the overall theory will cause large changes in the results of the primary analysis. When these corrections become large, a solution by Iteration Method may tend to oscillate or even diverge. Other factors such as the slope of the plate elements and the geometrical form of the cross-section also influence the magnitudes of the relative joint displacements. It is probably reasonable to assume that if an iteration solution does not converge for a prismatic folded plate of a certain cross-sectional shape, then the solution will not converge if the elements of the structure are tapered. In order to eliminate the uncertainties involved in applying the Iteration Method, all the analytical solutions presented in this dissertation were obtained on the basis of the Particular Load Method.

E. Solution Accuracy as Affected by the Number of Nodal Sections

The number of nodal sections that should be used in the analysis of a non-prismatic folded plate depends mainly on the particular geometry of the structure. In certain cases, the choice may also be governed by loading conditions. It is difficult to state any hard and fast rules concerning a particular choice of this variable. Some of the factors that should be considered in making this choice will be discussed in this section.

One of the main variables to consider is the degree of taper of the plate elements. In the proposed theory, the deflected shape of a structure is determined by a numerical integration of the curvature distribution. It is assumed that the curvature distribution is defined between nodes by a second degree parabola. In the region where tapered plate elements are narrow, the intensity of curvature may become quite large and the distribution may tend to be concentrated in this region. As a result, a larger number of nodal sections are required to accurately define the exact distribution. This factor is quite important because the entire correction analysis is dependent upon the accuracy of the deflected shape of the structure. As the taper of the plate elements becomes smaller and the shape of the plates approaches the prismatic case, the curvature is more uniformly distributed over the length of the plates. In these cases, an accurate approximation of the curvature distribution can be made with fewer nodal sections.

Other parts of the analysis are also influenced by the number of nodal sections. The matrix solution for removing the effects of the secondary holding forces is dependent on the number of concentrated holding forces and the assumption used to determine each force. Both of these factors depend upon the number of nodes. In regions where tapered plates are quite narrow, more nodal sections are required to account for the effects of larger concentrated holding forces. The matrix solution of the Modified Three Shear Equations is also dependent on both the number of nodes and the taper of the plates.

Loading distributions may govern the choice of the number of nodal sections. A sufficient number of sections must be considered to adequately define the longitudinal distributions of the applied loads as well as the joint loads which result from the applied loads.

Since the degree of taper of the plate elements is, in most cases, the main factor to consider when choosing the number of nodal sections, a study was conducted on the structure shown in Fig. 52 to investigate the effects of the number of nodal sections for one of the worst cases of taper. In this structure, the plate elements are tapered to a point and the degree of taper is quite large. The structure was analysed for the loading condition given in Fig. 52 on the basis of 7 and 15 nodal sections. The distributions of longitudinal stresses and transverse moments along the joints which resulted from these two solutions are shown in Figs. 53 and 54 respectively. The joint numbers designated on the graphs correspond to the numbering system of the joints shown on the structure in Fig. 52.

As shown in Fig. 53, the longitudinal stresses for both 7 and 15 nodal sections are generally much the same in the middle of the structure. Near the supports where the tapered plate elements are very narrow, the two solutions begin to differ. This deviation is slightly larger in the case of the transverse moments shown in Fig. 54, especially along joints 3 and 4. The main difference exists in the fact that the solution based on 7 nodal sections does not pick up the large changes in stress and moment in the immediate vicinity of the supports. These changes are mainly a result of the pointed effect of the plate elements which will be discussed further in the next chapter.

When prismatic folded plates are analysed by the proposed theory, an accurate solution can be obtained with fewer nodal sections. The prismatic structure shown in Fig. 39 was analysed on the basis of 7 nodal sections and accurate results were obtained as shown in Table 1 and Figs. 41 and 42.

VI. A STUDY OF FACTORS INFLUENCING THE STRUCTURAL BEHAVIOR OF NON-PRISMATIC FOLDED PLATES

The structural behavior of a folded plate is definitely influenced by the geometry of the structure. In this study, a number of structures are analysed to determine the influence of some of the main geometrical parameters. These parameters include the taper and slope of the plate elements as well as the geometrical shape of the cross-section. In addition, both free and simply supported edge boundary conditions are considered.

This study also investigates the possibility of using simplified theories to predict the behavior of non-prismatic folded plates. In certain types of prismatic structures, the analysis can be terminated at the end of the primary solution. It is also possible to use Beam Theory to predict the stress distributions for the interior plate elements of some prismatic structures. In the course of this presentation, a comparison will be made to determine if either of these approximations can be applied to non-prismatic folded plates.

A. Variations in the Plate Geometry

The structural shape shown in Fig. 55a is used in the study of the effects of taper and slope. The effects of other variables are eliminated by holding them constant, as indicated in Fig. 55a. In order to compare the behavior of non-prismatic folded plates to that of prismatic folded plates, the depths of all the plate elements at midspan are also held

constant. It is also assumed that all the plate elements in a structure have the same shape.

With the midspan depths, dm_i, and the span length, L, held constant, the taper of the plate elements can be defined by a parameter

$$\Omega_i = \frac{|dr_i - d\ell_i|}{L}$$

where $d\ell_i$ and dr_i are the plate depths at the left and at the right ends respectively, as shown in Fig. 55a. Notice that when the value of Ω_i is varied, different shapes of plates are obtained. In this study, the effects of taper and shape will be generally referred to as the effects of taper, expressed in terms of the single parameter Ω_i.

The basic objective of this study is to show how the structural behavior of a folded plate is influenced by changes in the plate geometry. It is not proposed that some of the results of this study should be used for design purposes without making modifications to the structure. In certain cases, the magnitudes of stresses and moments are quite large and it will be difficult to reinforce the structure if the thickness of the plates is not increased. In this study, the thickness is held constant in all cases so that the effects of other geometrical parameters can be studied. All the results presented in this section are based on solutions by the Particular Load Method using 15 nodal sections.

1. Taper and shape of the plates

In order to study the effects of taper, the slope, θ_i, is held constant at 30° to the horizontal. A list of the tapers that will be considered is given in Fig. 55b. The extreme cases of taper are defined by $\Omega_i = 0.30$ and $\Omega_i = 0$, which represent the cases of triangular and prismatic plate elements respectively. In all the other cases, the plates are trapezoidal in shape.

The stress distributions along the individual joints of the structure are shown in Fig. 56. In these graphs, the distributions have been plotted with respect to the joint notation and co-ordinate system shown in Fig. 55a. It should be noted that the stresses that are output from the computer analysis are directed parallel to the neutral axis of the plates and not parallel to the joints. The magnitudes of stress in these two directions should be very close; therefore, in this study the stresses parallel to the neutral axis are plotted to indicate the stresses along the joints. The stress distributions are influenced by both the taper of the plates and boundary conditions of the structure. As a result, the distributions along interior and exterior joints may be quite different. The shape of the stress distribution also depends upon the relative depths of the plates adjacent to a joint. Along the ridges, joints 3 and 5, the adjacent plates are always equal in depth. Near the supports where both plates are narrow, the stresses are larger. When the plates are tapered to a point, $\Omega_i = 0.30$, the stress tends to approach infinity. Near the wider ends of the plates the distributions are quite

similar for all cases of taper. This situation is also shown along joint 1; however, the shape of the distribution in this case is influenced by the free edge boundary condition.

A different trend is indicated along the valleys, joints 2 and 4. Along these joints, the shape of the stress distribution is quite similar for all cases of taper. This trend is introduced because at any position along these joints the high stress condition associated with the narrow end of one plate is dampened by the effect of a wider plate adjacent to it. An examination of the stresses near midspan along all joints shows that the magnitude of stress at this location is not affected a great deal by the amount of taper. In this region, the cross-section is the same for all cases and the stresses are quite close to those predicted for the prismatic structure.

In the regions where the points of triangular plate elements are located at the supports, singularity conditions are introduced by these pointed effects and the stresses in these regions approach infinity. Although the theory does not predict the stresses right at the points this trend is indicated in Fig. 56 by the stress predictions for the case of $\Omega_i = 0.30$. It is also evident by considering the case of taper where $\Omega_i = 0.25$ that a small increase in the plate area near the supports will decrease the stresses an appreciable amount. This effect tends to indicate that it would be much better to design the structure with an overhang, as shown in Fig. 1, so that the points are shifted to a region of lower stress and the singularity conditions are eliminated.

These singularity conditions also cause the stresses to change in sign over the depths of some of the plates, as shown in the case of Ω_i = 0.30. The stress near the narrow end of plate 3 is in tension at joint 3, and in compression at joint 4. A similar trend is indicated at the narrow end of plate 4. At the wide ends of certain plates, the stresses are also reversed in sign over the depths. This effect is shown in plate 4 where the stress at joint 5 is in tension, but at joint 4 the plate is in compression. It is difficult to interpret the physical significance of these predictions. It is also difficult to know what to expect in the vicinity of a singularity point. It should be noted that the curves are shown to be smooth and continuous. If the stresses at the singularity point along joint 5 must approach infinity, it seems natural for the stress distribution along this joint to follow its continuous trend and enter the region of tension. These predictions may also indicate that the theory is in error for predicting the stresses in the narrow region of pointed plate elements. Nevertheless, these predictions should be taken into account in designing structures until they are either disqualified or verified by some other theory.

The distributions of transverse moments are also influenced by the amount of taper. The behavior is mainly affected by the relative combinations of the plate depths at each transverse cross-section. In the case of non-prismatic elements the depth of each plate is different at every transverse nodal section. Consequently, the distribution of the plate stiffnesses is also different at each nodal section. This effect

is quite important in the overall behavior of non-prismatic folded plates because at any cross-section, the narrow plates are much stiffer than the wider plates; therefore, they attract larger transverse moments.

The distributions of transverse moments, plotted along the length of each joint, are shown in Fig. 57. Near the narrow ends of the plates along joints 3 and 5, the moments are very large. The sign of the transverse moment along these joints is reversed in the regions where both plates are wide. This effect results because the stiffer part of the transverse cross-section is always in the region of the narrower plates. The moment does not change sign along joint 4 because there is always a wide plate on one side of the joint. Along joint 2, the moment is determinate at all sections. Except for the case of $\Omega_i = 0.30$, the magnitudes of the transverse moments at midspan are quite similar to those predicted for the prismatic case.

In general, the distributions of the transverse moments follow the same basic trend along each joint, increasing in magnitude as the taper increases. This trend is not shown at joint 3 for the case of $\Omega_i = 0.30$. In this case, the maximum positive moment is not as large as that shown for the case where $\Omega_i = 0.25$. There is also a sharp decrease in moment near the support along both joints 3 and 5. These trends are similar to those indicated by the stress distributions in the immediate vicinity of a singularity point. The theory is invalid in this case, because it is based on one-way slab action and two-way action does exist near the

supports. The effects of two-way slab action should tend to reduce the magnitudes of the transverse moments in these regions.

The distribution of the shearing forces, $T_{no,j}$, are shown in Fig. 58. In a prismatic folded plate, the shear force distribution has the same shape as the longitudinal distribution of plate load bending moments if the applied loading is similar. When the structure is subjected to a uniform load, this shape is parabolic as shown along the joints for the case where $\Omega_i = 0$. The distributions along the joints of non-prismatic folded plates are completely different as indicated by the graphs. The trends that are shown for the case of $\Omega_i = 0.30$ are similar to those observed for both the stresses and transverse moments associated with this case.

The behavior of a non-prismatic folded plate is influenced a great deal by the effects of relative joint displacements and by the fact that the cross-section of the structure becomes distorted in certain regions. These effects can be studied by comparing the results of the primary analysis, which does not account for relative joint displacements, to the results of the final analysis. The stress distributions for two cases of taper, $\Omega_i = 0.25$ and $\Omega_i = 0.15$, are shown in Fig. 59 along an exterior valley, joint 2 and an interior ridge, joint 5. The largest variation between the primary and final stresses is shown for the case of the larger taper. It is also evident that the stresses predicted by the primary analysis are much closer to the final stresses along a valley as

compared to a ridge. This behavior results because there is always a wide part of one plate adjacent to a narrow part of another along the valleys while both plates are narrow in the region of one support adjacent to a ridge. These plates are very flexible to bending in their own plane at the narrow ends. As a result, large relative displacements occur in these regions along the ridges and the cross-section becomes quite distorted. This effect is greater in the case of larger tapers which in turn causes larger variations between the primary and final stresses.

The basic assumption involved in applying Beam Theory to predict the stress distribution in folded plates is that the cross-section of the structure retains its original shape. This assumption is usually quite valid when the effects of relative joint displacements are small. The stress distributions predicted by Beam Theory are shown in Fig. 59 for the case of the interior ridge, joint 5. It is evident that as the taper of the plates approach the prismatic case, the predictions of Beam Theory are closer to the results of the final analysis. In the case of larger tapers such as $\Omega_i = 0.25$, Beam Theory tends to be completely inaccurate because the cross-section becomes quite distorted in the narrow regions of the plates.

The influence of relative joint displacements is even greater on the transverse moments. A comparison of the transverse moments predicted by the primary and final analysis along joints 4 and 5 is shown in Fig. 60. Similar trends in the behavior are observed for the transverse

moments as were observed for the longitudinal stresses. The main difference, however, is that the corrections that are applied to the primary transverse moments to account for the effects of relative joint displacements are much larger. This behavior results because in the region where the plates are narrow and quite stiff in the transverse direction, large end moments are introduced even if the magnitudes of the relative displacements are quite small.

It is quite conclusive from this study that the primary transverse moments give a very poor indication of the final moments in non-prismatic folded plates. Consequently, primary transverse moments should not be used as a design approximation for non-prismatic folded plates, particularly if the structure has a developable surface.

In prismatic folded plates the correction analysis part of the solution also introduce larger corrections to the transverse moment than to the longitudinal stresses. The results of Simpson's problem presented in Table 1 can be used to make this comparison. One of the main differences between the behavior of prismatic and non-prismatic folded plates is related to the location in the structure where the effects of relative joint displacements are the largest. The displacements in a prismatic structure are usually largest at midspan. In a non-prismatic structure which has the same midspan cross-section, the magnitudes of the relative joint displacements at this location are approximately the same. However, relative joint displacements are also quite large near the narrow ends of the tapered plates and even small displacements in these regions will introduce large correction moments.

2. Slope of the plates

In some respects, the effect of changing the slope of the plates is similar to the effect of changing the taper. Both of these factors influence the magnitude of the relative joint displacements. The structure shown in Fig. 55 is also used for the purpose of this discussion where the taper is held constant at $\Omega_i = 0.25$. The plate slopes, θ_i, that are considered are listed in Fig. 55c.

The results of the primary analysis and the final analysis for the stresses and transverse moments are shown in Fig. 61 and 62 respectively. In each case, the distributions are plotted for a valley, joint 4, and a ridge, joint 5. The largest difference between the primary and final results occur when the slope is shallow, $\theta_i = 30°$, as compared to the steeper slope where $\theta_i = 45°$. As the slope of the plates is decreased, the deflection angles between the plates also decrease and the structure becomes flatter. As a result, the structure is more flexible and larger relative joint displacements occur along the entire length of the joints. This effect is shown by comparing the results of the primary and final analysis for both the stresses and the transverse moments. This comparison also shows that the corrections are larger along the ridges, especially in the region where both plates are narrow.

The final distributions of longitudinal stress for all the variations in the slope are shown in Fig. 63. In general, the magnitude of the stresses at all regions along the joints are affected by

varying the slope. There is definitely an elementary explanation for this effect on the basis of beam theory. As the slope of the plates is decreased, the effective section modulus of the structure also decreases. The section modulus is basically a function of the square of the height; therefore, it should be expected that the magnitudes of the stress should get increasingly larger for each decrease in the slope. This trend is clearly indicated by the distributions of stress along joints in Fig. 63.

There is also another basic reason for these increases in stress. The area of the horizontal projection of the structure increases as the structure becomes shallower. As a result, the structure must carry more live load and the stresses would tend to increase due to this effect. The effect of relative joint displacements does tend to alter these trends.

A comparison of the variations in the transverse moments resulting from changing the slope of the plates is shown in Fig. 64. The magnitudes of these moments are shown to increase as the slope decreases. This effect is once again related to the fact that both the load and the magnitude of the relative joint displacements increase as the structure becomes shallower.

B. Geometrical Form of the Cross-Section

Each structure considered in the previous parts of this study consisted of plates of identical shapes folded to form ridges and valleys

alternatively in a regular pattern. Aside from the effects of taper and slope, the behavior of a folded plate is also affected by the geometrical arrangement of the plates in the cross-section. In this section, the analysis of two other geometrical forms will be presented to illustrate some other behavior characteristics of folded plates and also to show that other types of non-prismatic folded plates can be analysed by the proposed theory. These structures were analysed on the basis of the Particular Load Method using 10 nodal sections.

The geometry and loading conditions for the first structure considered in connection with the study of cross-sectional form are given in Fig. 65. This structure consists of a combination of rectangular and trapezoidal elements. One practical advantage of this particular cross-section is that the lower horizontal plates provide a region for placing longitudinal tension reinforcement and the top horizontal plate supplies a considerable area for resisting compression forces.

The structural behavior in this case is affected by the arrangement of the plates which gives the result of small deflection angles between the plates, $\gamma_{i,i+1} = 35°$. As shown in Figs. 67 and 68, there are large differences between the primary and final results for both the stresses and transverse moments. In addition, these corrections are shown to be large along the entire length of the joints. This condition results because large relative displacements are introduced all along the joints by the effect of relatively small plate deflection angles. It should also

be noted that the magnitudes of the stresses are generally decreased by the effect of relative joint displacements, but the transverse moments are increased. In particular, the stresses along joint 3 should be noted. In this case, the stresses predicted by the primary analysis are in compression, but the final analysis shows that the state of stress is completely reversed to tension along the joint. There is only a slight evidence of the effects of taper, shown by the skew in the shape of some stress distributions. The taper effect is still quite evident in the distribution of the determinate transverse moments along joint 2.

As shown in Fig. 67, the predictions of Beam Theory are fairly close along joint 4, but there is a larger deviation along joint 3. The stresses predicted by Beam Theory will depend upon the cross-section that is considered in the analysis. The results presented in Fig. 67 are based on the portion of the cross-section designated in Fig. 65. Beam Theory is shown to yield slightly better predictions in this case because the effects of relative displacements are more uniformly distributed over the length of the structure and the localized displacements introduced by the effects of taper are small.

Another geometrical form to be considered is shown in Fig. 66. The arrangement of the plates in this structure is obtained by alternating the plate elements in groups of three. Although it is not apparent from the sketch in Fig. 66, the middle module of three plates can be repeated many times to form an attractive structure. The geometrical properties and loading conditions for this case are also given in Fig. 66.

The basic trends in the behavior of this structure are similar to those observed for the structure shown in Fig. 65. This structure also contains some cases where the deflection angles between the plates are quite small, in this case 45°. As a result, the effects of relative joint displacements are large over the entire length of the structure as shown by comparing the primary and final stress distributions in Fig. 69. The stresses in all regions of this structure are low, even near the outer edge. The effect of taper which is more evident in the primary analysis along joint 1 is dampened out in the final results. It is interesting to note that the stresses near the narrow end of plate 1 along joint 1 are in tension while beam theory would indicate compressive stresses in this region. In this case, the indications of beam theory are definitely wrong because the plate load which is introduced into plate 1 by resolving a downward vertical joint load at joint 2 tends to bend the outer plate such that tension will exist along the outer joint. An illustration of this force resolution is shown on the cross-section in Fig. 66. A similar trend is frequently indicated when small edge beams are projected upward along the outer edges of prismatic folded plates. In this case, the outer edge of the edge beam is usually in compression while beam theory would tend to indicate that this edge should be in tension.

The predictions of Beam Theory for an interior portion of the structure shown in Fig. 66 are given in Fig. 69. The results along the

valley, joint 3, seem to be quite close, but the predictions along the ridge, joint 4, are much more inaccurate.

The magnitudes of the transverse moments shown in Fig. 70 are small along all joints except in joint 3. In this case, the effects of relative joint displacements introduce large correction moments. Although the moments along joint 3 are larger than those along the other joints, the maximum moment is still much smaller than those that were observed in some of the other structures studied in this chapter.

G. Edge Boundary Conditions

The structural behavior of a folded plate is definitely influenced by the boundary conditions along the outer longitudinal edges of the structure. In all the previous studies in this chapter, a free edge boundary condition has been considered. A study was conducted to determine if some of the highly stressed regions in these non-prismatic folded plates can be relieved by providing a simple support along the outer longitudinal edges. The same structural shape used in the study of the effects of taper and slope, shown in Fig. 55, is used in this investigation. The particular case where $\Omega_i = 0.25$ and $\theta_i = 30°$ is considered. The general behavior of this structure is studied by comparing the effects of a simple support condition to the effects of a free edge condition.

A simply supported edge condition can be provided by constructing bearing walls along the outer longitudinal edges of the structure. It is assumed in this study that support displacements are prevented in the

vertical direction, but the structure is free to translate in the horizontal plane perpendicular to the outer edge. It is also assumed that the structure is free to deform along the length of the outer edge such that shear stresses do not develop at this edge.

The stress distributions along the exterior edge, joint 1 and the interior ridge, joint 5, are shown in Fig. 71 for the cases of the simply supported edge and the free edge condition. The stress predictions for both the primary analysis and the final analysis are included. It is evident by comparing the final results at the exterior edge and at the interior ridge, that the effects of providing a simple support along the outer edge are quite localized. In the case of the outer edge, joint 1, there is a large difference between the stress distributions. The large stresses associated with the free edge condition are lowered a great deal by providing a simple support along this edge. A comparison along the interior ridge, joint 5, shows that the boundary conditions do not affect the stresses in the interior of the structure because the magnitudes and distributions of stress are practically the same for both cases. This condition should be expected because boundary conditions usually cause only localized effects in any boundary value problem. These localized effects are quite important in this case to relieve the high stresses along the outer plate and to provide edge stability for the structure.

The effects of providing a simple support along the outer edge have a similar influence on the transverse moments as shown in Fig. 72. In the case of a free edge, the moments along joint 2 are large because of

the large cantilever effect. These moments are reduced in magnitude by providing vertical restraint along the outer edge. The general distribution of the transverse moments along the outer edge is also changed a considerable amount. The moments along the interior ridge, joint 5, are practically the same for both boundary conditions. This result is unfortunate, since the magnitudes of the transverse moment in interior parts of the structure are not reduced by providing a simple support along the outer edges of the structure.

VII. SUMMARY

A theory is developed in this study to analyse long simply supported non-prismatic folded plates. In many respects, the theory is similar to Ordinary Folded Plate Theory used in the analysis of prismatic folded plates. The basic concepts of Ordinary Folded Plate Theory are generalized in this study to account for the conditions of non-similar loading and the effects of non-prismatic plate elements.

Because of the non-prismatic nature of the structures, a method of nodal analysis is used. A structure is analysed at a finite number of nodal sections in the transverse direction on the basis of a one-way slab analysis. In the longitudinal direction, the plate elements are assumed to act as beams. Stresses are matched at a number of nodal sections along each interior joint by applying a Modified Three Shear Equation which is derived to account for the effects of tapered plate elements.

A complete analysis of a structure consists of a primary analysis in which the effects of relative joint displacements are neglected and a correction analysis which takes these effects into account. In the correction analysis, the deflected shape of the structure is based on a numerical integration of the curvature distribution.

The theory is formulated by two methods of analysis, namely, the Iteration Method and the Particular Load Method. Computer programs were written for both of these methods since the only practical means of analysing non-prismatic folded plates by these methods is with the aid

of a digital computer. When the Iteration Method is applied to analyse structures in which the effects of relative joint displacements are large or whenever the plate elements taper to a point at the supports, the solution may tend to oscillate around the true solution or it may even diverge. This problem is not encountered in applying the Particular Load Method since a complete solution is obtained by this method.

As a special case, the theory can be used in the analysis of prismatic folded plates. One particular advantage of this method is that conditions of non-similar loading can be considered in a single analysis of a structure.

The theory is used to analyse prismatic folded plates subjected to conditions of similar and non-similar loading. It is shown that the results of the proposed theory are practically identical to those obtained by applying Ordinary Folded Plate Theory. The predicted results of the theory also correlate very well with the experimental results of a model study conducted on two non-prismatic folded plates. In most cases, the theoretical results are within 14% of the experimental data.

In the behavior study conducted on a number of non-prismatic folded plates, many interesting trends were noticed. The observations made in this study are summarized below:

1. In the narrow regions of tapered plate elements, large transverse moments are developed mainly as a result of relative joint displacements. These moments are larger in regions where the narrow ends of two tapered plates are adjacent to a common joint.

The moments are usually smaller along a joint where the narrow end of one plate is adjacent to the wide end of another plate.

2. The effects of relative joint displacements are larger in flatter structures or in structures where the deflection angles between the plates are small. In these structures the effects of relative joint displacements introduce large corrections to the stresses and transverse moments predicted by the primary analysis.
3. The effects of relative joint displacements are usually largest near the midspan of prismatic folded plates. In non-prismatic folded plates, the effects of relative joint displacements near midspan may be quite small compared to those in the narrow regions of tapered plate elements.
4. The boundary condition of a simple support along the outer longitudinal edge of a structure helps to reduce the large stresses and transverse moments that are associated with a free edge boundary condition. However, this effect is localized to regions near the boundary.
5. The stresses and transverse moments predicted by the primary analysis are usually a poor indication of the final magnitudes and distributions of stresses and moments in non-prismatic folded plates. The predictions of the primary analysis are more inaccurate in cases where the plate elements have larger tapers. Consequently, the primary analysis is usually not

adequate for even the preliminary design of a non-prismatic folded plate, especially if the structure has a developable surface.

6. In regions near the narrow ends of tapered plate elements, the original cross-section of the structure becomes distorted and the stresses predicted by Beam Theory for interior plate elements are usually very inaccurate. The predictions of Beam Theory are more accurate if the plate elements are more prismatic in shape.
7. It is definitely not advisable to design a non-prismatic folded plate in which the pointed ends of triangular plate elements are located at the supports of the structure. The pointed effect of a plate element introduces a singularity condition and theoretically, the stresses near the point approach infinity. This condition can be relieved by providing a slight over-hang so that the points are shifted to regions of lower stress and the singularity conditions are eliminated.

The computer programs written for this investigation can be modified so that structures with more general geometrical conditions can be analysed. With the addition of a subroutine in which the longitudinal plates of the structure can be analysed as continuous beams, non-prismatic folded plates that are continuous over intermediate support diaphragms could also be considered. The method of nodal analysis offers another advantage that was not taken into account in the present

computer programs. By modifying the programs so that the geometrical properties of each plate at each nodal section are read into the computer, non-prismatic plate elements which vary in thickness along the longitudinal span of the plates could be considered. In addition, the Modified Three Shear Equation could be extended to account for variations in thickness over the depths of the plates. The present computer programs were not written to take advantage of temporary data transfer to magnetic tapes. By using this technique, it may be possible to consider structures which consist of a larger number of plate elements.

Although the theory presented in this study is quite general, it can only be applied in the analysis of long non-prismatic folded plates where the degree of plate taper is not too large. In order to analyse structures with shorter spans and larger plate tapers, a theory must be developed which is based on elastic plate theory and the elasticity solution of the plane stress problem.

VIII. LITERATURE CITED

1. American Society of Civil Engineers. Task Committee on Folded Plate Construction. Phase I report on folded plate construction. American Society of Civil Engineers Proceedings 89, No. ST1: 117-140. 1963.

2. Beaufaut, F. W. Analysis of continuous folded plate surface. American Society of Civil Engineers Proceedings 91, No. ST6: 117-140. 1965.

3. Beaufaut, F. W. and Gray, G. A. Experimental analysis of continuous folded plates. American Society of Civil Engineers Proceedings 92, No. ST1: 11-19. 1966.

4. Benito, C. Scale model tests on shell roofs. In Proceedings of the Second Symposium on Concrete Shell Construction, Oslo, July 1957. pp. 279-283. Oslo, Norway, Teknish Ukeblad. 1958.

5. Born, J. Beitrage zur berechnung pyramidisher faltwerke nach der technischen elastizitatstheorie. In Proceedings of the Colloquium on Simplified Calculation Methods of Shell Structures, Brussells, Sept. 1961. pp. 86-154. Amsterdam, Holland, North-Holland Publishing Company. 1962.

6. Born, J. Hipped-plate structures. London, England, Crosby Lockwood and Sons, Ltd. 1962.

7. Del Pozo, F., Torroja, J. A. and Lopez Palanco, R. Tribune for the dog racing stadium of Madrid: [in Proceedings World Conference on Shell Structures, San Francisco, Oct. 1962]. National Academy of Science Publication 1187: 379-382. 1964.

8. Faerber, N. A. You can raise the roof with concrete. American Concrete Institute Proceedings 59: 1047-1055. 1962.

9. Gere, J. M. and Weaver, W. Analysis of framed structures. Princeton, N.J., D. Van Nostrand Company, Inc. 1965.

10. Graham, F. M. The behavior of a folded plate roof system. Unpublished Ph.D. thesis. Ames, Iowa, Library, Iowa State University of Science and Technology. 1966.

11. Perry, C. C. and Lissner, H. R. The strain gage primer. 2nd ed. New York, N.Y., McGraw-Hill Book Co., Inc. 1962.

12. Powell, G. H. Comparison of simplified theories for folded plates. American Society of Civil Engineers Proceedings 91, ST6: 1-31. 1965.

13. Scordelis, A. C. and Gerasimenko, P. V. Strength of reinforced concrete folded plate models. American Society of Civil Engineers Proceedings 92, ST1: 351-365. 1966.

14. Simpson, H. Design of folded plate roofs. American Society of Civil Engineers Proceedings 84, Paper 1508: 1-21. 1958.

15. Timoshenko, S. Applied elasticity. East Pittsburg, Pa., Westinghouse Technical Night School Press. 1925.

16. Timoshenko, S. and Goodier, J. N. Theory of elasticity. 2nd ed. New York, N.Y., McGraw-Hill Book Co., Inc. 1951.

17. Traum, E. The design of folded plates. American Society of Civil Engineers Proceedings 85, ST8: 103-123. 1959.

18. Welch, L. Folded plate dome ideal for auditorium. American Concrete Institute Proceedings 30: 441-446. 1958.

19. Whitney, C. S. Cantilever folded plate. American Concrete Institute Proceedings 30: 417-430. 1958.

20. Whitney, C. S., Anderson, B. G. and Birnbaum, H. Reinforced concrete folded plate construction. American Society of Civil Engineers Proceedings 85, ST8: 15-43. 1959.

21. Yamahara, S. Analysis of non-prismatic folded plate structures. Unpublished graduate research report. Berkeley, Calif., Department of Civil Engineering, University of California. 1962.

22. Yitzhaki, D. Prismatic and cylindrical shell roofs. Haifa, Israel, Haifa Science Publishers. 1958.

23. Yitzhaki, D. and Reiss, M. Analysis of folded plates. American Society of Civil Engineers Proceedings 88, ST5: 107-141. 1962.

IX. ACKNOWLEDGMENTS

The writer is most grateful to his Major Professor, Dr. C. E. Ekberg, Jr., Head of the Department of Civil Engineering for his guidance and encouragement during the course of the writer's doctoral study program.

The writer wishes to express his sincere appreciation to his Technical Advisor, Dr. Ti-ta Lee, Assistant Professor of Civil Engineering for his advice, guidance and encouragement during the course of this investigation.

The author is also grateful to Dr. H. A. Elleby, Assistant Professor of Civil Engineering for his helpful suggestions during the computer programming phase of this study.

A note of thanks is due to Al Miller, programmer at the Iowa State University Computational Center for his suggestions.

The experimental phase of this study was financed by a grant from the President's Permanent Objective Committee Alumni Achievement Fund at Iowa State University. The generous support of the Iowa State University Computational Center is also gratefully acknowledged.

X. APPENDIX A: NOTATION

The following subscript and superscript notation is used in this investigation:

no = node or nodal section.

i = plate or member.

j,k = joint.

ij = interior joint.

nn = number of nodes or last node.

m = number of plates or members.

nj = number of joints.

nij = number of interior joints.

nr = number of restraints.

n = number of degrees of freedom.

p = the primary analysis.

s = the secondary analysis.

c = the correction analysis, not including the secondary transverse moments.

r = a particular loading system.

f = the final solution.

The subscript notation on the variables is used to refer to a particular location on the structure. For example, $\bar{f}_{no,i,j}$ is the longitudinal stress parallel to the neutral axis at nodal section "no" for plate "i" at joint "j". The notation $RC_{no,j}$ is used to refer to

the concentrated holding force intensity at nodal section "no" along joint "j". Whenever a specific reference is made to a particular part of the analysis, a superscript notation is used. For example, $TM^{p}_{no,j}$ refers to the transverse bending moment at nodal section "no" along joint "j" for the primary analysis, p.

The following notation is used to define the variables:

$TM_{no,j}$ = transverse bending moment per unit width of slab.

$MO_{no,i}$ = longitudinal plate load bending moment.

$T_{no,j}$ = shear force.

$AR_{no,j}$ = joint reaction intensity or holding force intensity.

$RC_{no,j}$ = concentrated holding force.

$RI_{no,j}$ = joint load intensity.

$F_{no,j}$ = concentrated force of a particular loading system.

$FI_{no,j}$ = complimentary holding force intensity of a particular loading system.

$FC_{no,j}$ = concentrated complimentary holding force of a particular loading system.

$K_{no,j}$ = concentrated nodal force used to initiate a particular loading system.

β_r = linear constant expressing the proportional amount of a particular load system r.

$PI_{no,j,k}$ = component of the plate load intensity.

$PL_{no,i}$ = plate load intensity.

$PC_{no,i}$ = concentrated plate load.

$R\ell_i$ = modified reaction at left support of a plate.

$f_{i,j}$ = longitudinal stress parallel to the edge of a plate.

$\bar{f}_{no,i,j}$ = longitudinal stress at the edge of a plate parallel to the neutral axis.

$q_{no,j}$ = shearing force per unit length along a joint.

$\bar{\varepsilon}_{no,i,j}$ = longitudinal strain at the edge of the plate parallel to the neutral axis.

σ_η = stress parallel to the neutral axis of a plate.

σ_ξ = stress perpendicular to the neutral axis of a plate.

ε_η = strain parallel to the neutral axis of a plate.

ε_ξ = strain perpendicular to the neutral axis of a plate.

L = span between end diaphragms.

Le = edge length of the plates.

Lna_i = length of the neutral axis of a plate.

ℓna_i = length of neutral axis between nodal sections.

ℓe = edge length of a plate between nodal sections.

$d_{no,i}$ = plate depth.

$d\ell_i$ = plate depth at the left end.

dr_i = plate depth at the right end.

dm_i = plate depth at midspan.

$h_{no,i}$ = horizontal projection of the depth of a plate.

t_i = thickness of a plate.

$A_{no,i}$ = cross-sectional area of a plate.

$Z_{no,i}$ = section modulus of a plate.

$I_{no,i}$ = moment of interia of the transverse slab per unit width.

$\theta_{no,i}$ = sloping angle of a plate with respect to the horizontal in a cross-sectional view.

$\gamma_{i,i+1}$ = deflection angle between plates in a cross-sectional view.

α_i = angle of plate taper.

Ω_i = taper parameter defines as $\frac{|dr_i - d\ell_i|}{L}$.

$\phi_{no,i}$ = curvature intensity.

$\bar{\phi}_{no,i}$ = concentrated angle change.

$\delta_{no,i}$ = plate deflection in the plane of a plate.

$\delta v_{no,j}$ = vertical joint deflection.

$\Delta_{no,i}$ = translational deflection perpendicular to the cross-section of a plate or member.

$\theta\ell_i$ = modified slope at left support of a deflected plate.

E = modulus of elasticity.

μ = Poisson's ratio.

γ' = unit weight of the material.

w_{LLi} = distributed live load based on the horizontal projection, per unit width of slab.

w_{DLi} = distributed dead load per unit width of slab.

$W_{Tno,i}$ = resultant vertical load applied to a member.

The following matrix notation is used in this investigation:

$[SJ]_{no}$ = the overall joint stiffness matrix corresponding to the degrees of freedom and the restrained portions of the structure.

$[S]_{no}$ = the stiffness matrix corresponding to the degrees of freedom.

$[SRD]_{no}$ = the stiffness matrix of end-actions corresponding to the support restraints which are caused by unit displacements corresponding to the degrees of freedom.

$[SDR]_{no} = [SRD]_{no}^{T}$ the matrix of actions corresponding to the degrees of freedom and caused by unit displacements corresponding to the joint restraints.

$[SRR]_{no}$ = the matrix of actions corresponding to the support restraints caused by unit displacements corresponding to the same set of restraints.

$[SM]_{no,i}$ = the basic member stiffness matrix for member i.

$\{AD\}_{no}$ = the column vector of actions (shears and moments) corresponding to the degrees of freedom of the system.

$\{AM\}_{no,i}$ = the column vector of unknown end-actions for the member i.

$\{AML\}_{no,i}$ = the column vector of fixed end-actions for the member i.

$\{AR\}_{no}$ = the column vector of unknown reactions.

$\{ARL\}_{no}$ = the column vector of reactions in the restrained structure resulting from the applied load, corresponding to the unknown reactions.

$\{AE\}_{no}$ = the column vector of equivalent joint loads.

$\{AJ\}_{no}$ = the column vector of actual joint loads.

$\{AC\}_{no}$ = the column vector of combined joint loads.

$\{DJ\}_{no}$ = the over-all joint displacement matrix containing all the degrees of freedom and restrained displacements.

$\{D\}_{no}$ = the column vector of unknown displacements corresponding to the degrees of freedom.

$\{DM\}_{no,i}$ = the column vector of displacements corresponding to the ends of the member i.

$[AA]$ = the coefficient matrix in the Modified Three Shear Equation matrix formulation.

$\{T'\}$ = the shear force vector arranged in order of the numbering system shown in Fig. 30.

$\{T\}_{no,j}$ = the shear force vector arranged according to the actual node-joint notation given in Fig. 30.

$\{C\}$ = constant vector in the Modified Three Shear Equation matrix formulation.

$[F]$ = the coefficient matrix in the Particular Load Method matrix formulation which contains the concentrated loads $F^{r}_{no,j}$ of all the particular loading systems.

$\{\beta\}$ = the column vector of linear constants expressing the proportion of each particular loading system required to remove the effects of the secondary holding forces.

$\{R\}$ = the column vector containing the concentrated secondary holding forces, $RC_{no,j}$, at all the interior nodes of the structure.

XI. APPENDIX B: TABLES

Table 1. Comparison of theories in the analysis of a prismatic folded plate with a similar loading[a]

Joint	Longitudinal stress at midspan, $\bar{f}$ (psi.)				Transverse moments at midspan, TM (lb.-in./in.)			
	Primary analysis		Final analysis		Primary analysis		Final analysis	
	Proposed theory[b]	Ordinary theory[c]	Proposed theory	Ordinary theory	Proposed theory	Ordinary theory	Proposed theory	Ordinary theory
1	-856	-855	-826	-826				
2	+717	+717	+706	+708	-1194	-1194	-1194	-1194
3	-564	-565	-563	-564	- 284	- 284	- 749	- 751
4	+504	+505	+501	+501	- 587	- 587	-428	- 429

[a]Structure and loading conditions shown in Fig. 39.

[b]Based on 7 nodal sections.

[c]Results presented by Simpson (14).

Table 2. Comparison of theories in the analysis of a prismatic folded plate with a non-similar loading[a]

Joint	Longitudinal stress at midspan, $\bar{f}$ (psi.)				Transverse moments at midspan, TM (lb.-in./in.)			
	Primary analysis		Final analysis		Primary analysis		Final analysis	
	Proposed theory[b]	Ordinary theory[c]	Proposed theory	Ordinary theory	Proposed theory	Ordinary theory	Proposed theory	Ordinary theory
1	-870	-867	-840	-845				
2	+757	+753	+746	+747	-1194	-1194	-1194	-1194
3	-654	+656	-653	-656	- 391	- 391	- 868	- 872
4	+628	+624	+624	+617	- 908	- 909	- 714	- 717

[a]Structure and loading condition shown in Fig. 40.

[b]Based on 15 nodal sections.

[c]Analysis for similar loading cases of dead load and live load superimposed.

Table 3. Theoretical and experimental longitudinal stresses[a]

Model 1				Model 2			
Gage location[b]	Theor. (psi.)	Expr.[c] (psi.)	Error[d] (%)	Gage location[e]	Theor. (psi.)	Expr.[f] (psi.)	Error[d] (%)
1	-648	-470	+38	1A	-505	-584	-14
				1B	+254	+270	- 6
2	-789	-739	+ 7	2	-676	-710	- 5
3	+143	+115	+24	3	+451	+425	+ 6
4	-581	-597	- 3	4	-655	-702	- 7
5	-203	-183	+11	5	-275	-303	-10
6	+185	+207	-11	6	+107	+ 65	+65
7	+563	+549	+ 3	7	+641	+576	+11
8	-410	-372	+10	8	-428	-418	+ 2
9	+612	+573	+ 7	9	+545	+576	- 5
10	-289	-242	+19	10	-344	-356	- 3
11	-478	-453	+ 6	11	-573	-586	- 2
12	-712	-625	+14	12	-635	-666	- 5
13	+231	+218	+ 6	13	+229	+221	+ 4
14	+286	+261	+10	14	+338	+301	+12
15	+ 38	+ 57	-33	15	+286	+304	- 6
16	-176	-164	+ 7	16	-166	-171	- 3

[a]Per load increment as defined in Fig. 49, parallel to the neutral axis.

[b]Given in Fig. 50.

[c]Based on strain measurements from top and bottom gages.

[d]+ Error indicates theory over-predicts experimental results.

[e]Given in Fig. 51.

[f]Based on strain measurements from top gages only.

Table 4. Theoretical and experimental vertical joint deflections[a]

Model 1				Model 2			
Dial location[b]	Theor. (in.)	Expr. (in.)	Error[c] (%)	Dial location[d]	Theor. (in.)	Expr. (in.)	Error[c] (%)
A	0.0069	0.0067	+ 3	A	0.0031	0.0031	0
B	0.0065	0.0062	+ 5	B	0.0038	0.0039	- 3
C	0.0038	0.0043	-12	C	0.0025	0.0024	+ 4
D	0.0064	0.0068	- 6	D	0.0037	0.0039	- 5
E	0.0033	0.0038	-13	E	0.0021	0.0023	- 9
F	0.0058	0.0058	0	F	0.0034	0.0031	+10
G	0.0064	0.0061	+ 5	G	0.0027	0.0026	+ 4

[a]Per load increment defined in Fig. 49.

[b]Given in Fig. 50.

[c]+ Error indicates theory over-predicts experimental results.

[d]Given in Fig. 51.

Table 5. Theoretical and experimental transverse moments in Model 1[a]

Gage location[b]	Theor. (lb.-in./in.)	Expr. (lb.-in./in.)	Error[c] (%)
1	0.868	0.709	+22
2	0.299	0.346	-14
12	0.313	0.333	- 6
15	0.085	0.071	+19

[a]Per load increment defined in Fig. 49.

[b]Given in Fig. 50.

[c]+ Error indicates theory over-predicts experimental results.

XII. APPENDIX C: FIGURES

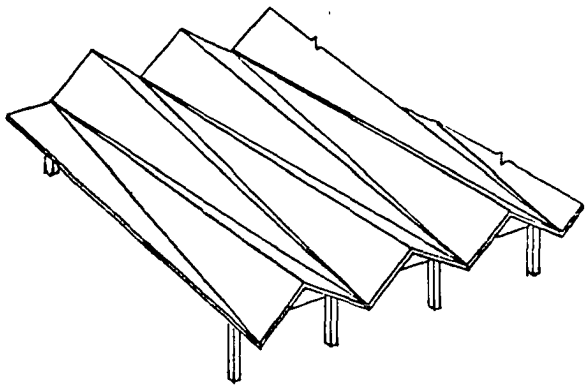

Fig. 1. Non-prismatic folded plate structure

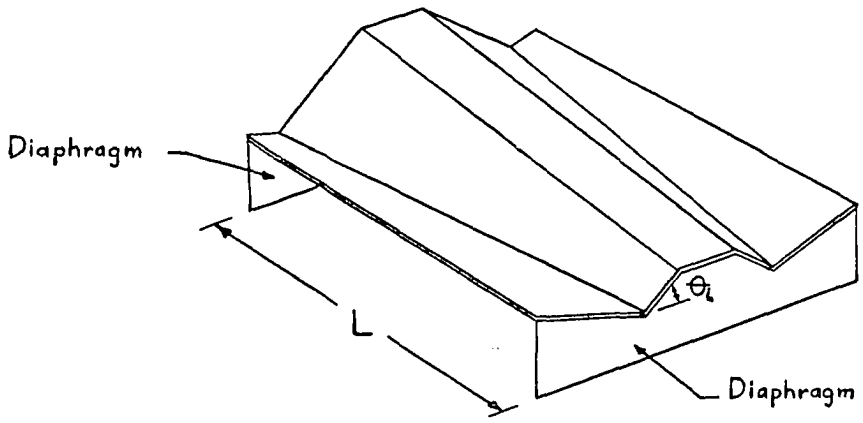

Fig. 2. Typical non-prismatic folded plate

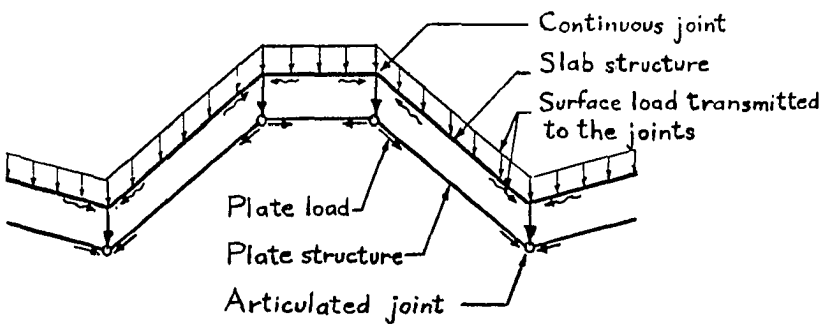

Fig. 3. Basic slab and plate structures

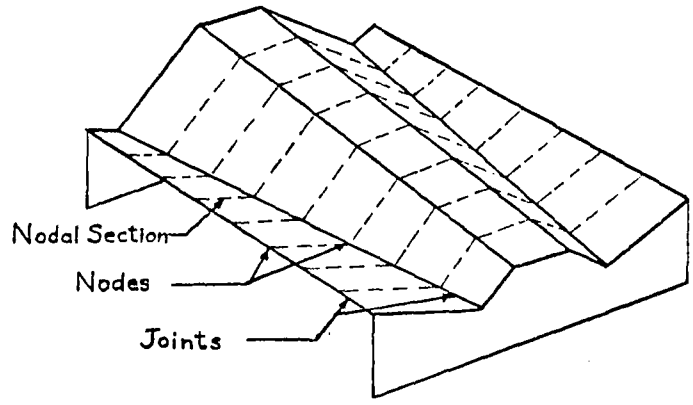

Fig. 4. Structure divided into transverse nodal sections

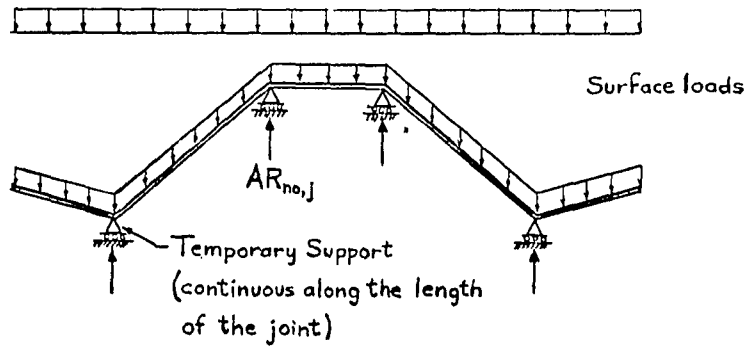

Fig. 5. Transverse nodal section of the slab structure

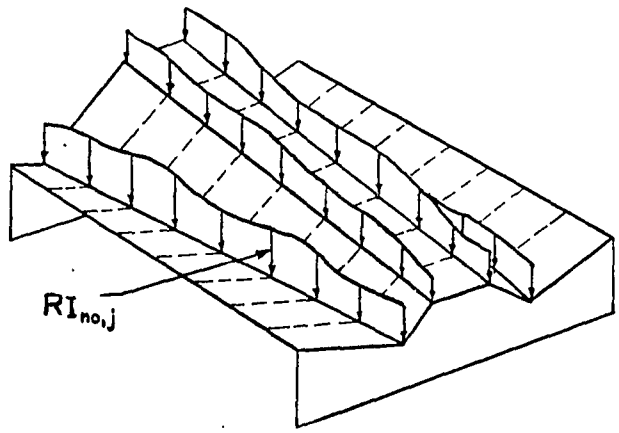

Fig. 6. Distributed joint loads applied to the plate structure

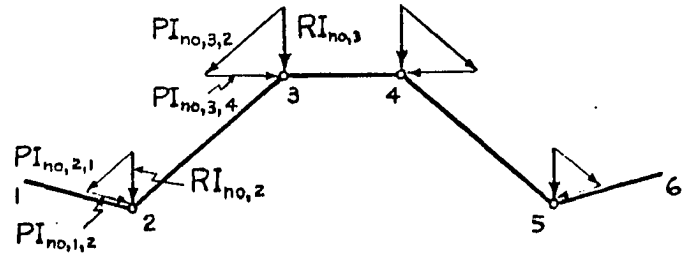

Fig. 7. Resolution of joint loads

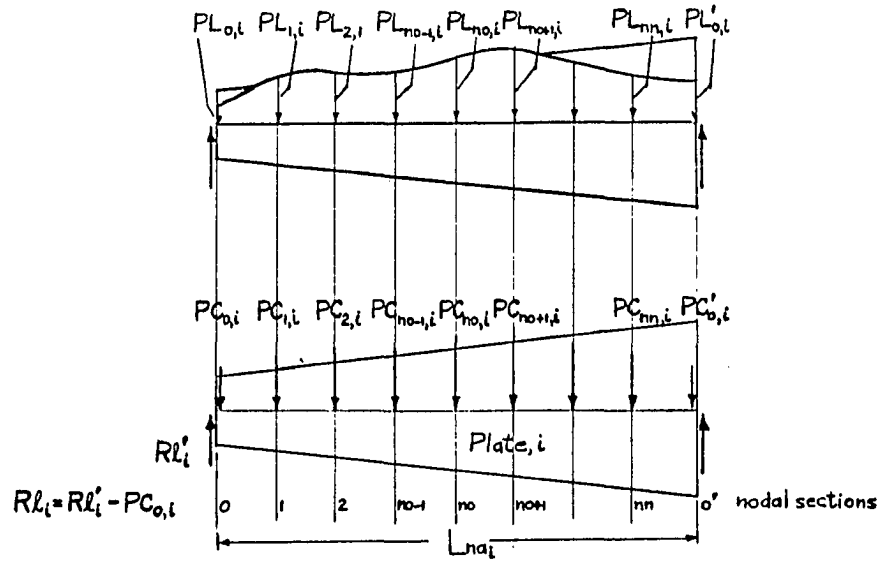

Fig. 8. Plate load bending analysis

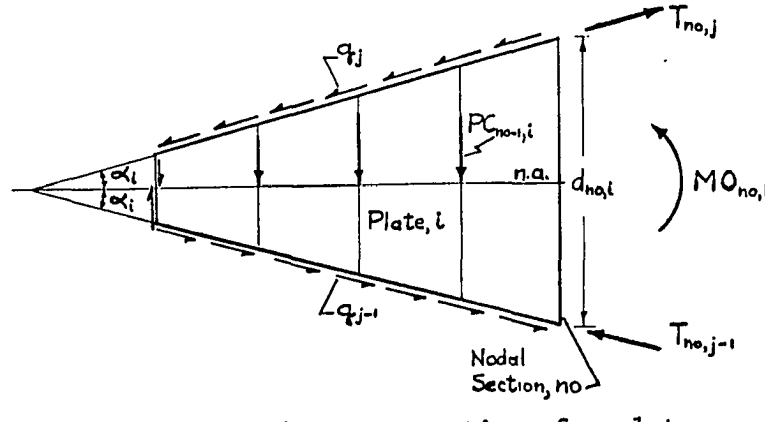

Fig. 9. Forces acting on a section of a plate

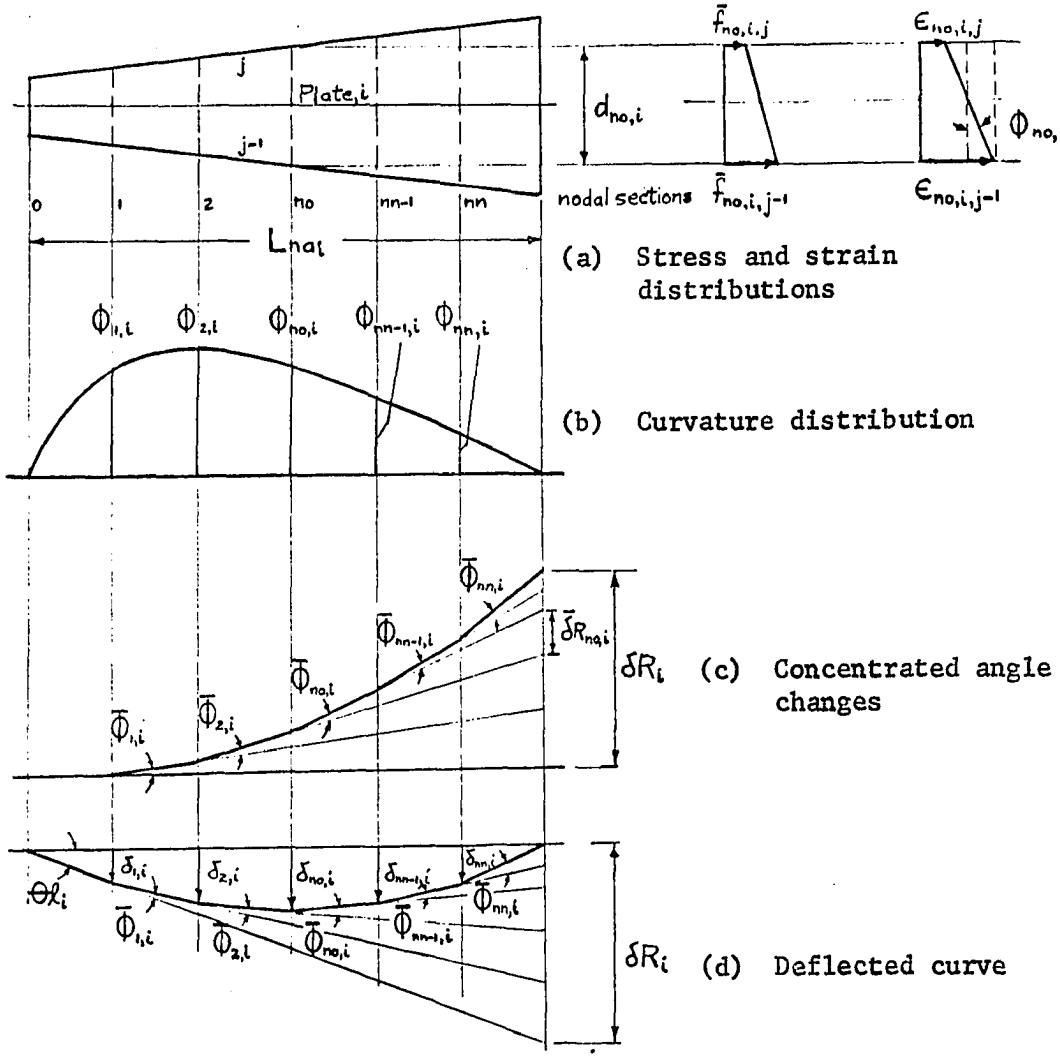

Fig. 10. Plate deflection analysis

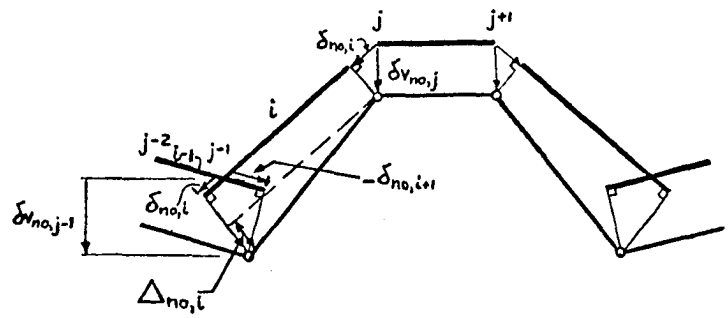

Fig. 11. Williot geometry applied to the disconnected plate problem

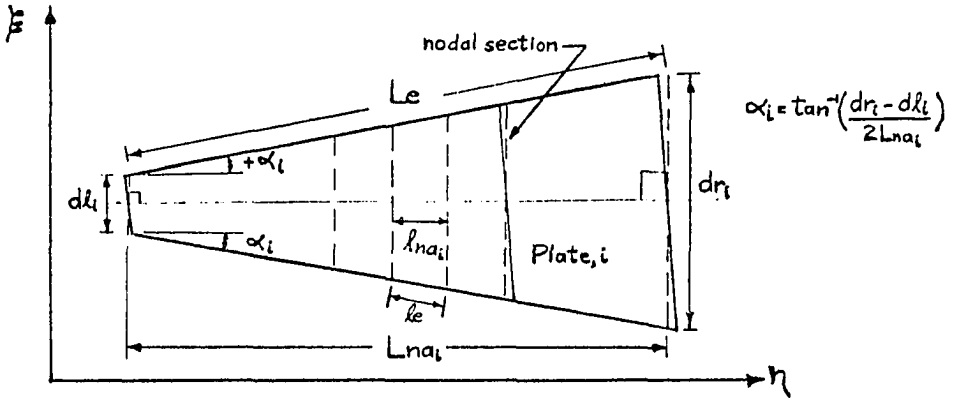

Fig. 12. Plate geometry approximations and co-ordinate system

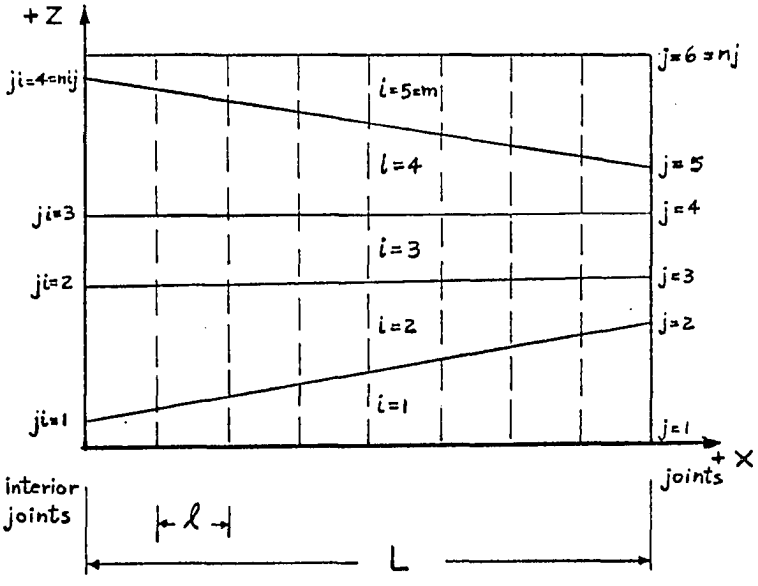

Fig. 13. Co-ordinate system for a structure in plan view and node-joint notation

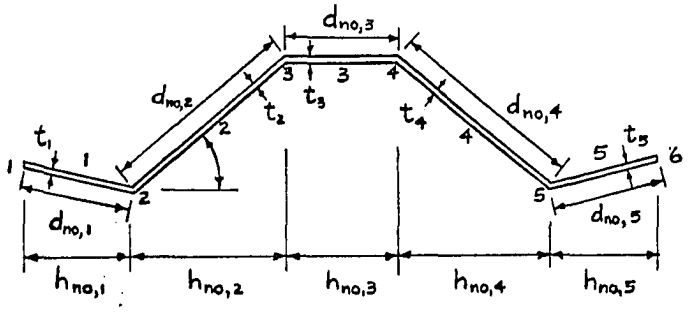

Fig. 14. Geometry of a typical nodal section

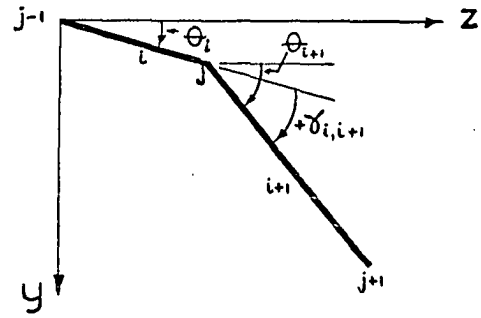

Fig. 15. Sign convention for the angles defining the slope of the plates and the deflection angles between plates

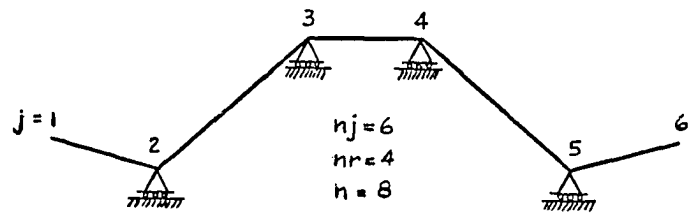

Fig. 16. Temporary vertical restraints at the joints of a typical nodal section

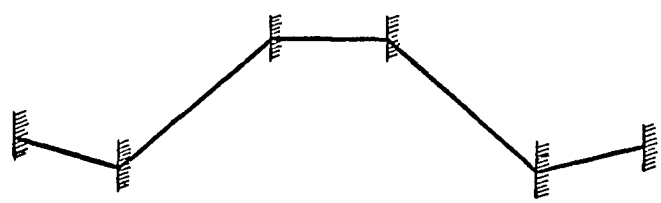

Fig. 17. Typical restrained nodal section

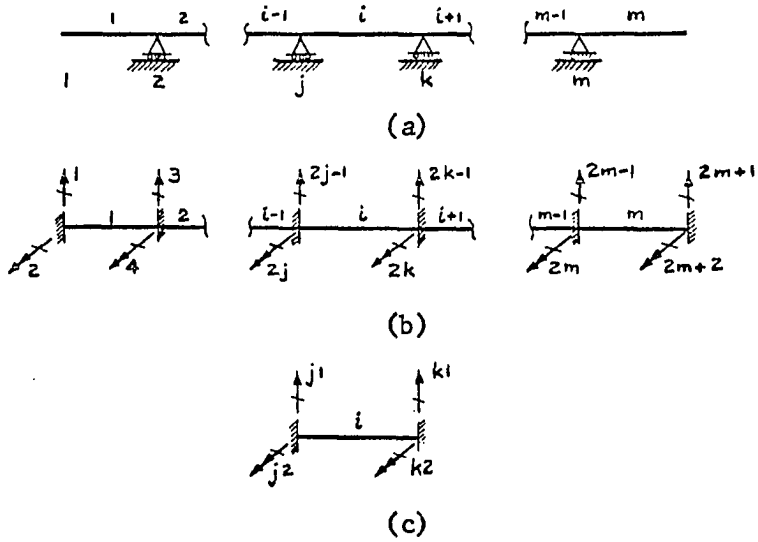

Fig. 18. Displacement vector notation

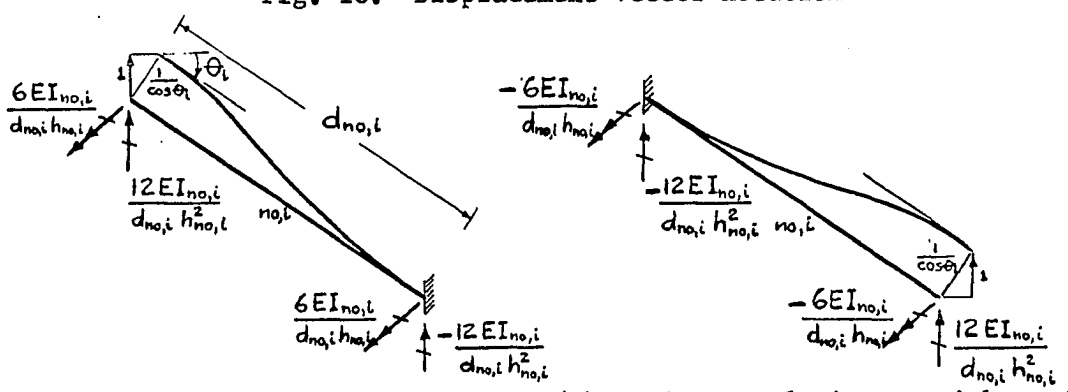

(a) Unit translation at left end (c) Unit translation at right end

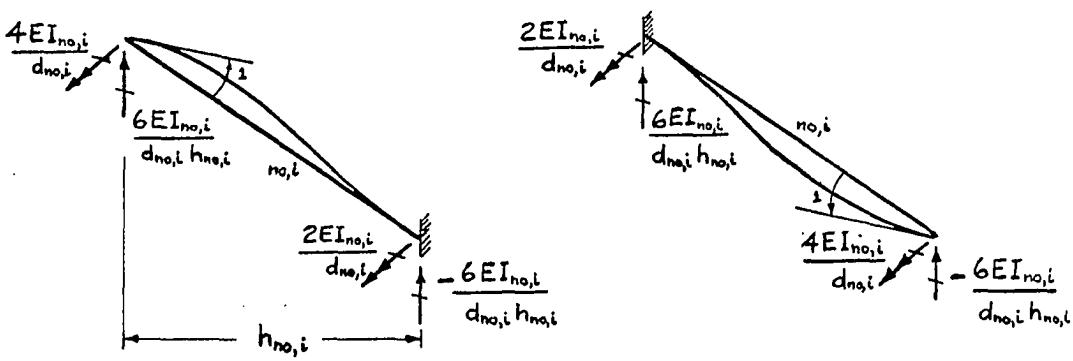

(b) Unit rotation at left end (d) Unit rotation at right end

Fig. 19. Generating a typical member stiffness matrix

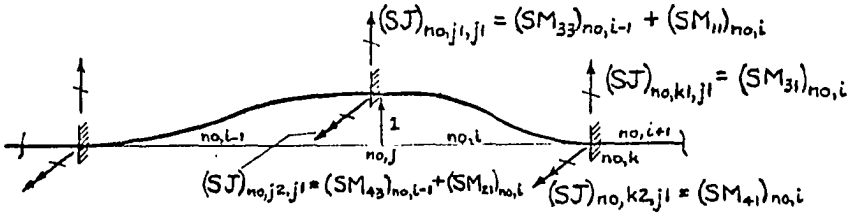

(a)

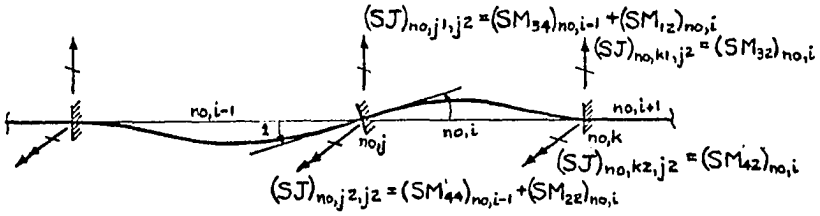

(b)

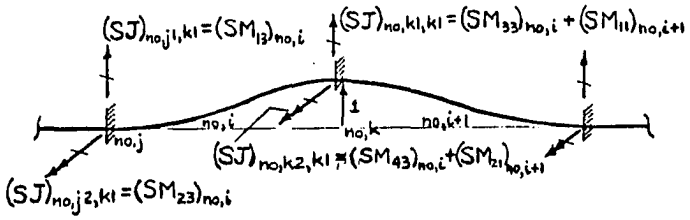

(c)

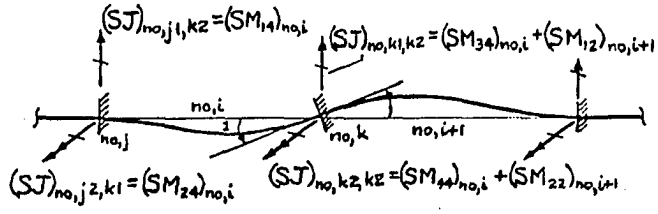

(d)

Fig. 20. Joint stiffness matrix coefficients

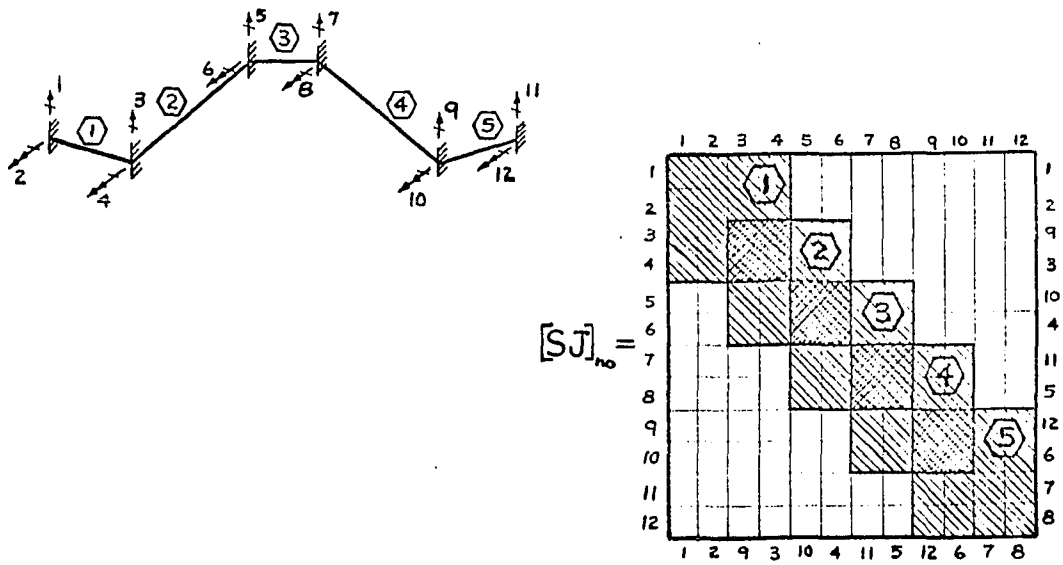

Fig. 21. Original over-all joint stiffness matrix

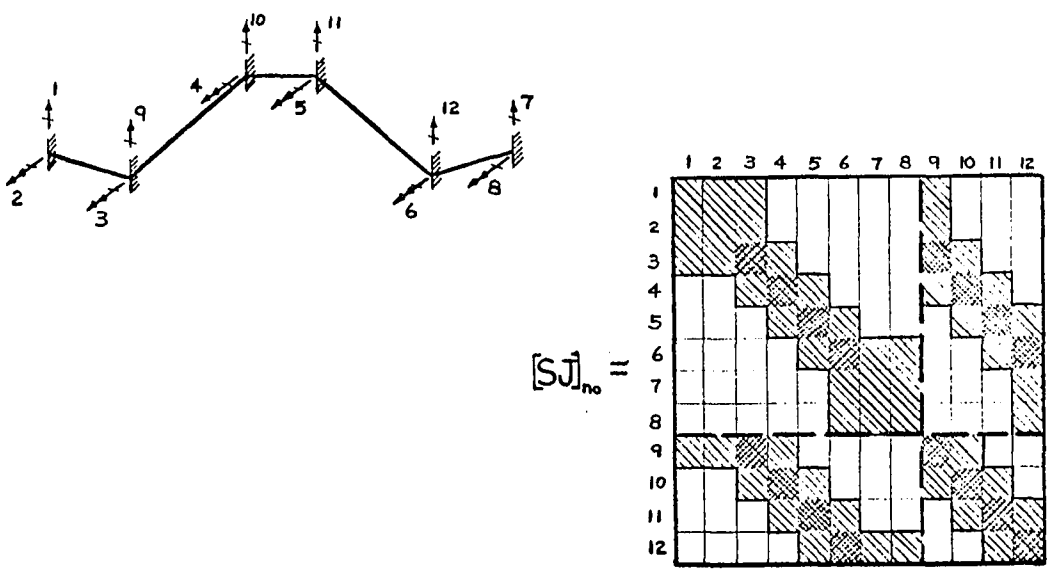

Fig. 22. Rearranged over-all joint stiffness matrix

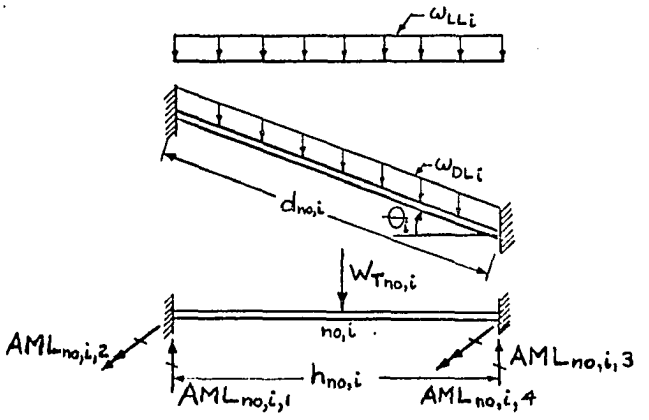

Fig. 23. Fixed end-actions caused by surface loads

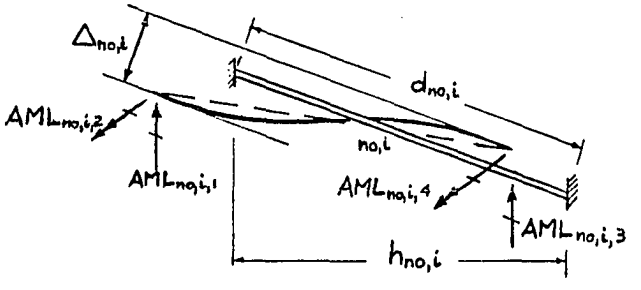

Fig. 24. Fixed end-actions caused by relative joint displacements

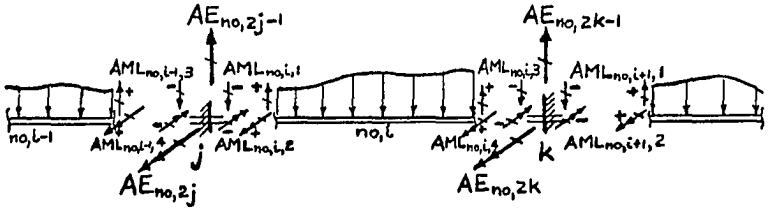

Fig. 25. Forming equivalent joint loads

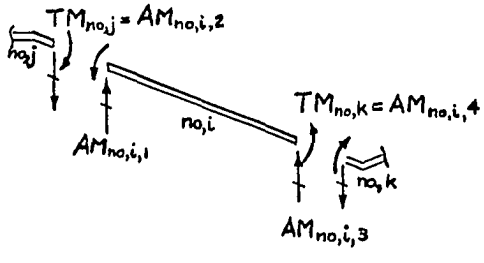

Fig. 26. Member end-actions and transverse moments at the joints

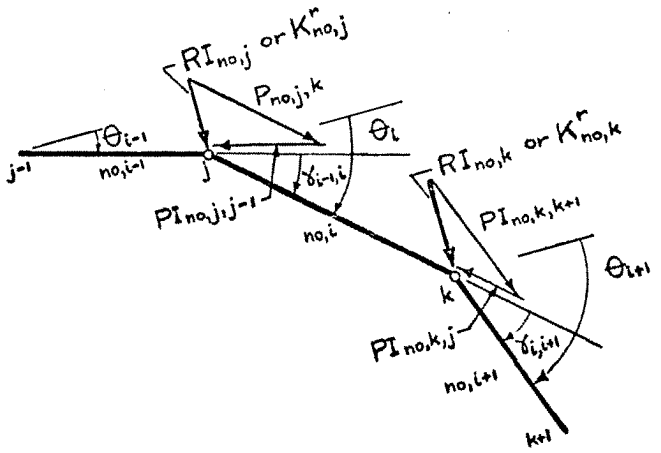

Fig. 27. Resolution of joint loads into plate loads

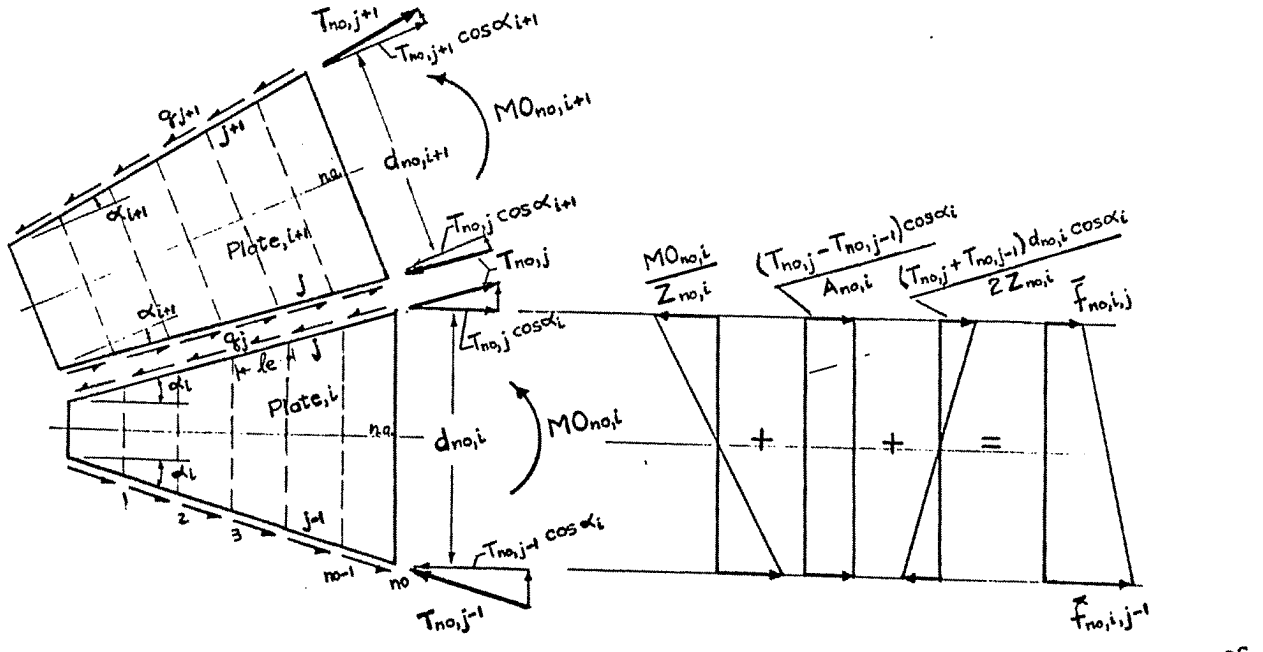

Fig. 28. Forces and stresses developed in two adjacent plates

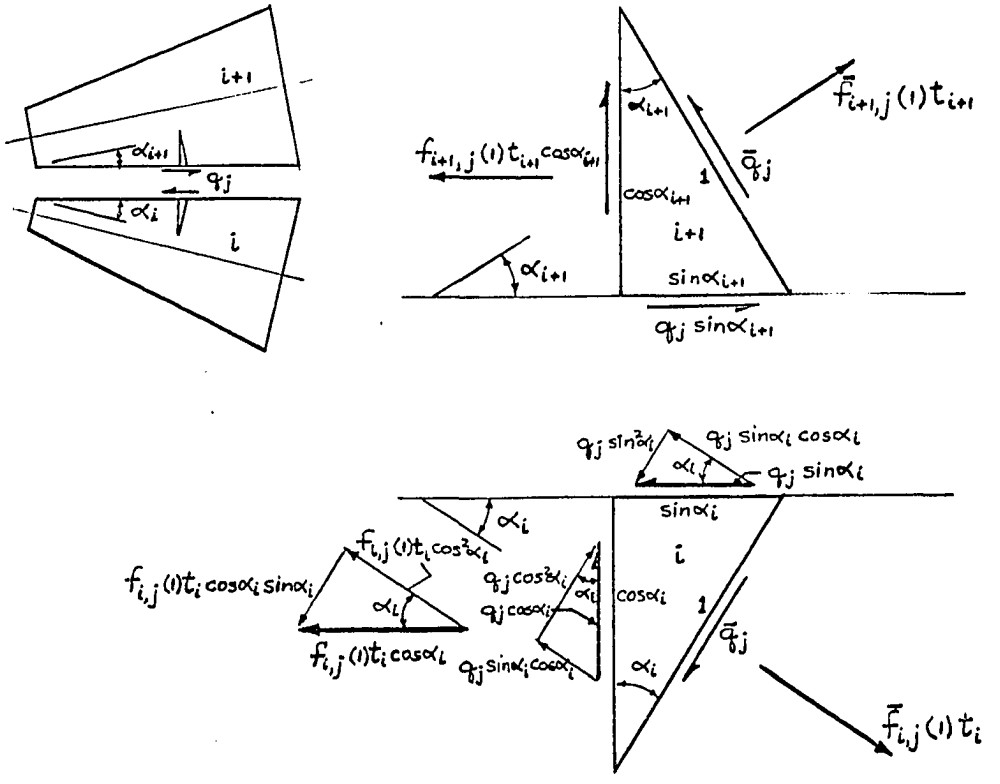

Fig. 29. Equilibrium of forces on two elemental sections of plate adjacent to a common joint

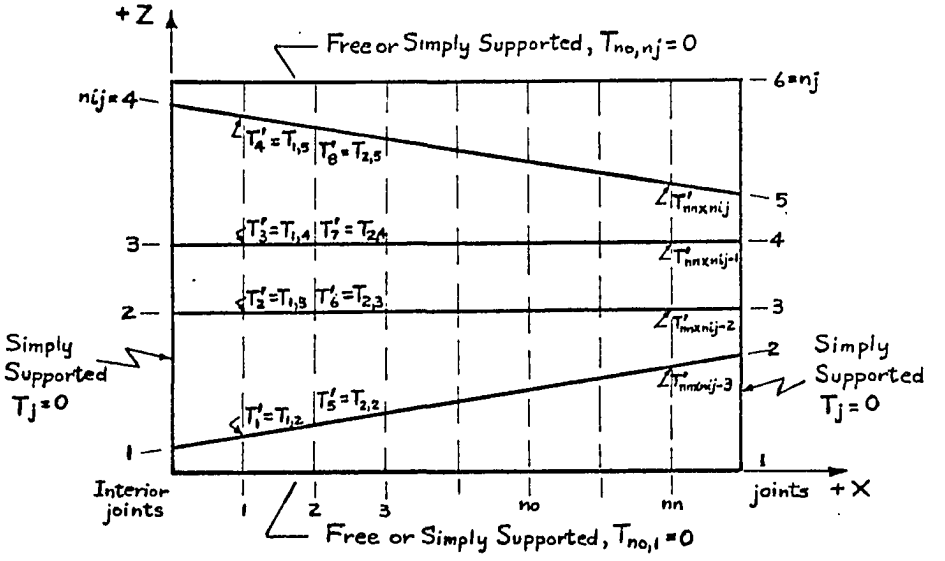

Fig. 30. Shear force notation and boundary conditions

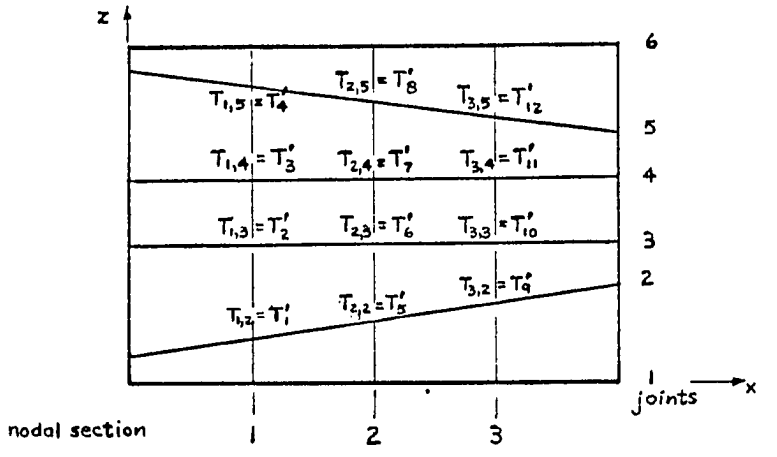

(a)

$$
\begin{array}{c|cccccccccccc|c|c}
no,j & & & & & & & & & & & & & & \\
\hline
1,2 & AA_{1,1} & AA_{1,2} & 0 & 0 & AA_{1,5} & 0 & 0 & 0 & 0 & 0 & 0 & 0 & T'_1 & C_1 \\
1,3 & AA_{2,1} & AA_{2,2} & AA_{2,3} & 0 & 0 & AA_{2,6} & 0 & 0 & 0 & 0 & 0 & 0 & T'_2 & C_2 \\
1,4 & 0 & AA_{3,2} & AA_{3,3} & AA_{3,4} & 0 & 0 & AA_{3,7} & 0 & 0 & 0 & 0 & 0 & T'_3 & C_3 \\
1,5 & 0 & 0 & AA_{4,3} & AA_{4,4} & 0 & 0 & 0 & AA_{4,8} & 0 & 0 & 0 & 0 & T'_4 & C_4 \\
2,2 & AA_{5,1} & 0 & 0 & 0 & AA_{5,5} & AA_{5,6} & 0 & 0 & AA_{5,9} & 0 & 0 & 0 & T'_5 & C_5 \\
2,3 & 0 & AA_{6,2} & 0 & 0 & AA_{6,5} & AA_{6,6} & AA_{6,7} & 0 & 0 & AA_{6,10} & 0 & 0 & T'_6 & C_6 \\
2,4 & 0 & 0 & AA_{7,3} & 0 & 0 & AA_{7,6} & AA_{7,7} & AA_{7,8} & 0 & 0 & AA_{7,11} & 0 & T'_7 & C_7 \\
2,5 & 0 & 0 & 0 & AA_{8,4} & 0 & 0 & AA_{8,7} & AA_{8,8} & 0 & 0 & 0 & AA_{8,12} & T'_8 & C_8 \\
3,2 & 0 & 0 & 0 & 0 & AA_{9,5} & 0 & 0 & 0 & AA_{9,9} & AA_{9,10} & 0 & 0 & T'_9 & C_9 \\
3,3 & 0 & 0 & 0 & 0 & 0 & AA_{10,6} & 0 & 0 & AA_{10,9} & AA_{10,10} & AA_{10,11} & 0 & T'_{10} & C_{10} \\
3,4 & 0 & 0 & 0 & 0 & 0 & 0 & AA_{11,7} & 0 & 0 & AA_{11,10} & AA_{11,11} & AA_{11,12} & T'_{11} & C_{11} \\
3,5 & 0 & 0 & 0 & 0 & 0 & 0 & 0 & AA_{12,8} & 0 & 0 & AA_{12,11} & AA_{12,12} & T'_{12} & C_{12}
\end{array}
$$

(b)

Fig. 31. Matrix formulation of Modified Three Shear Equations

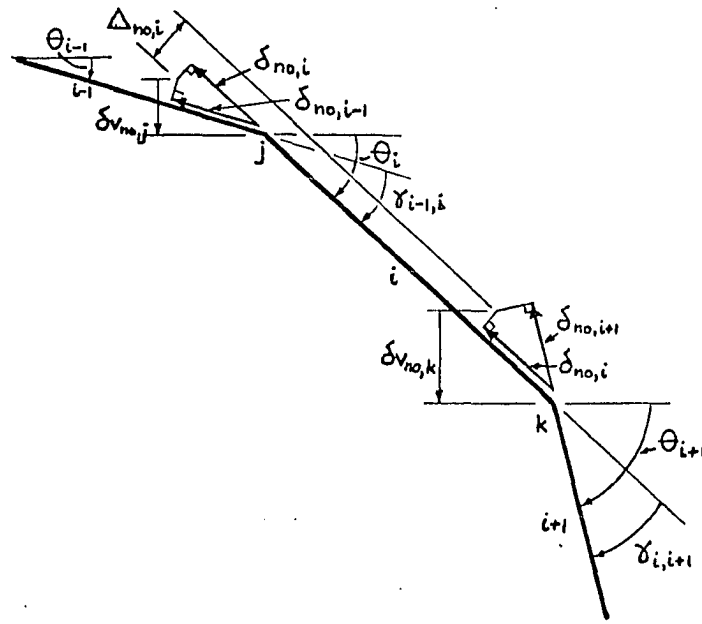

Fig. 32. Matching joint deflections by Williot geometry

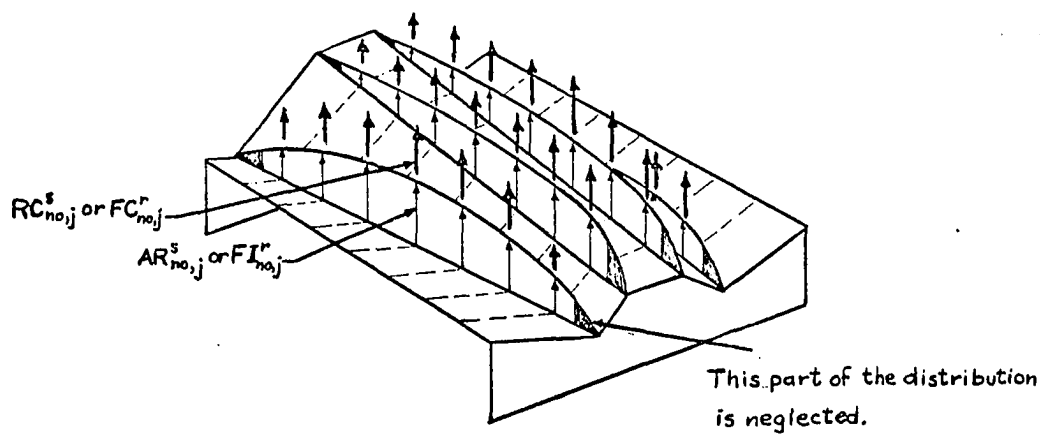

Fig. 33. Distributed and equivalent concentrated holding forces

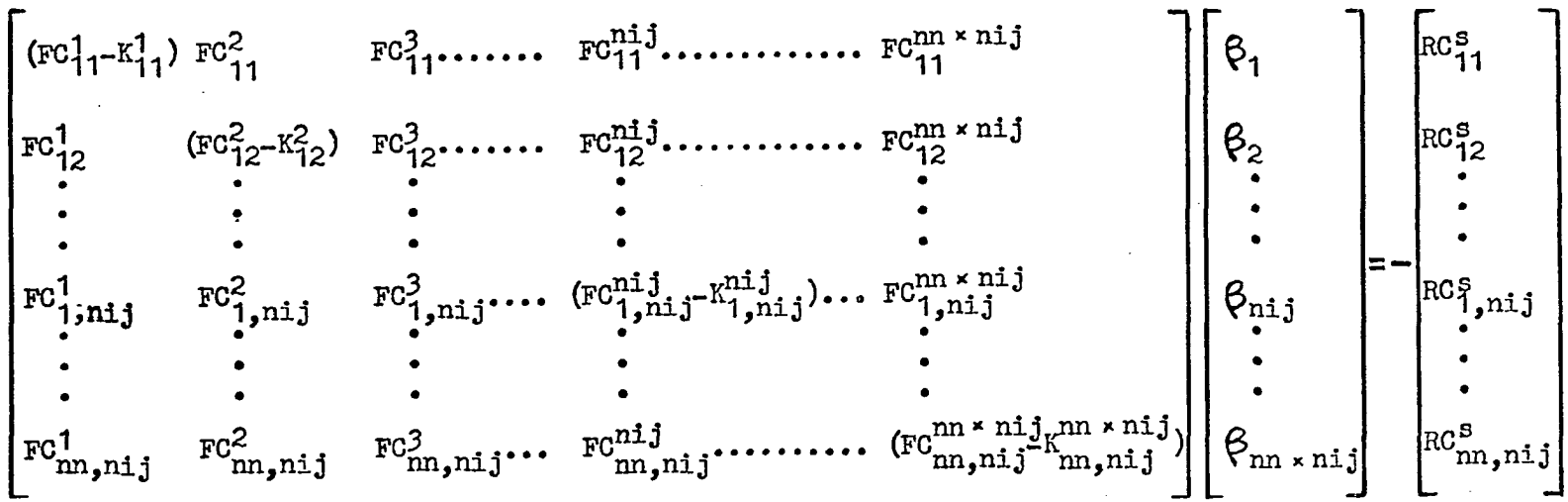

Fig. 34. Matrix formulation for the Particular Load Method

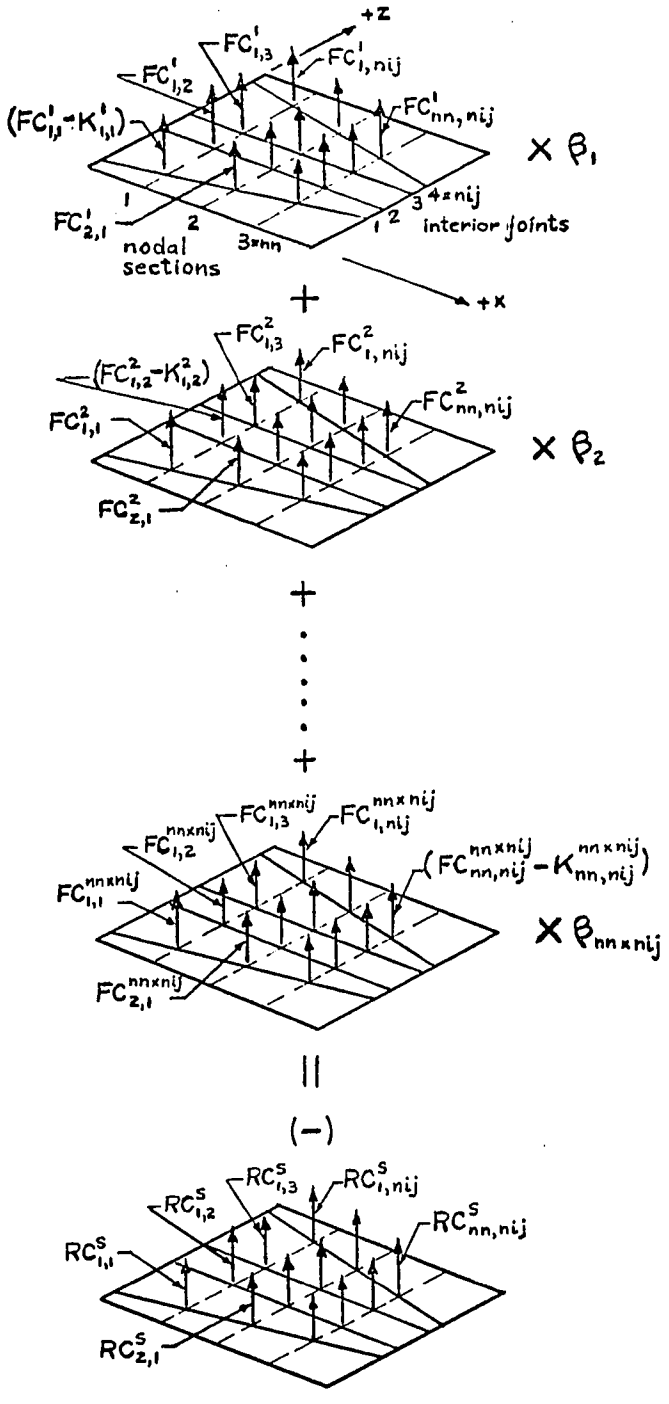

Fig. 35. Removing the effects of the secondary holding forces by the Particular Load Method

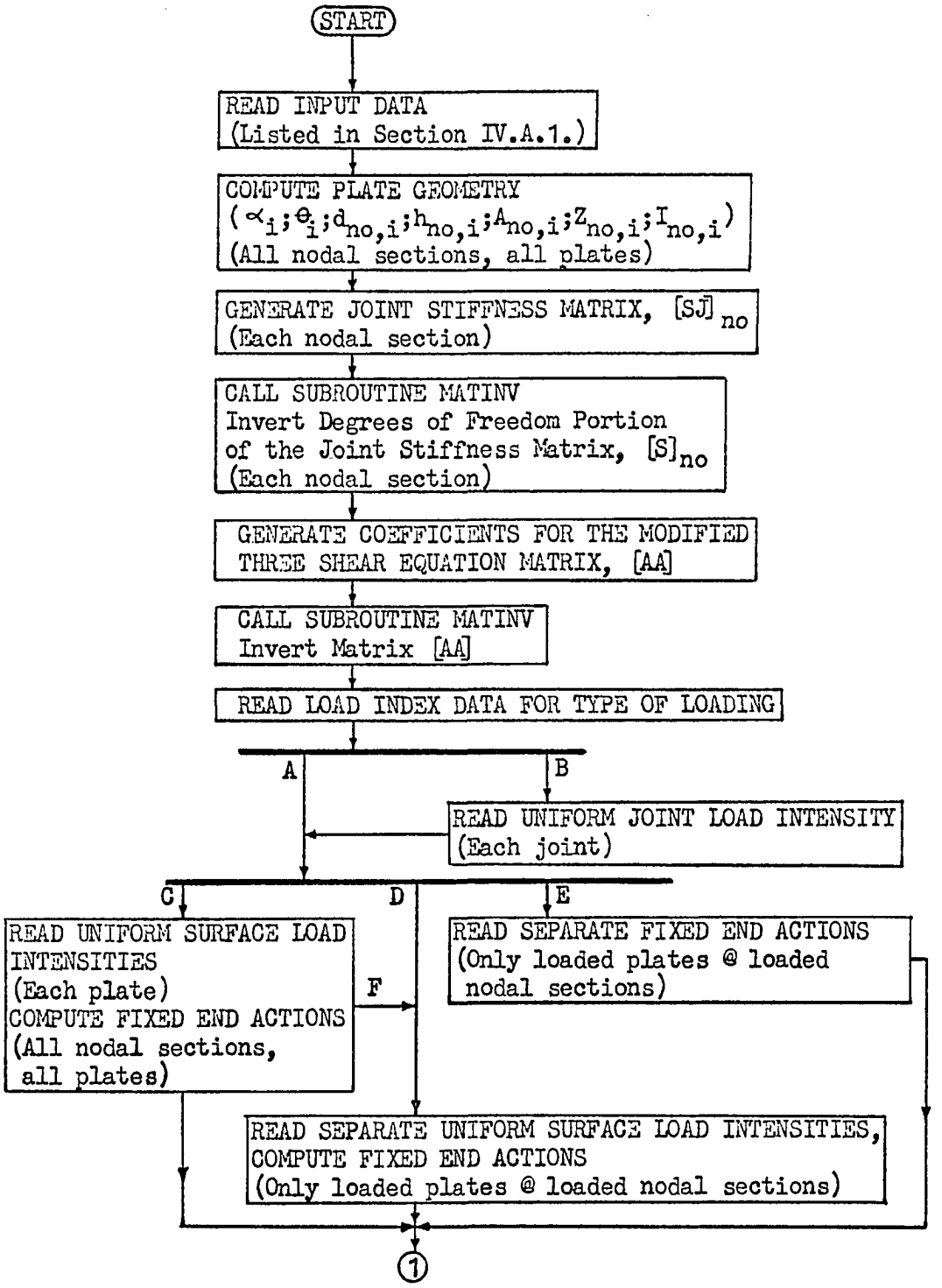

Fig. 36. Common flow chart

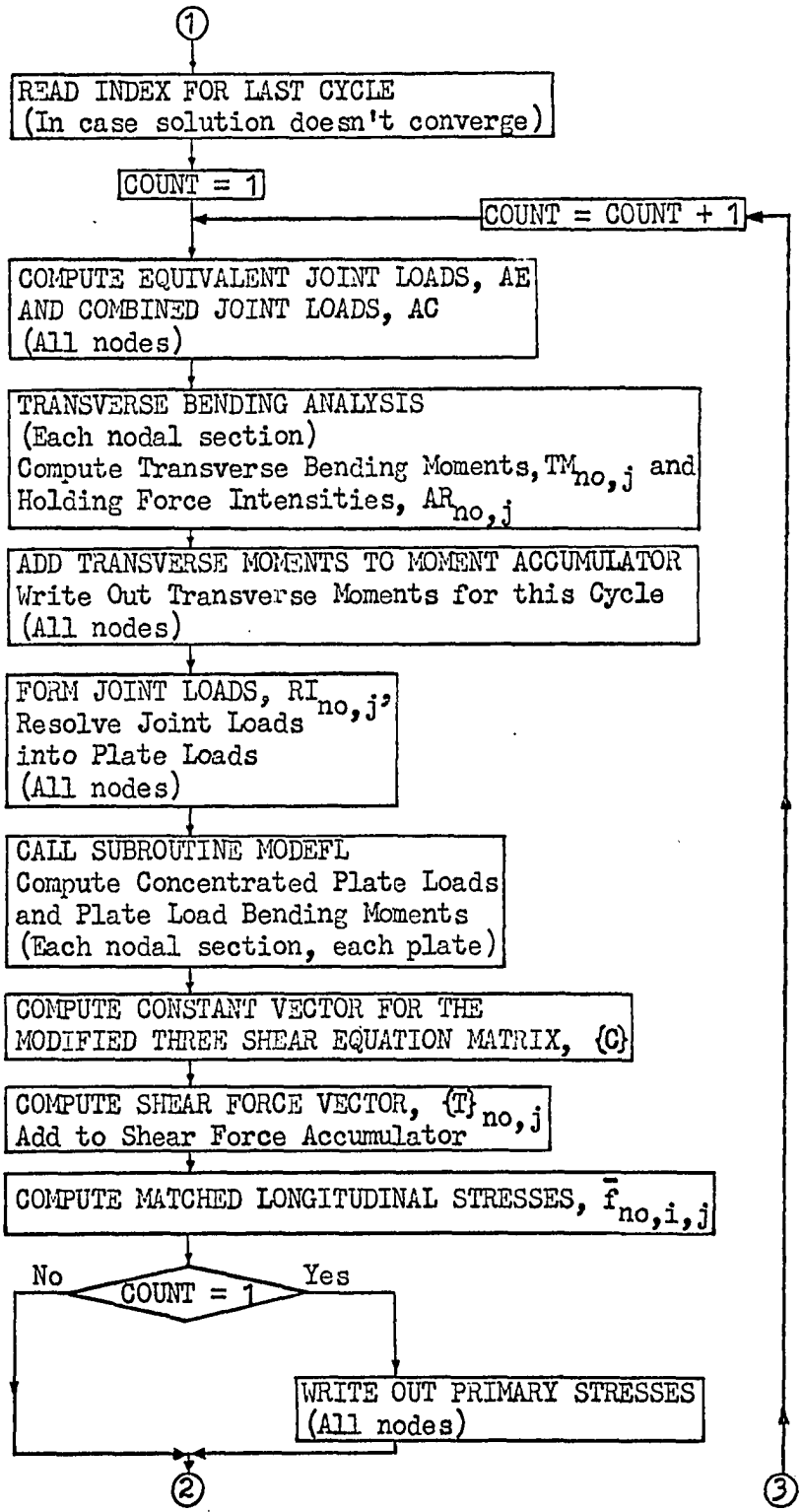

Fig. 37. Flow chart for the Iteration Method

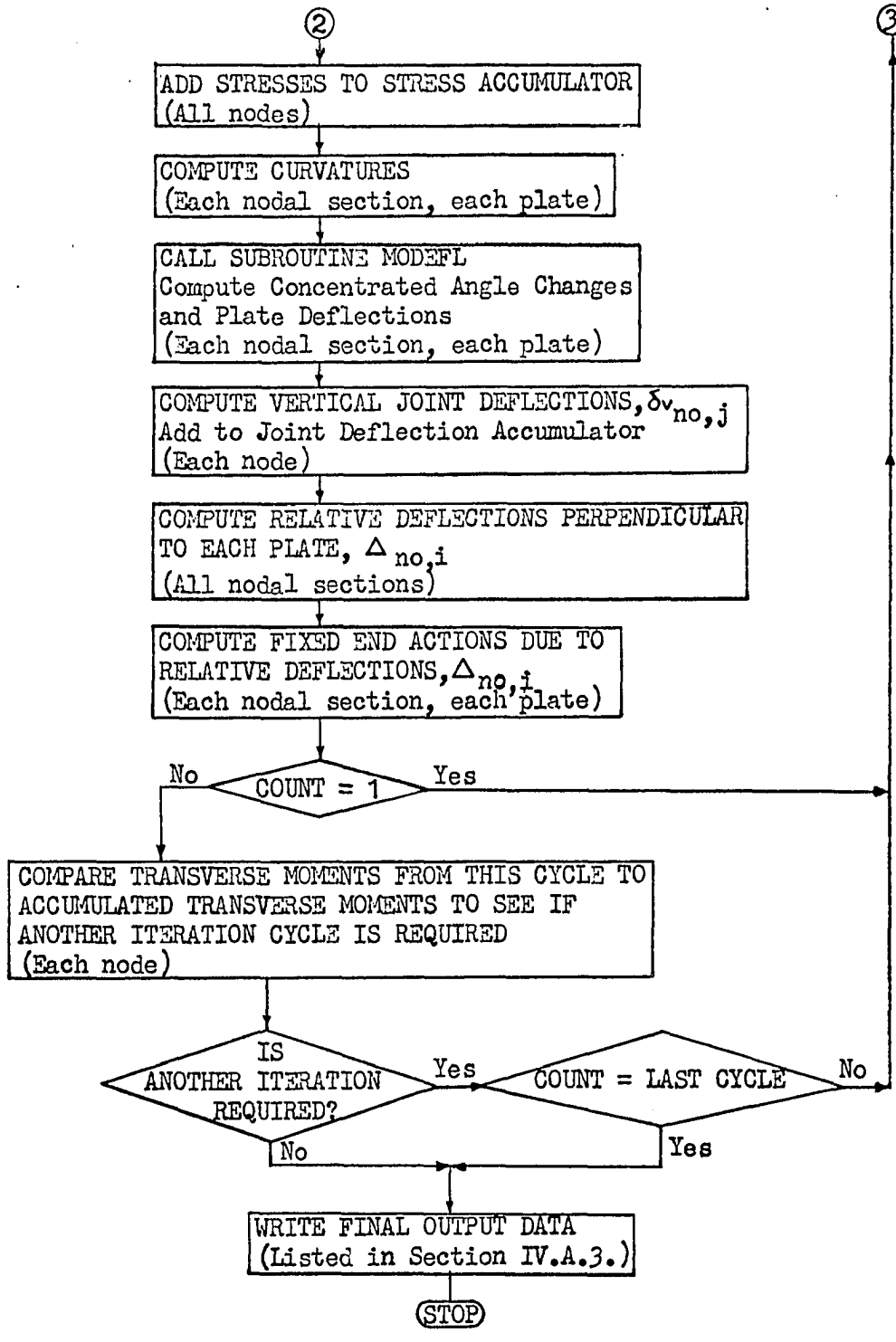

Fig. 37 (Continued)

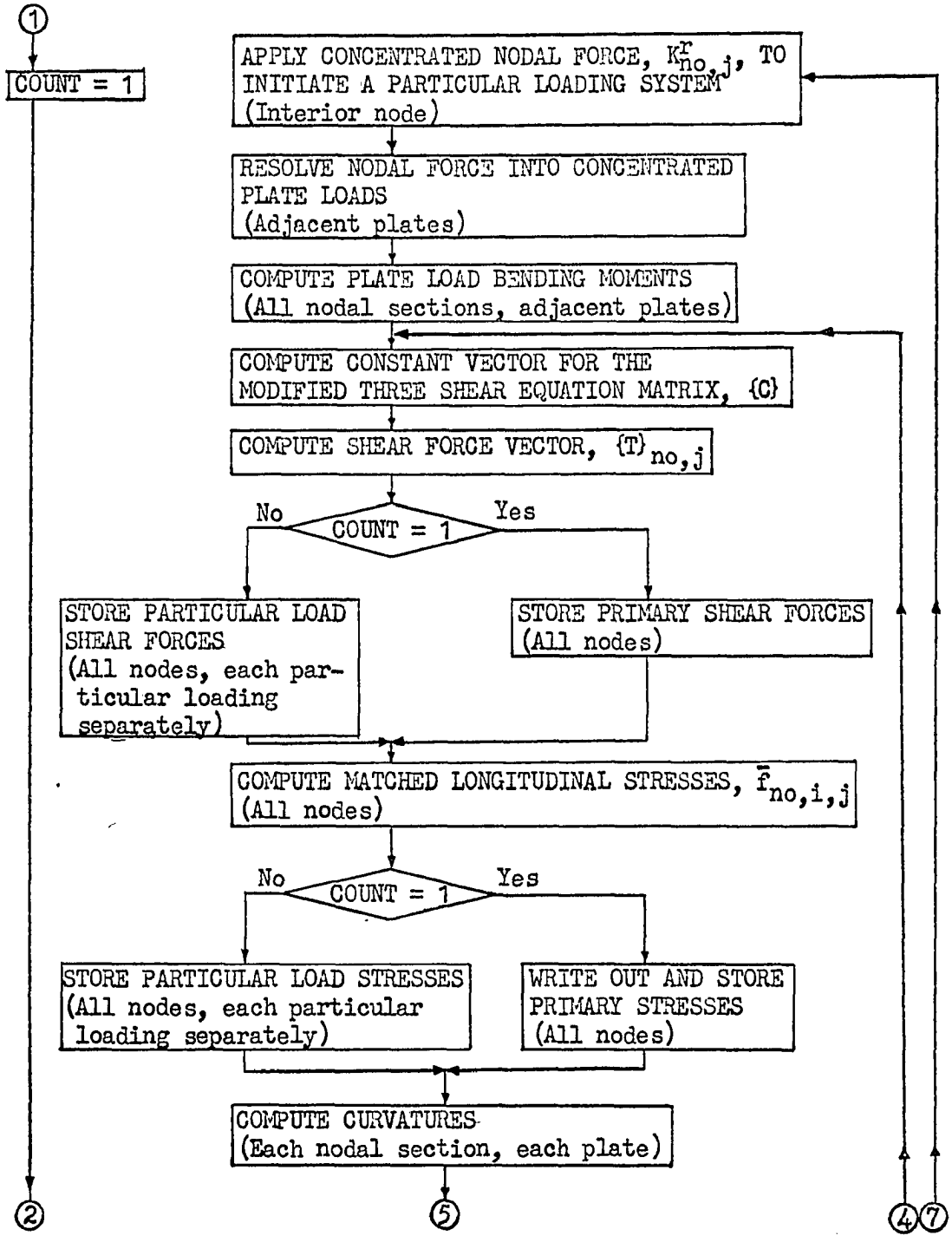

Fig. 38. Flow chart for the Particular Load Method

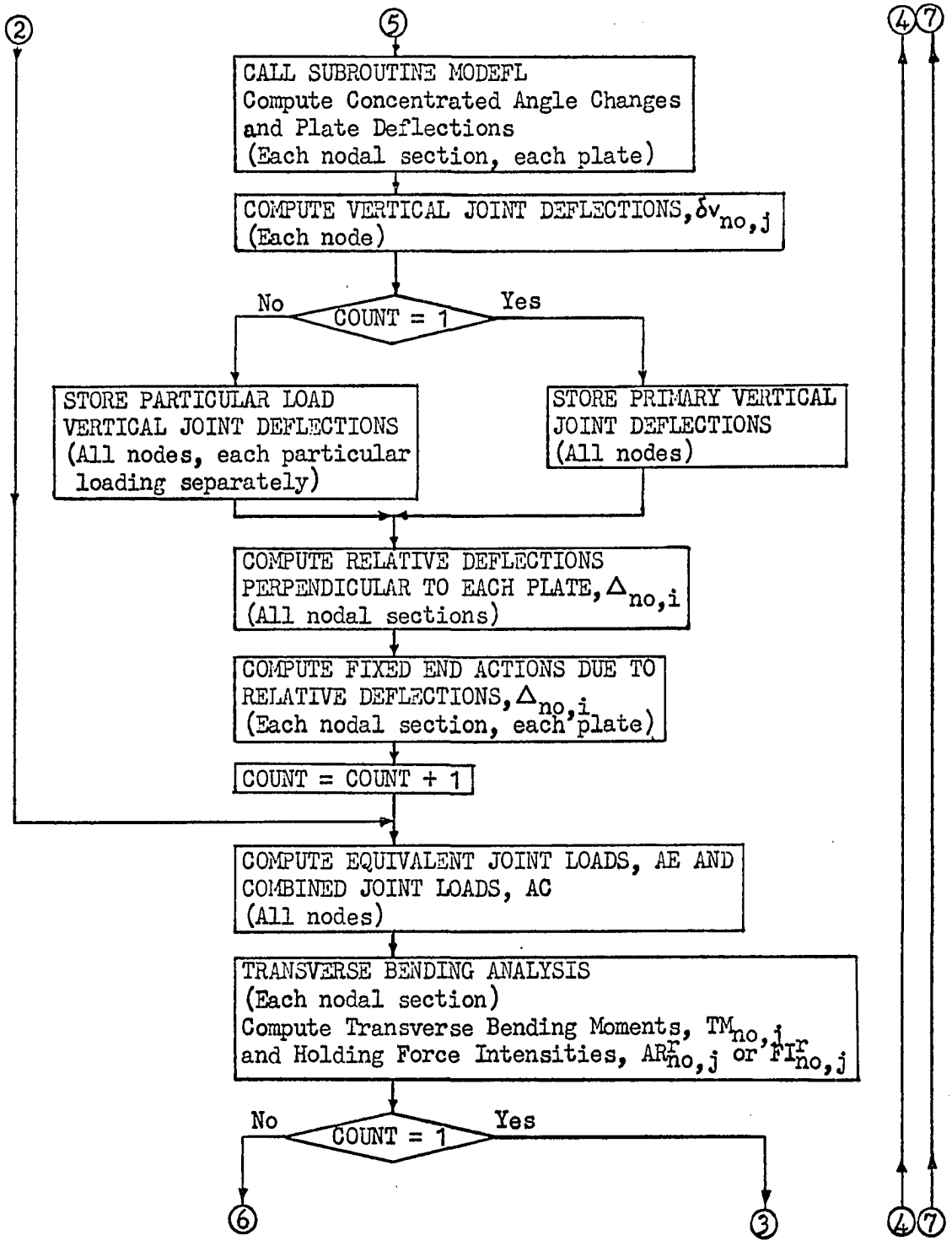

Fig. 38 (Continued)

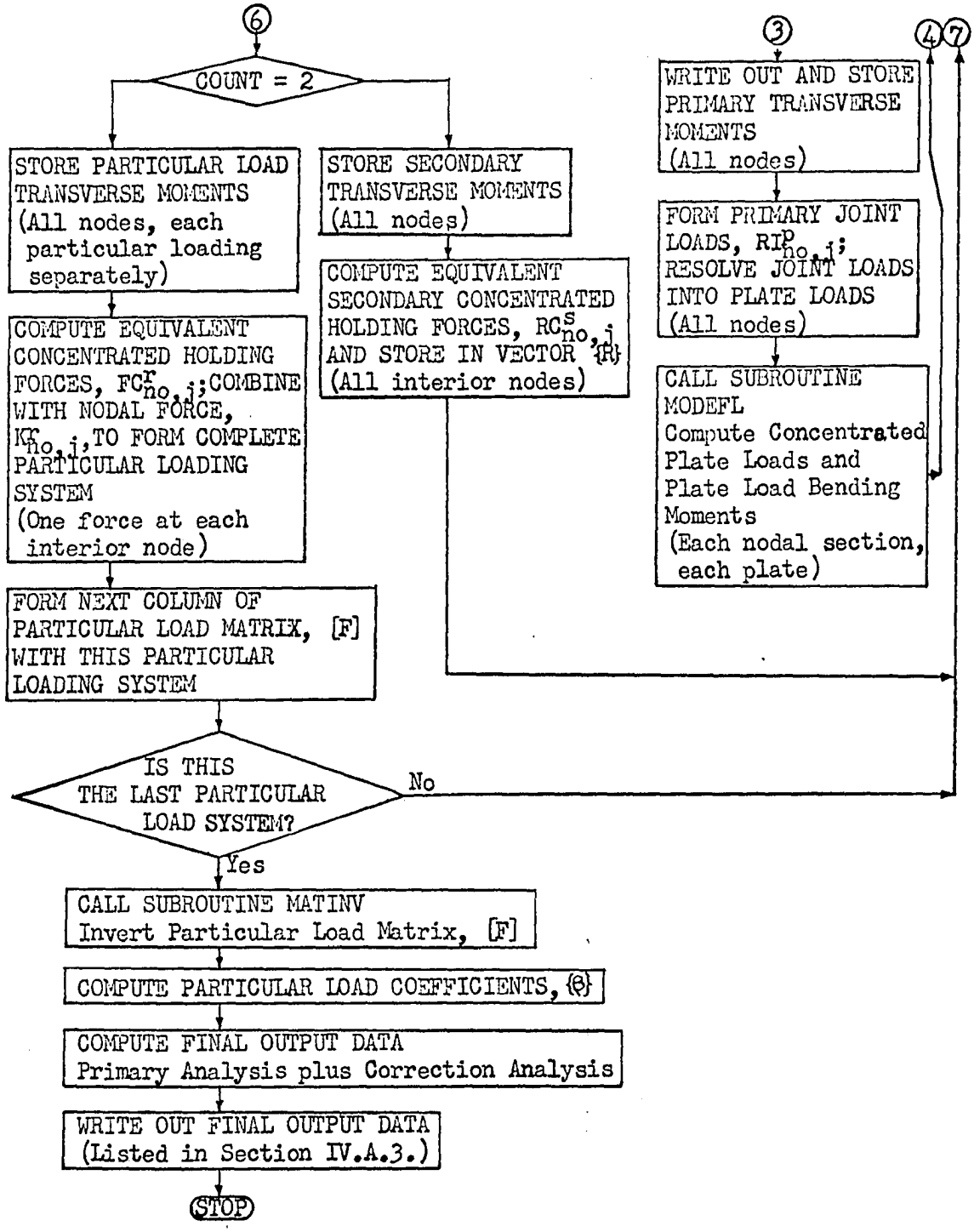

Fig. 38 (Continued)

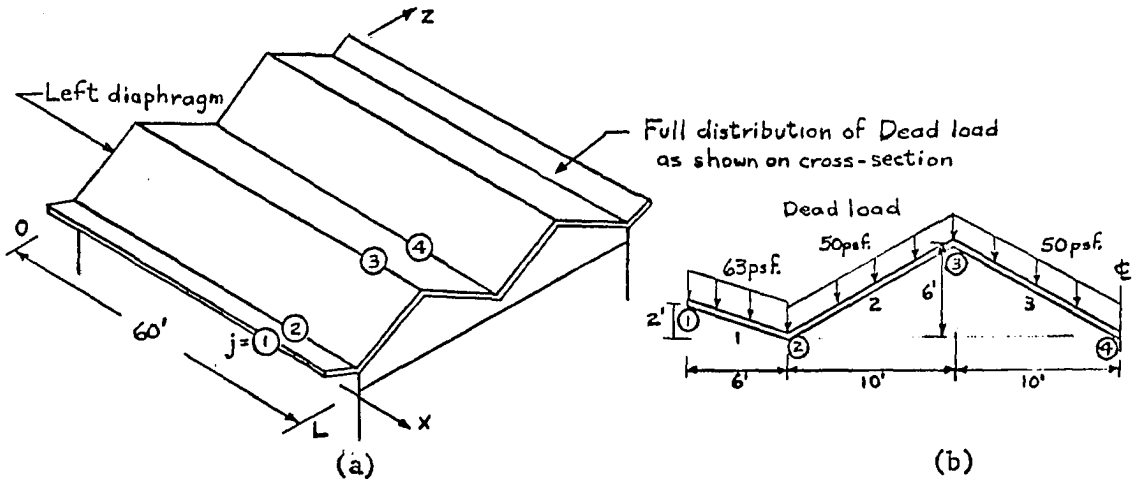

Fig. 39. Prismatic folded plate with similar loading

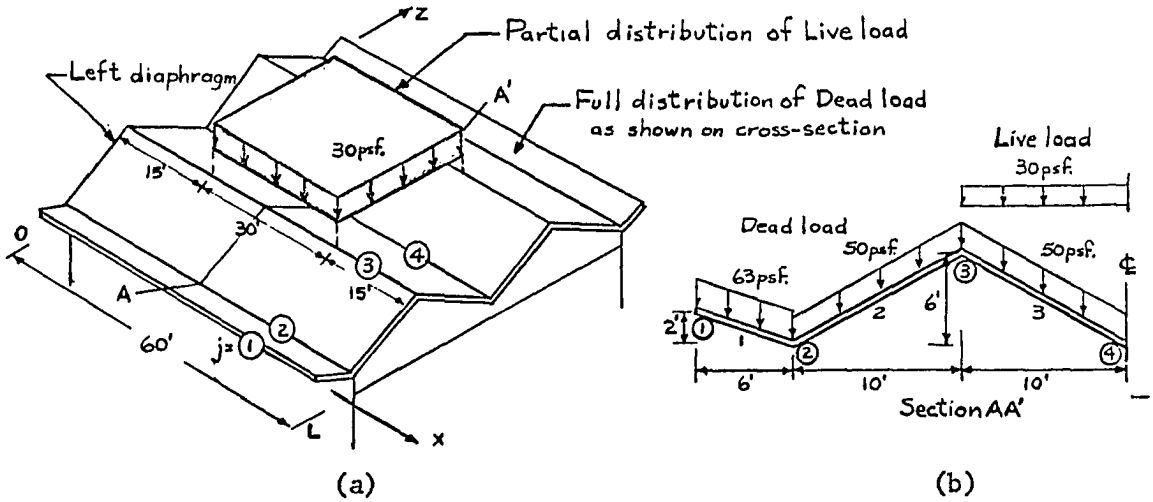

Fig. 40. Prismatic folded plate with non-similar loading

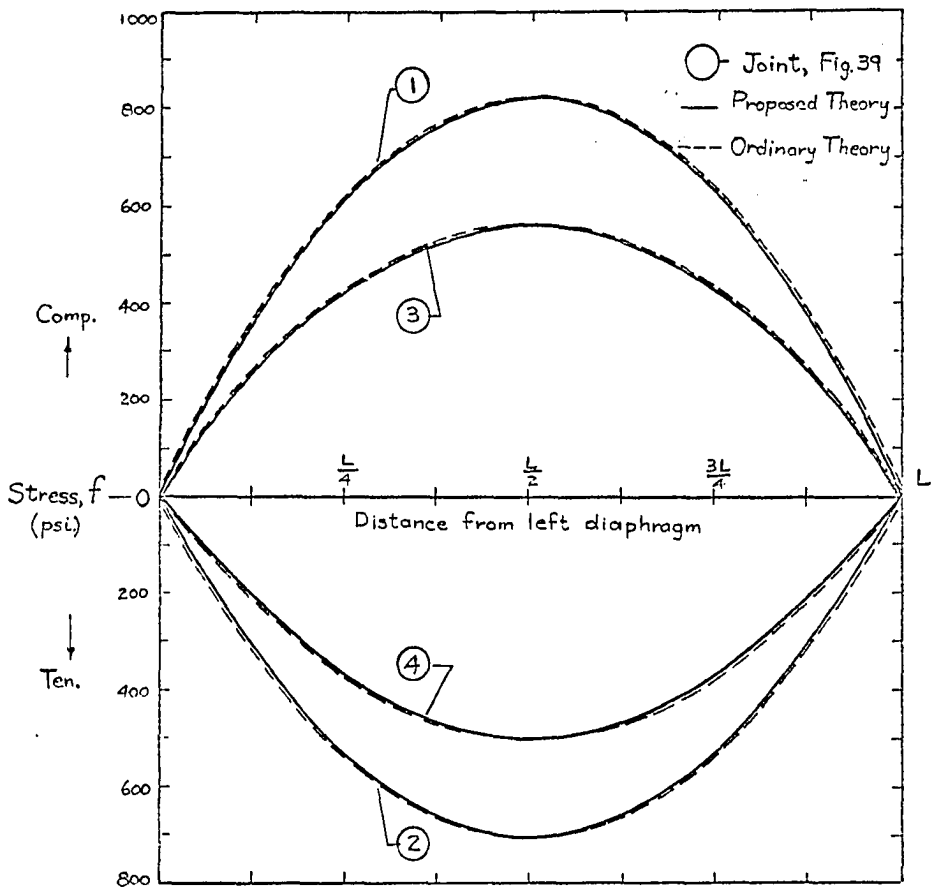

Fig. 41. Stress distributions along the joints of a prismatic folded plate with similar loading (Fig. 39)

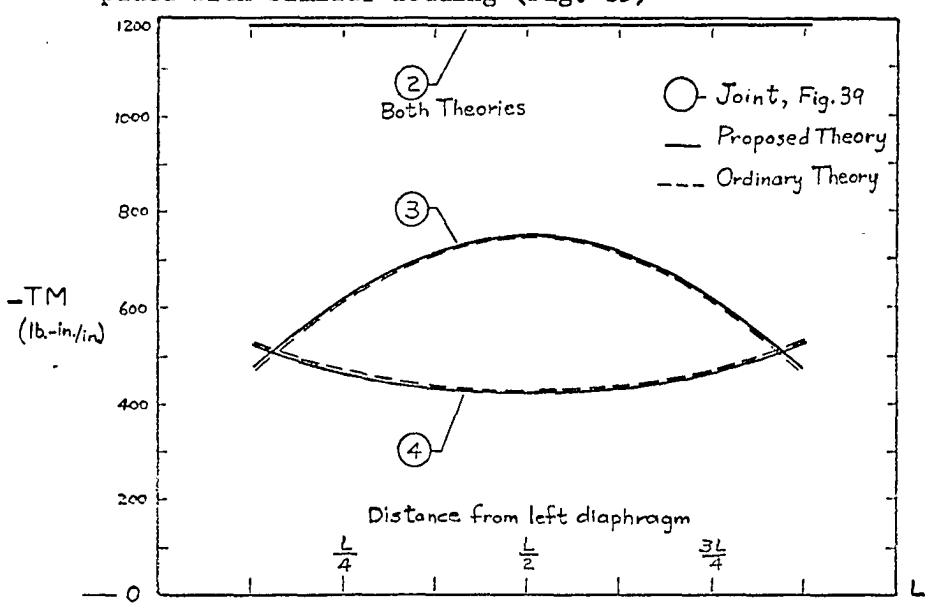

Fig. 42. Distribution of transverse moments along the joints of a prismatic folded plate with similar loading (Fig. 39)

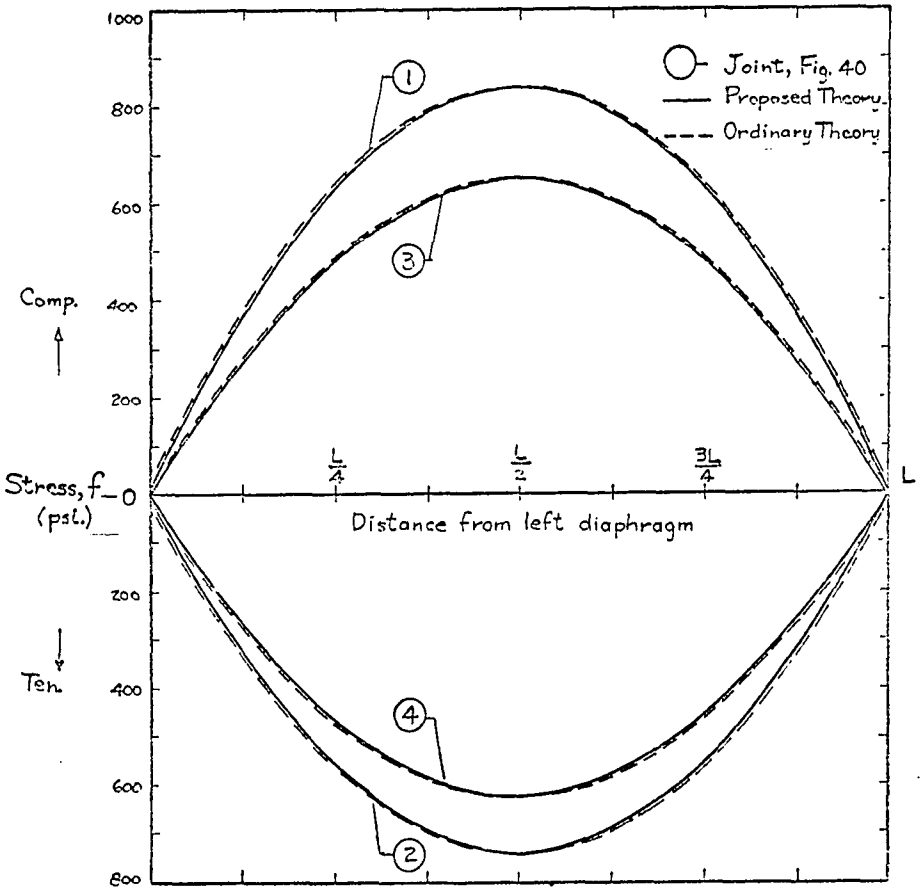

Fig. 43. Stress distributions along the joints of a prismatic folded plate with non-similar loading (Fig. 40)

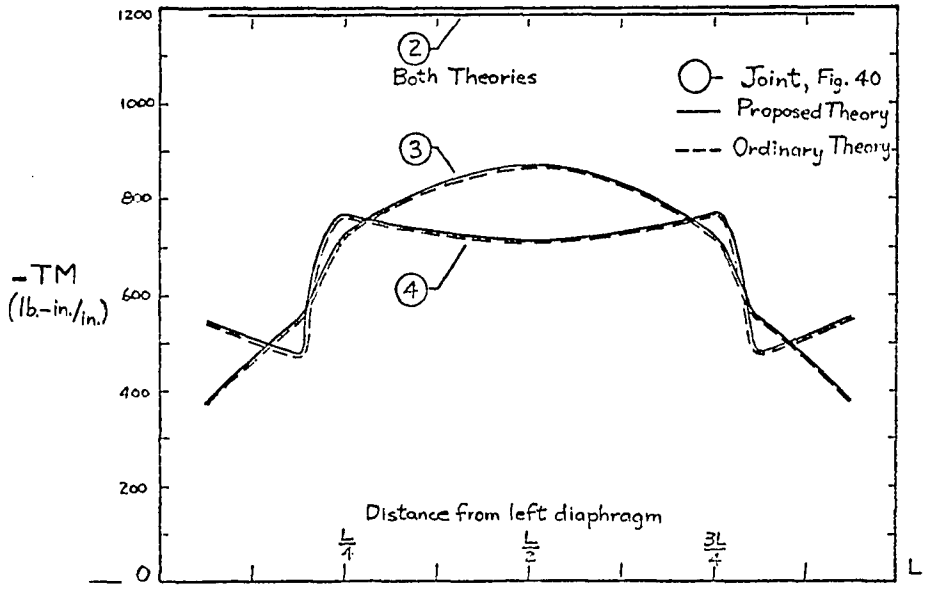

Fig. 44. Distribution of transverse moments along the joints of a prismatic folded plate with non-similar loading (Fig. 40)

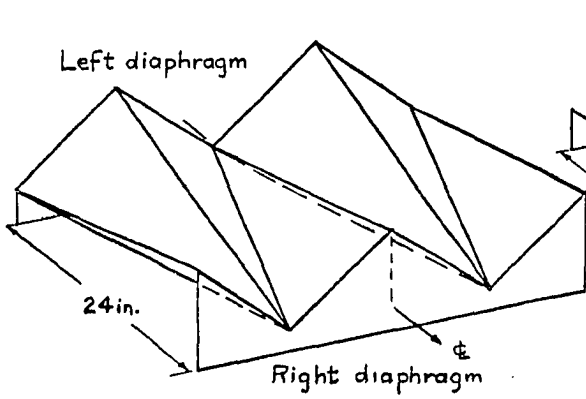

(a) Model 1

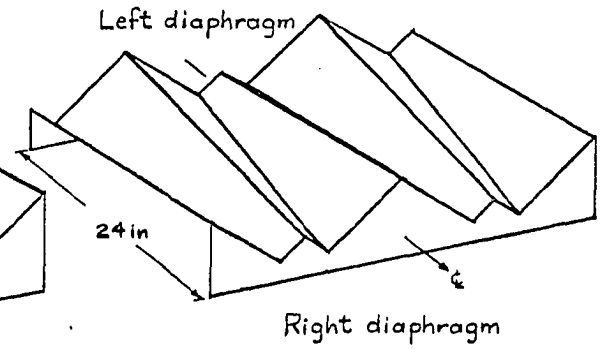

(b) Model 2

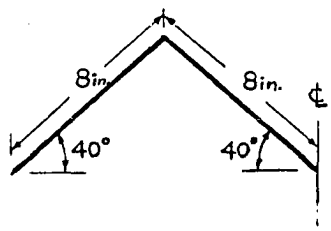

(c) Cross-section at left diaphragm of Model 1

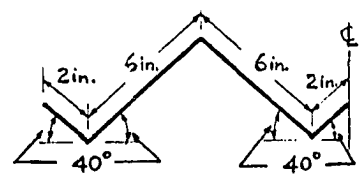

(e) Cross-section at left diaphragm of Model 2

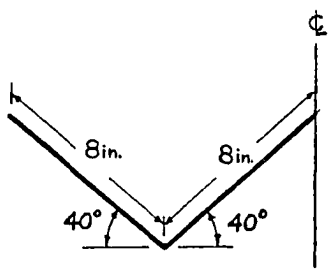

(d) Cross-section at right diaphragm of Model 1

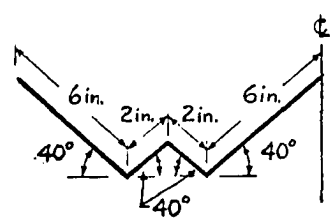

(f) Cross-section at right diaphragm of Model 2

Fig. 45. Geometry of the model structures

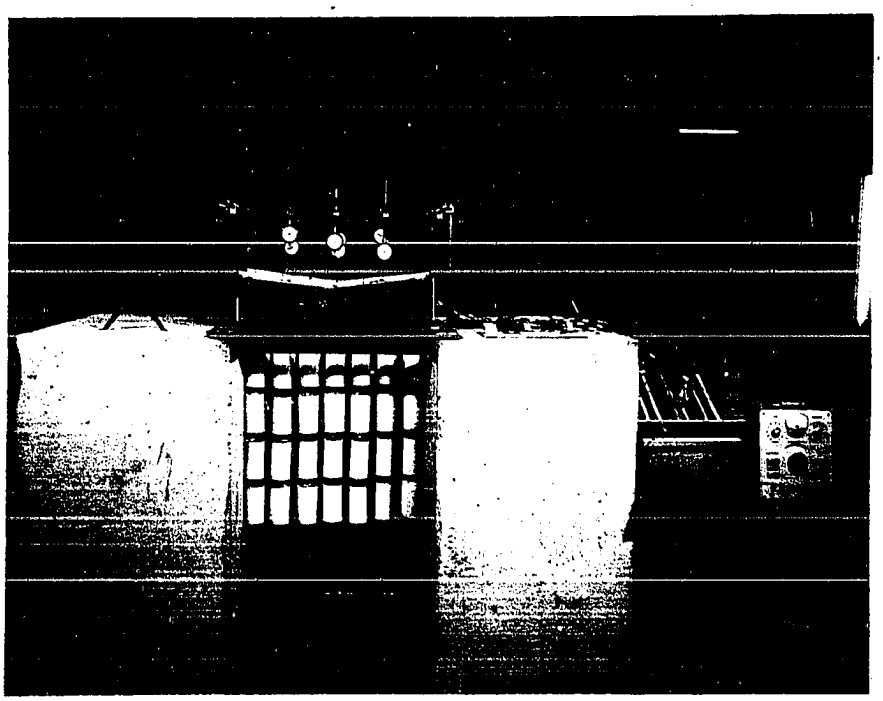

Fig. 46. Test apparatus

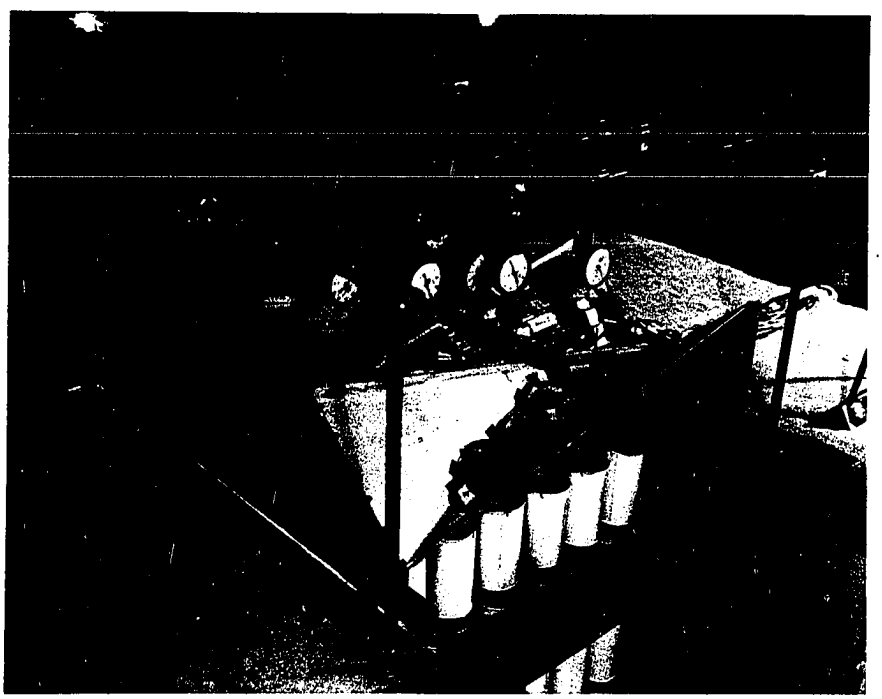

Fig. 47. Model 1, load and support systems

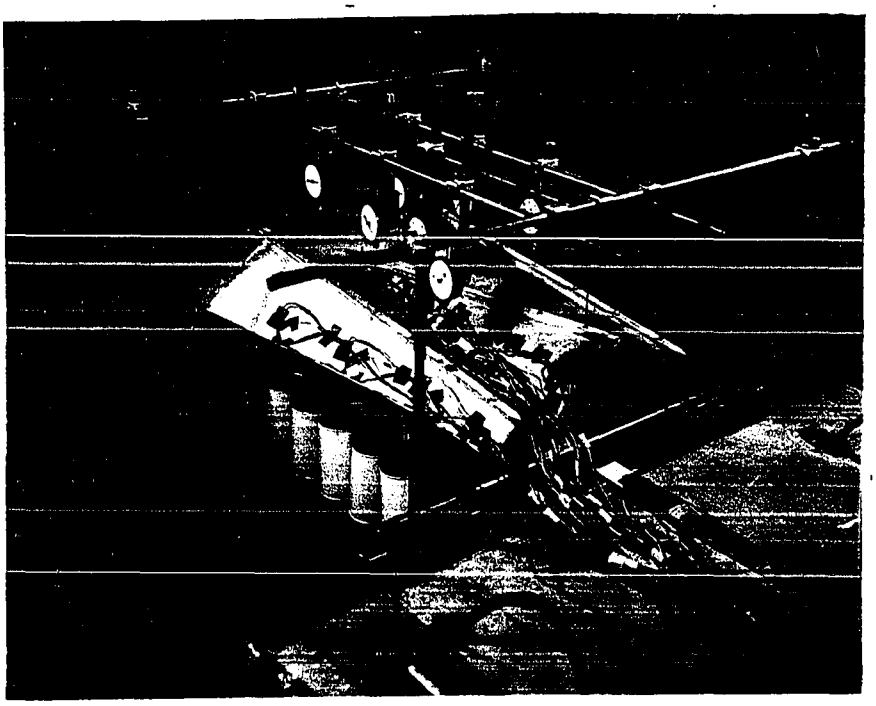

Fig. 48. Model 2 and the deflection frame

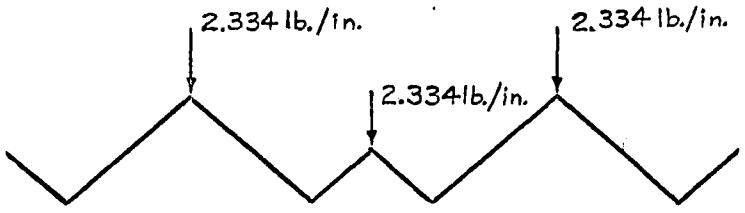

(Intensities based on the horizontal projection of the ridges)

Fig. 49. Increment of joint load applied to both models

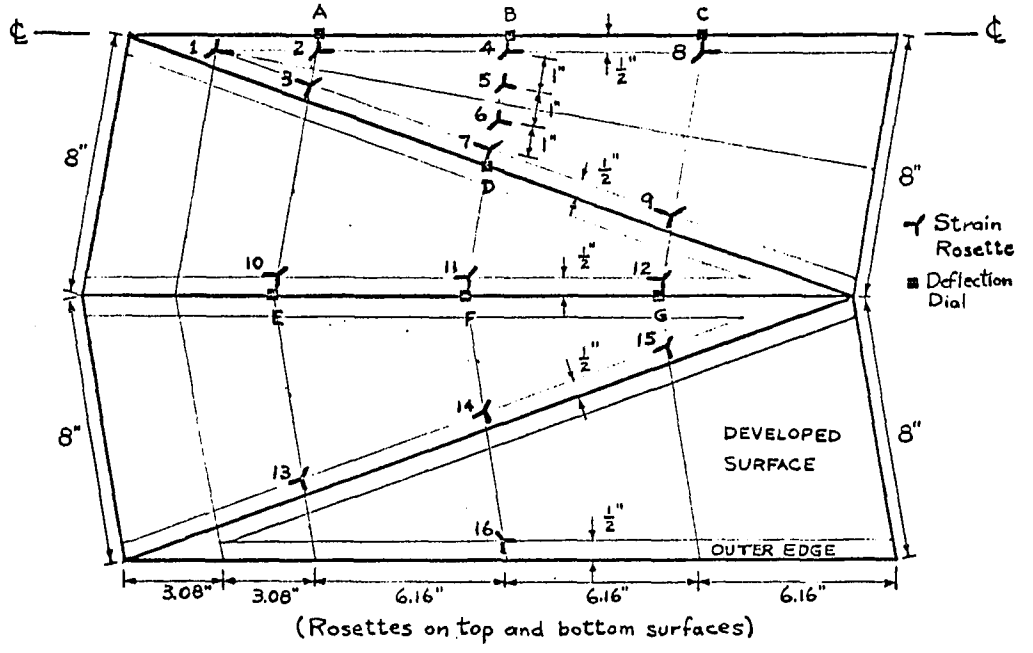

Fig. 50. Locations of strain rosettes and deflection dials on Model 1

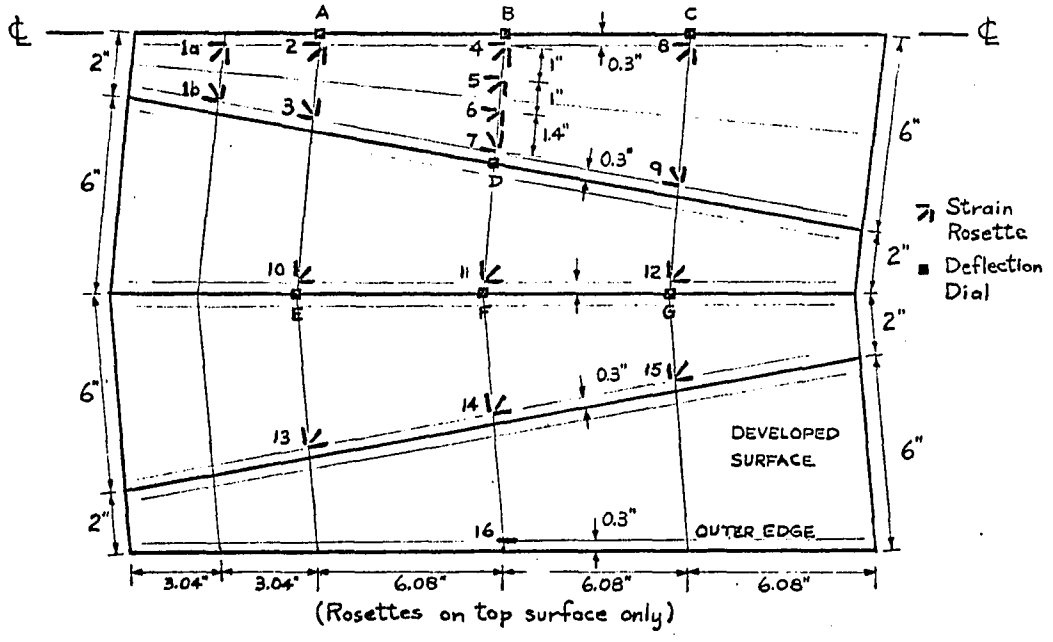

Fig. 51. Locations of strain rosettes and deflection dials on Model 2

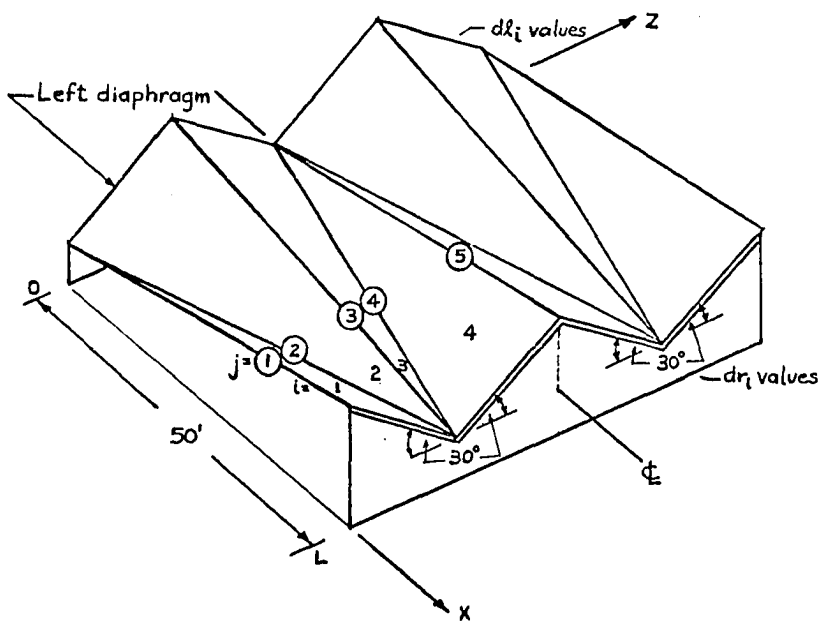

ω_{DL} = 75 lbs./ft²
ω_{LL} = 30 lbs./ft²
t_i = 6 in
L_{na_i} = 50.56 ft.

Plate	$d\ell_i$ (ft.)	dr_i (ft.)
1	0	15.0
2	15.0	0
3	15.0	0
4	0	15.0

Fig. 52. Structure used in the study of the solution accuracy of the proposed theory as it is affected by the number of nodal sections

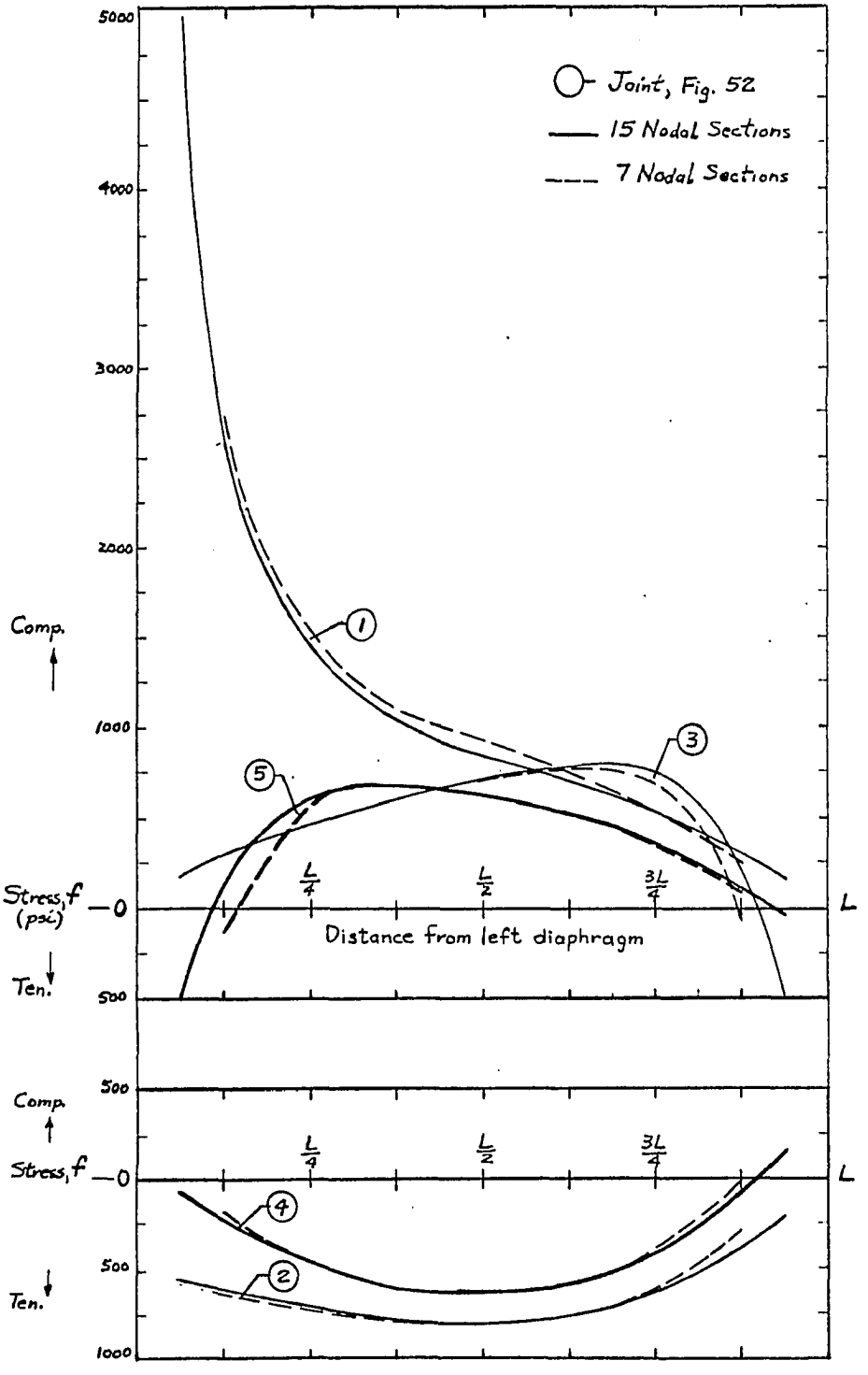

Fig. 53. Stress distributions in the study of the accuracy of a solution as affected by the number of nodal sections

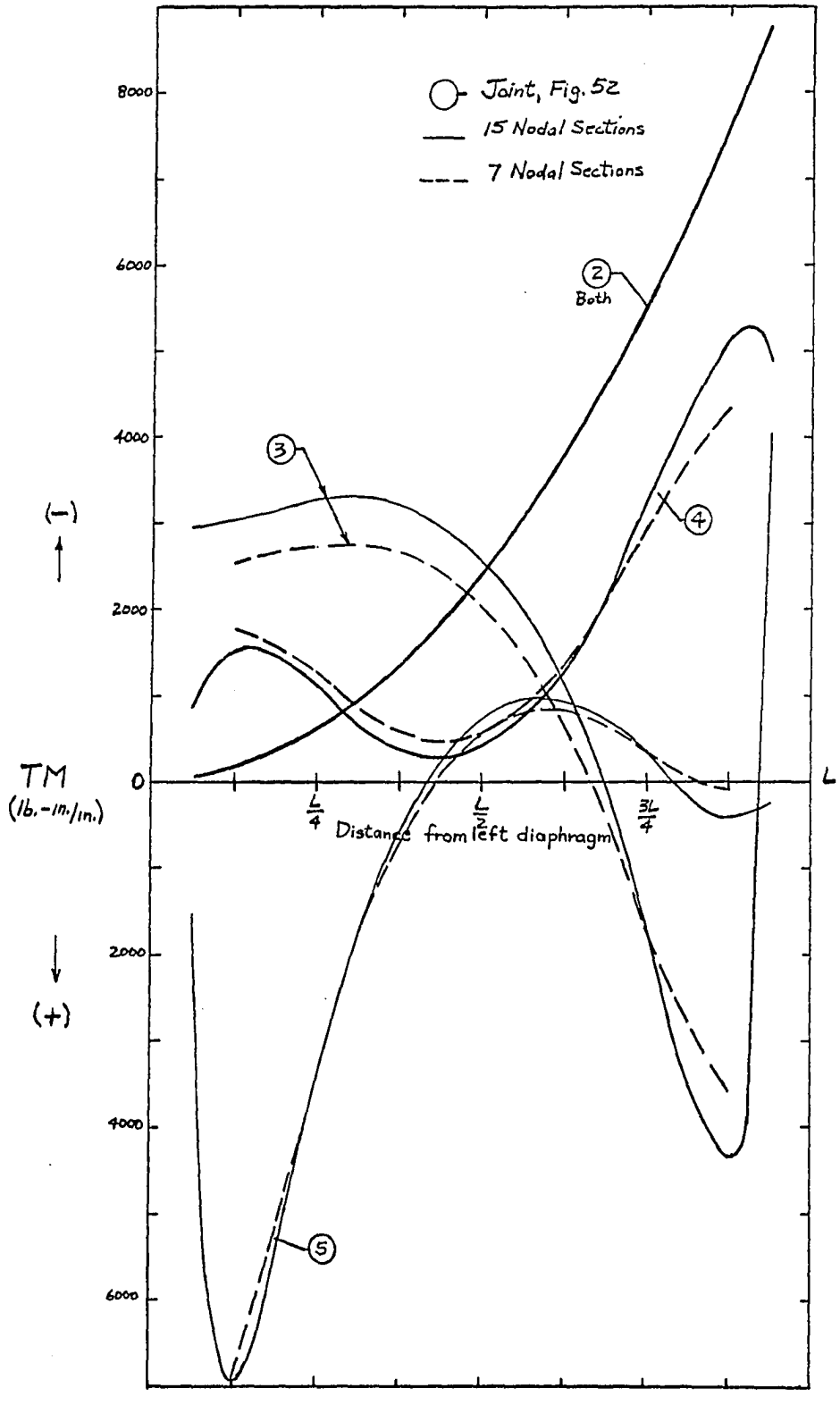

Fig. 54. Transverse moments in the study of the accuracy of a solution as affected by the number of nodal sections

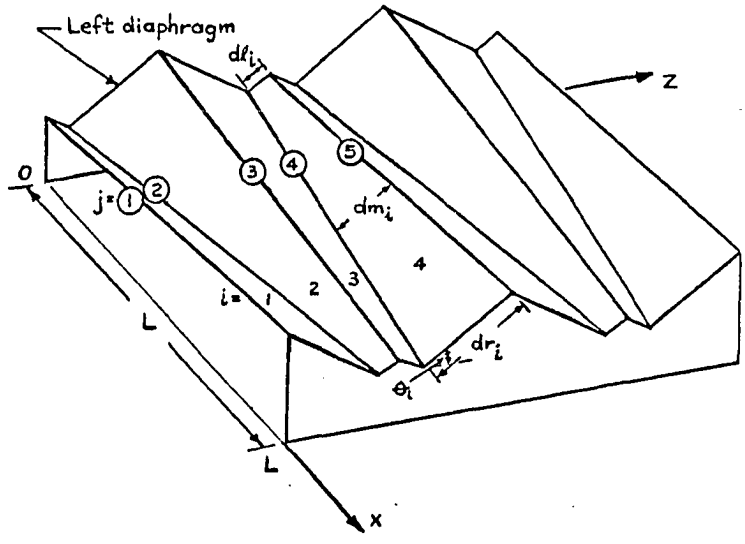

Constant Parameters

$L = 50$ ft.

$t_i = 6$ in.

$dm_i = 7.5$ ft.

$\omega_{DL_i} = 75$ lbs./ft.^{2}

$\omega_{LL_i} = 30$ lbs./ft.^{2}

All plates have the same shape in each case considered

(a) Structural plan and loading conditions

(b) Variations in Plate taper

($\theta_i = 30° = $ Constant)

Case	$d\ell_i$ (ft.)	dr_i (ft.)	L_{na_i} (ft.)	α_i (approx.) (degrees)	Ω_i
1	0.0	15.00	50.56	8.5	0.30
2	1.25	13.75	50.40	7.0	0.25
3	2.50	12.50	50.25	5.7	0.20
4	3.75	11.25	50.14	4.2	0.15
5	7.50	7.50	50.00	0.0	0.0

(c) Variations in plate slope

($\Omega_i = 0.25 = $ Constant)

Case	θ_i (degrees)
1	22.5
2	30.0
3	37.5
4	45.0

Fig. 55. Structure used in the study of the effects of taper and slope

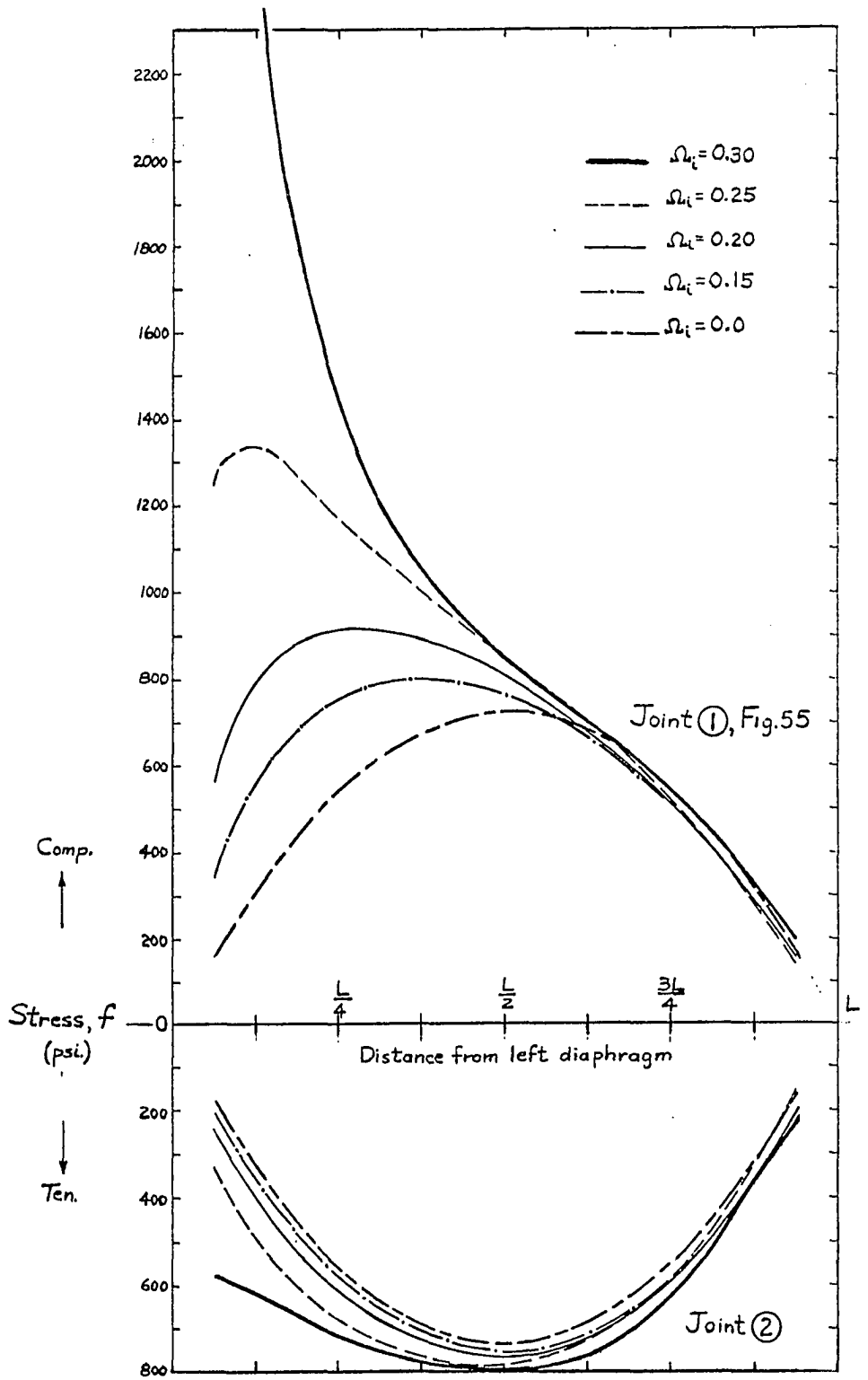

Fig. 56. Stress distributions in the study of the effects of taper

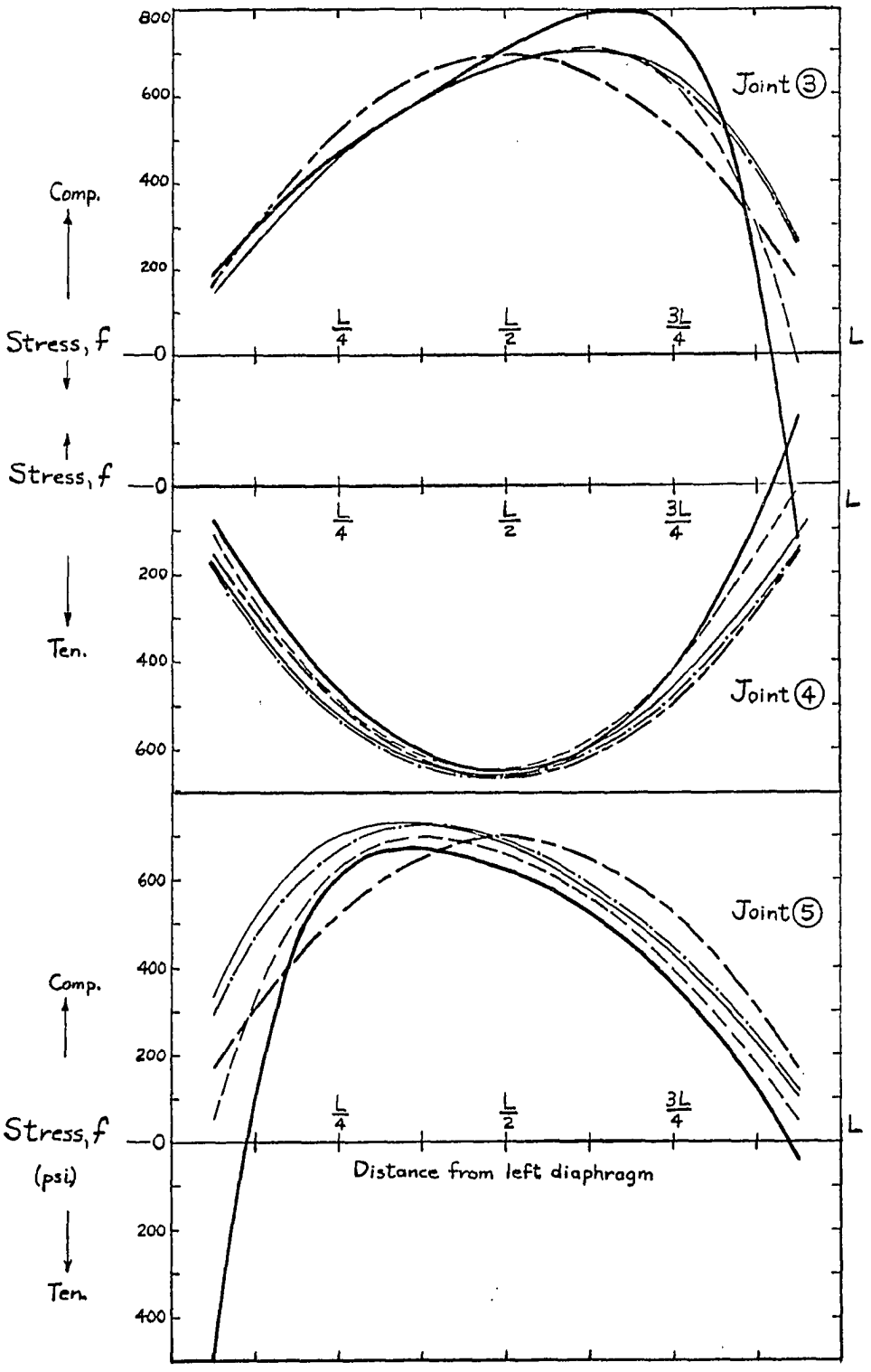

Fig. 56 (Continued)

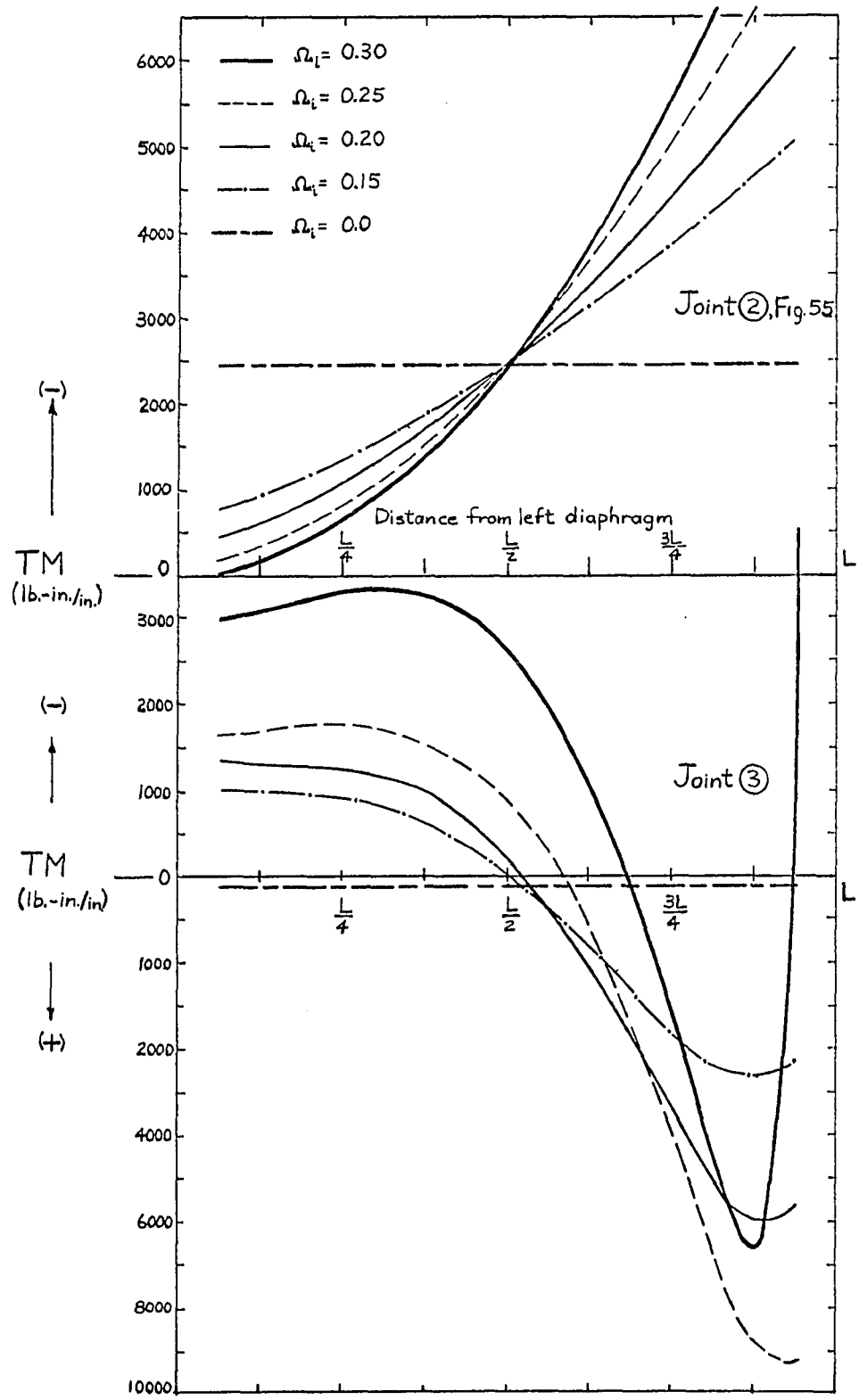

Fig. 57. Distributions of transverse moments in the study of the effects of taper

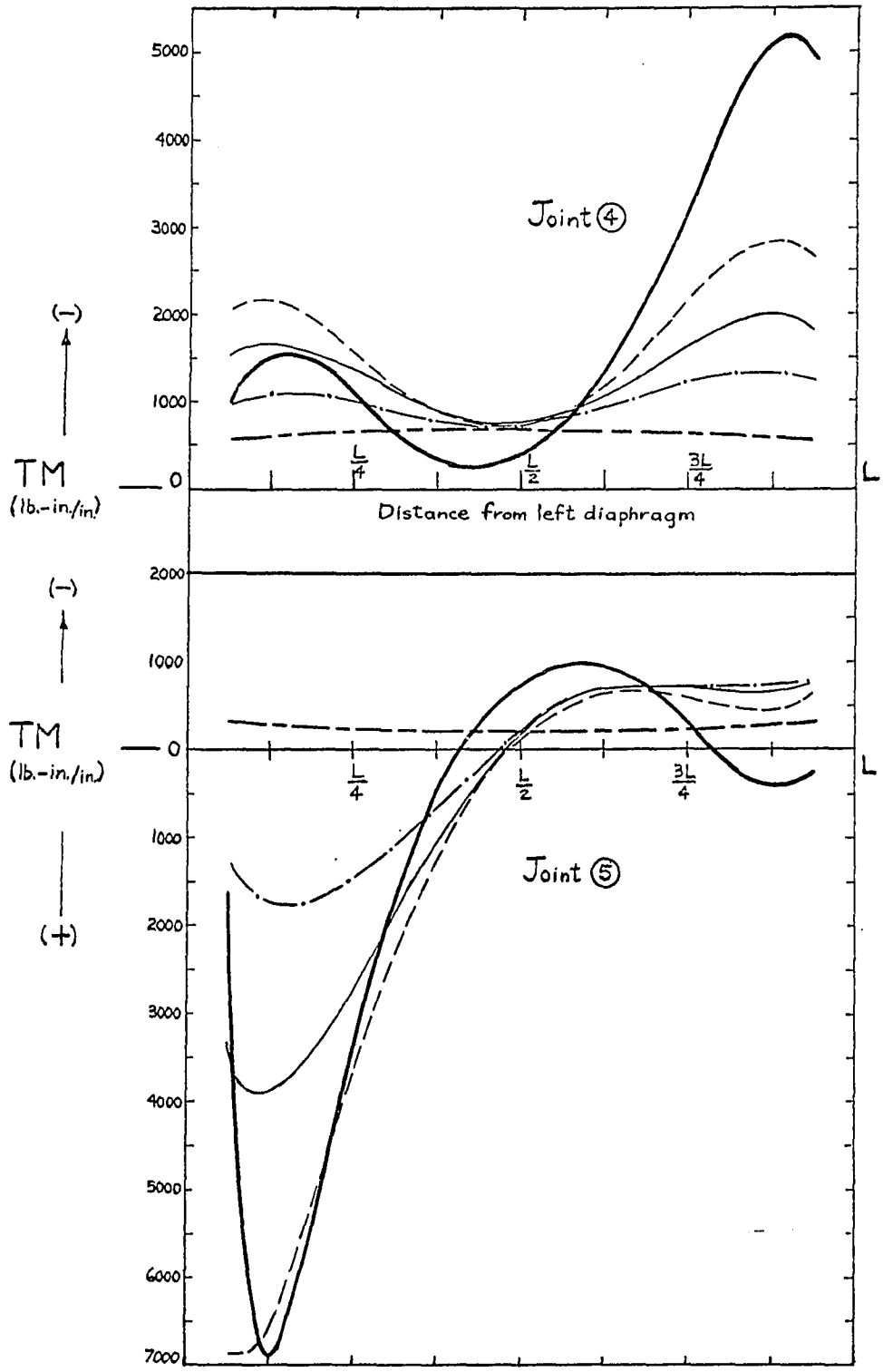

Fig. 57 (Continued)

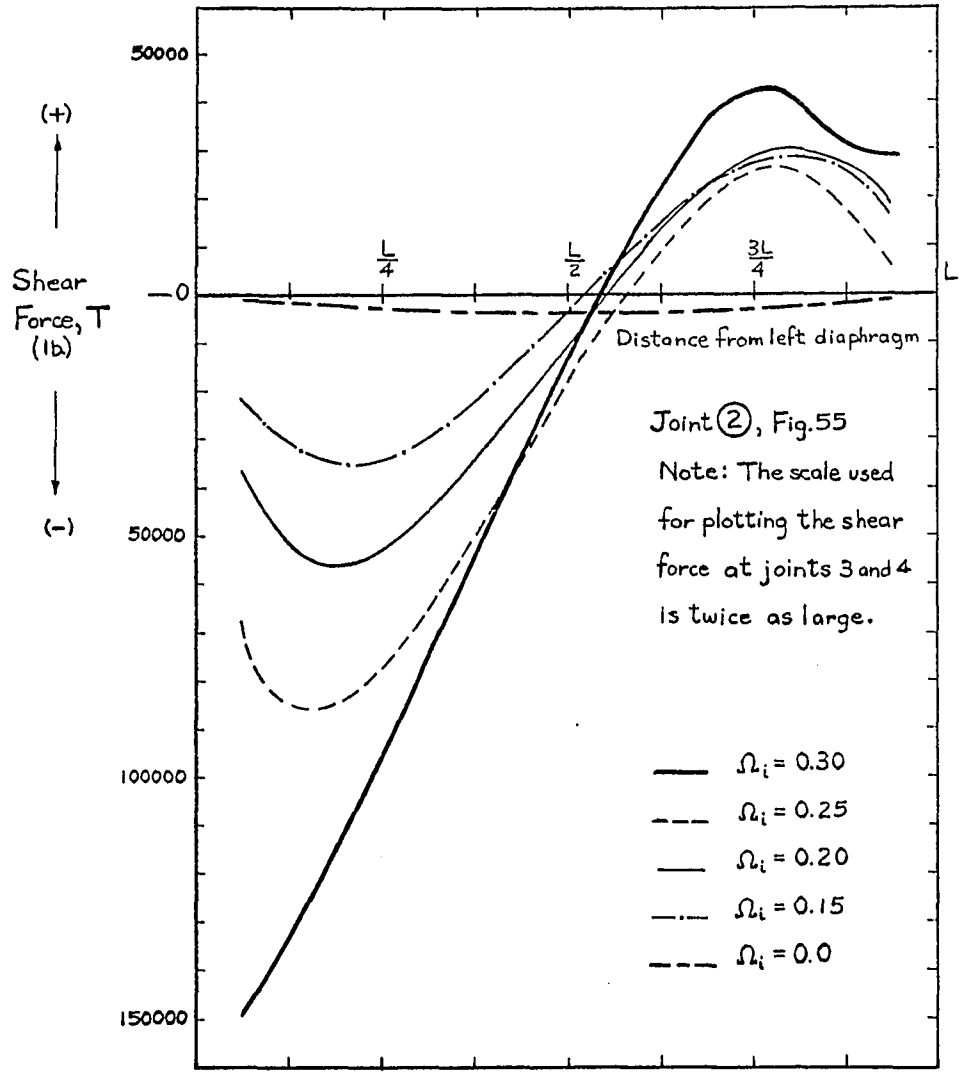

Fig. 58. Shear force distributions in the study of the effects of taper

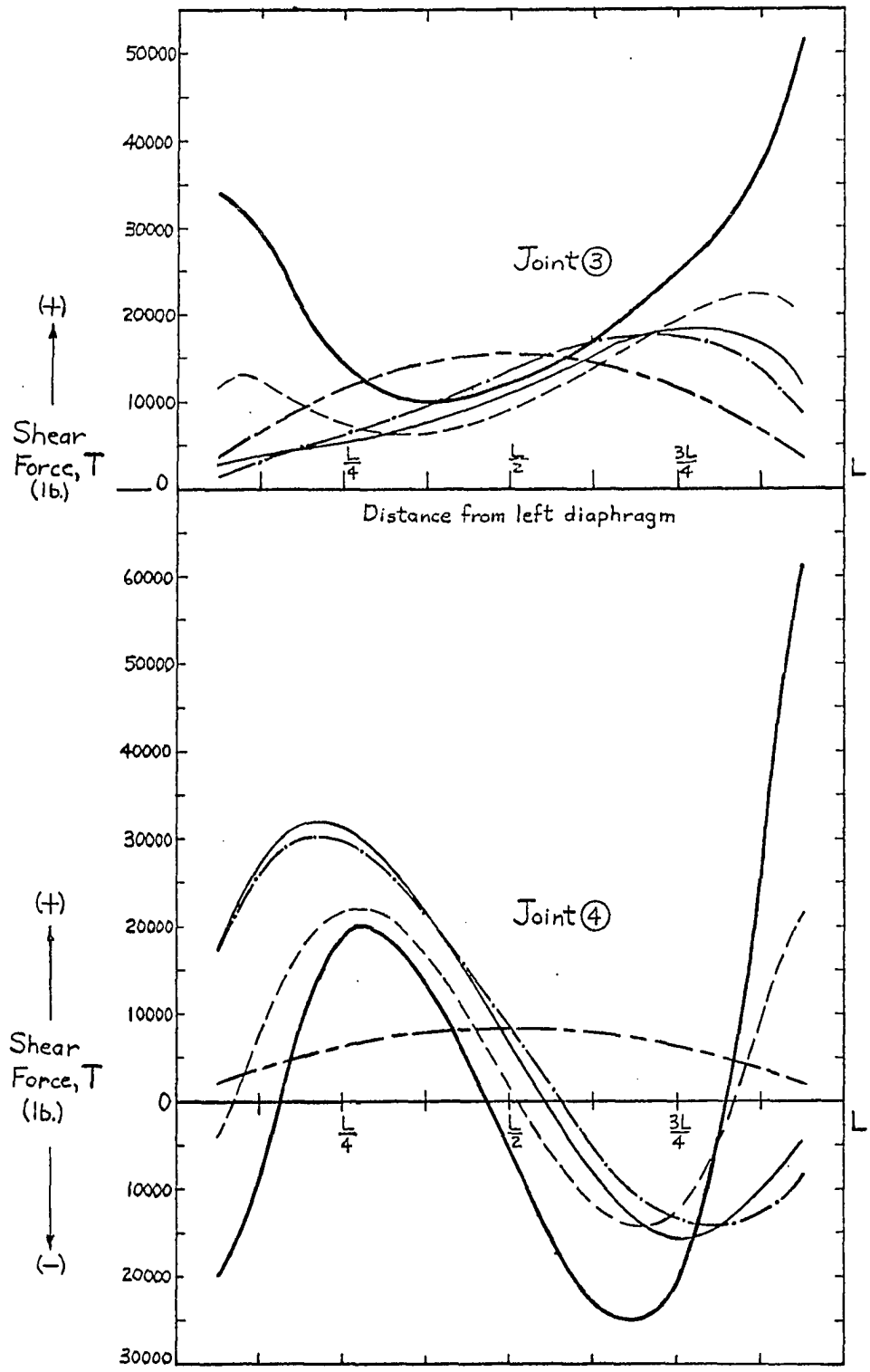

Fig. 58 (Continued)

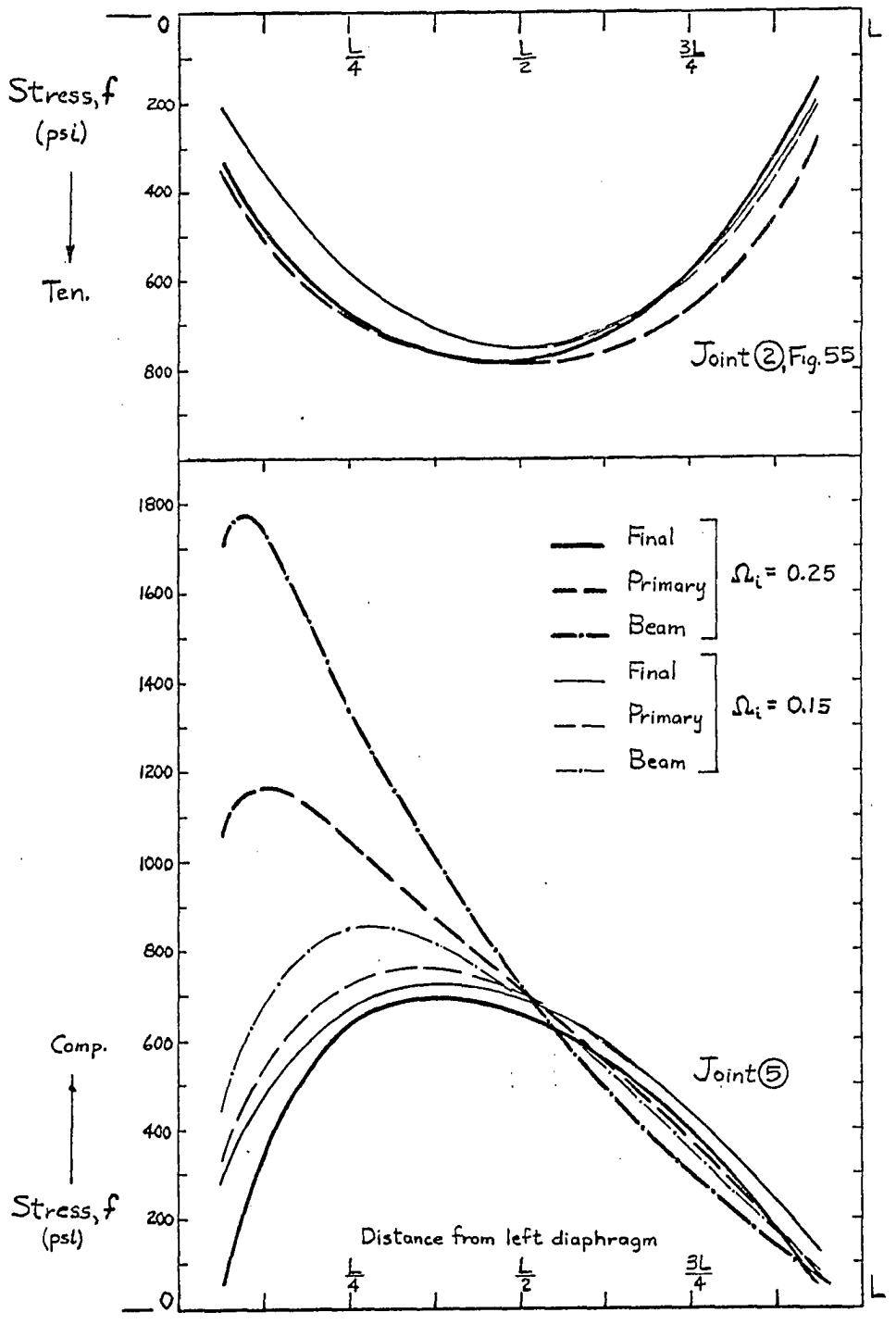

Fig. 59. Primary and final stress distributions in the study of the effects of taper

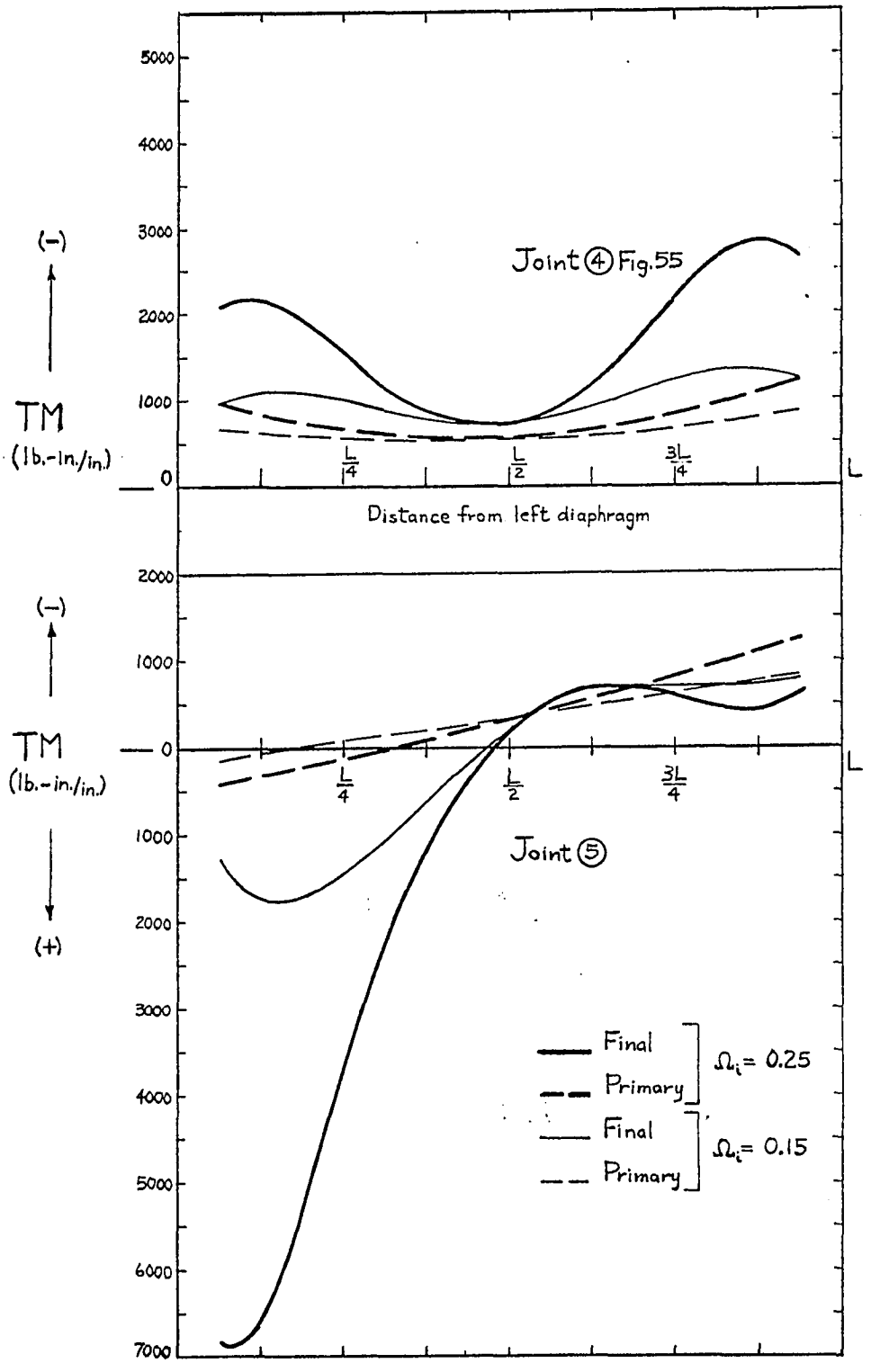

Fig. 60. Primary and final distributions of transverse moments in the study of the effects of taper

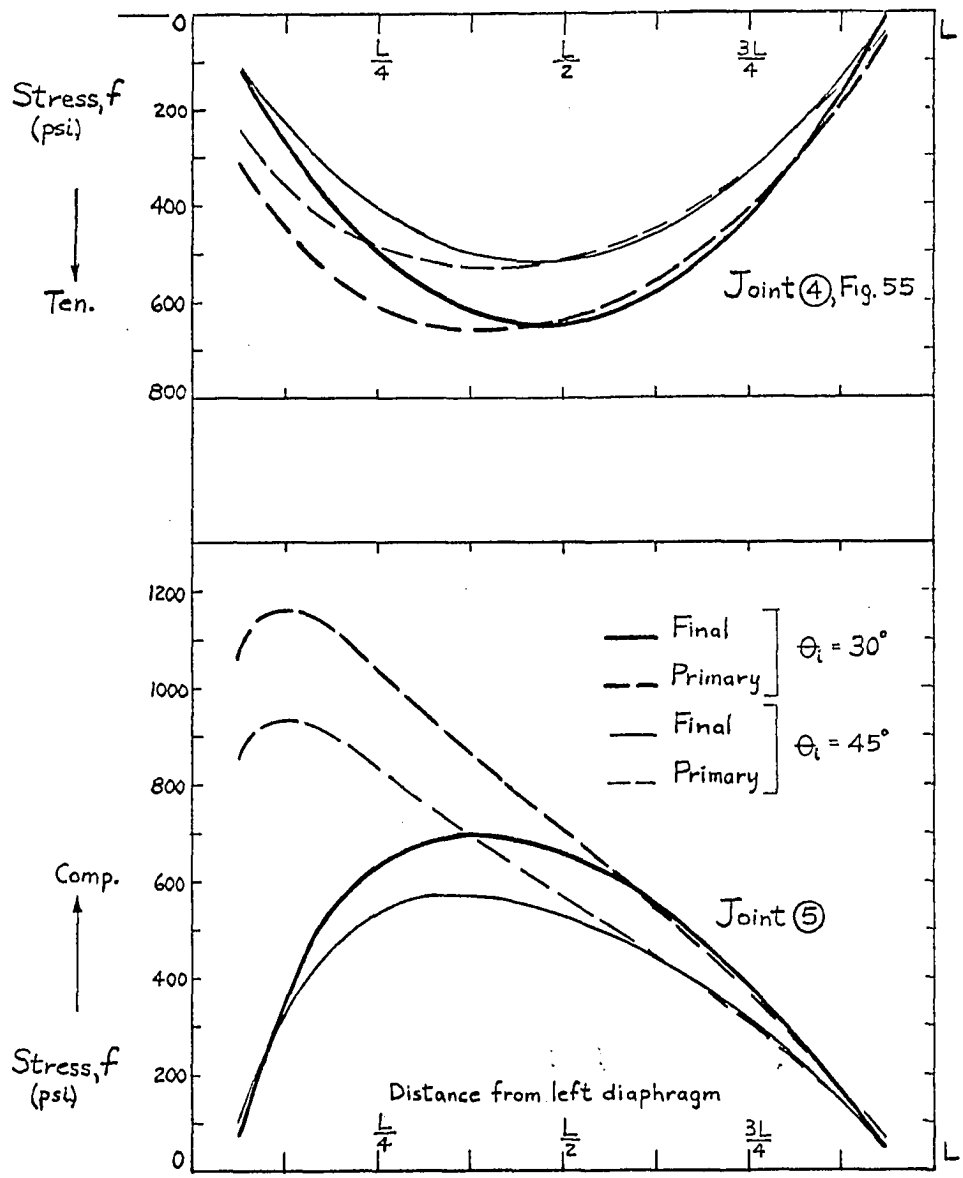

Fig. 61. Primary and final stress distributions in the study of the effects of slope

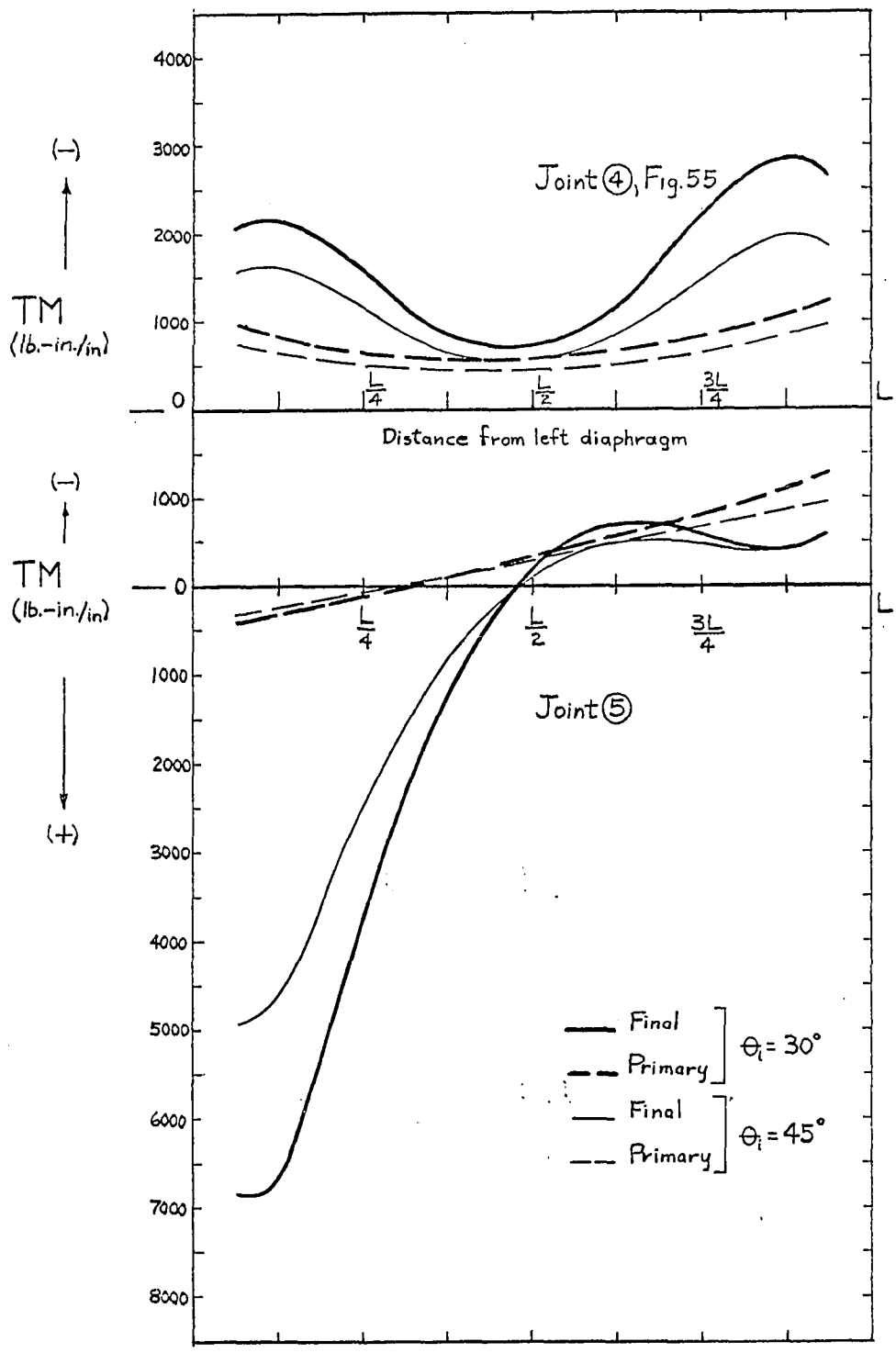

Fig. 62. Primary and final distributions of transverse moments in the study of the effects of slope

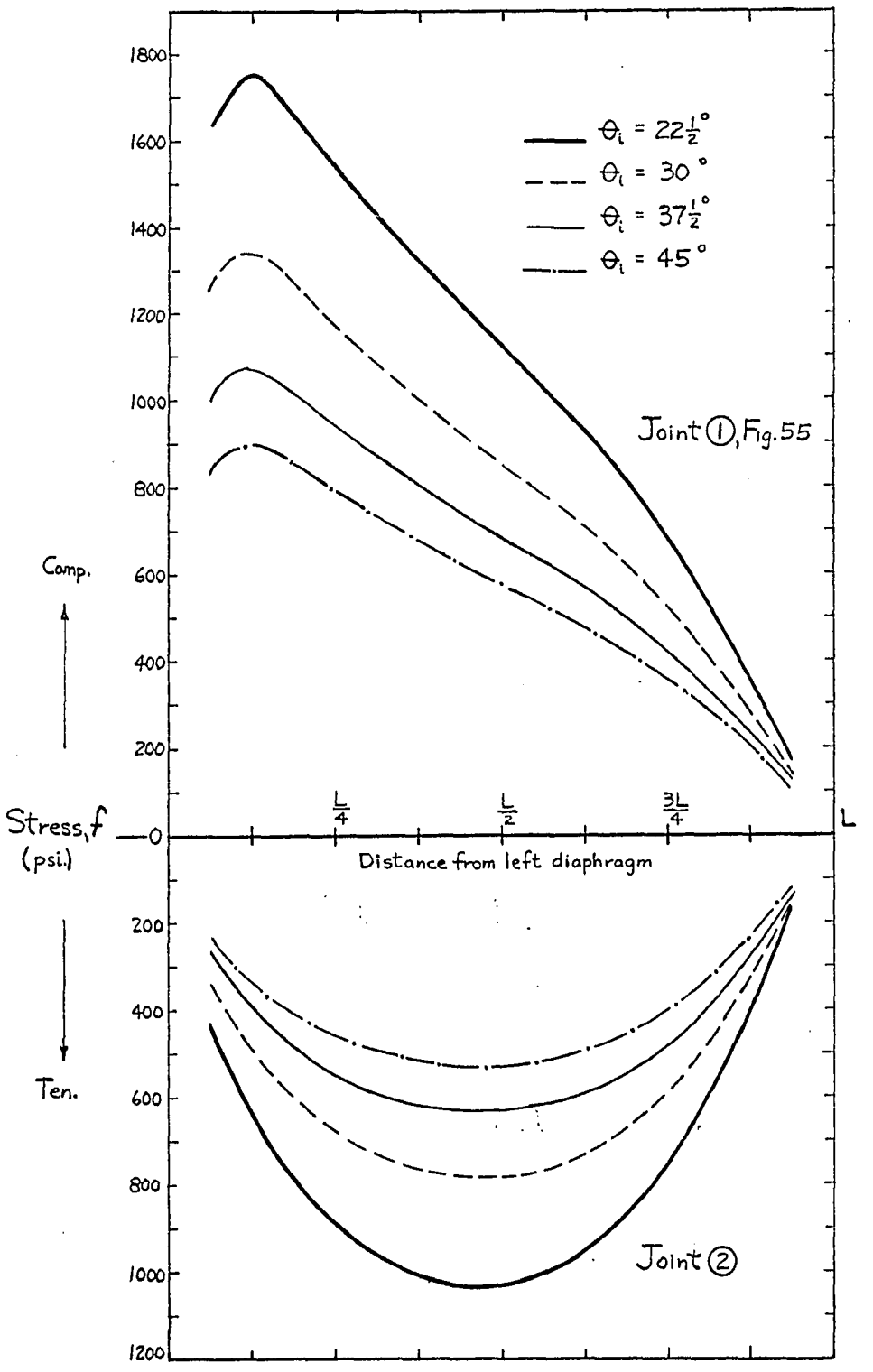

Fig. 63. Stress distributions in the study of the effects of slope

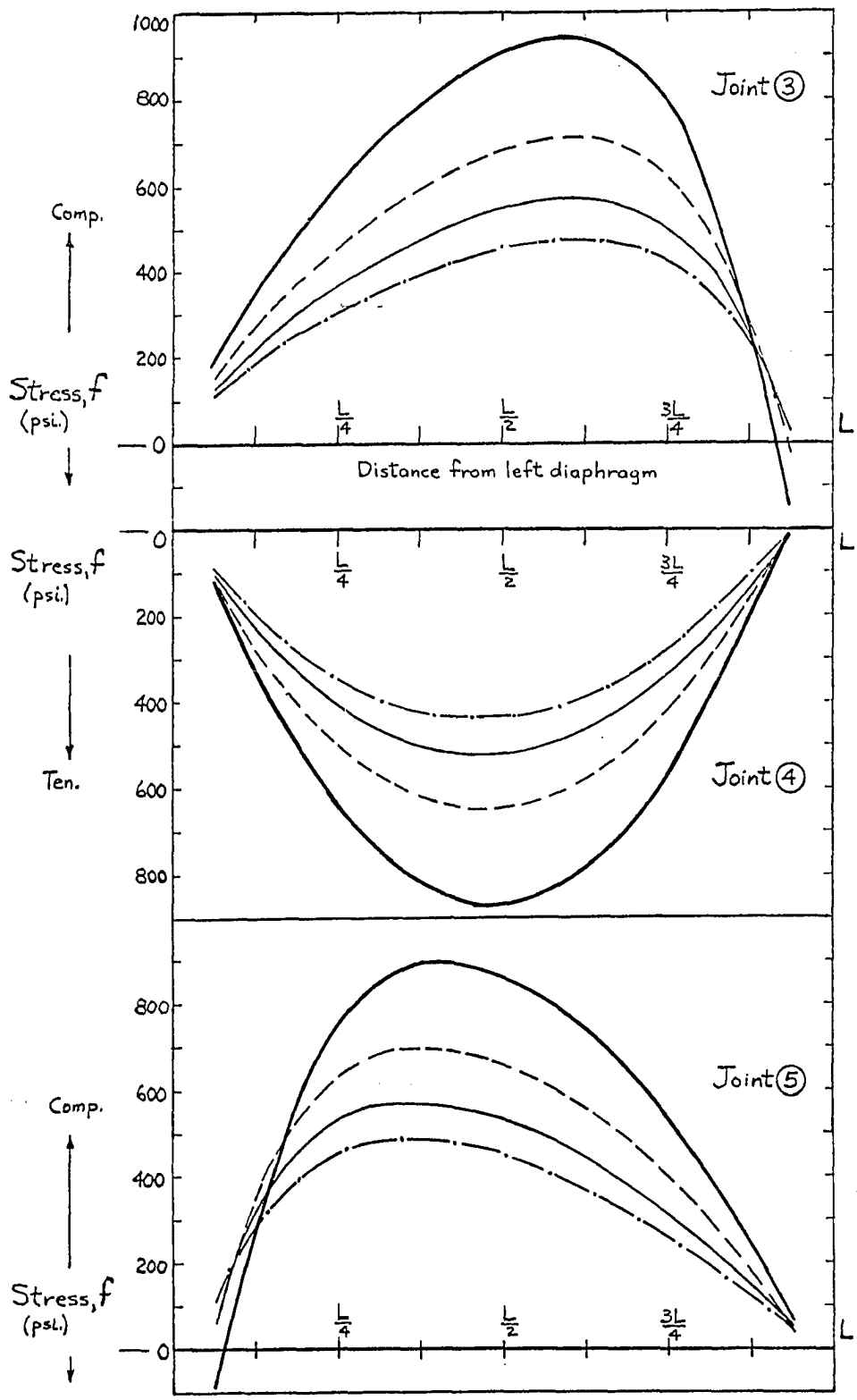

Fig. 63 (Continued)

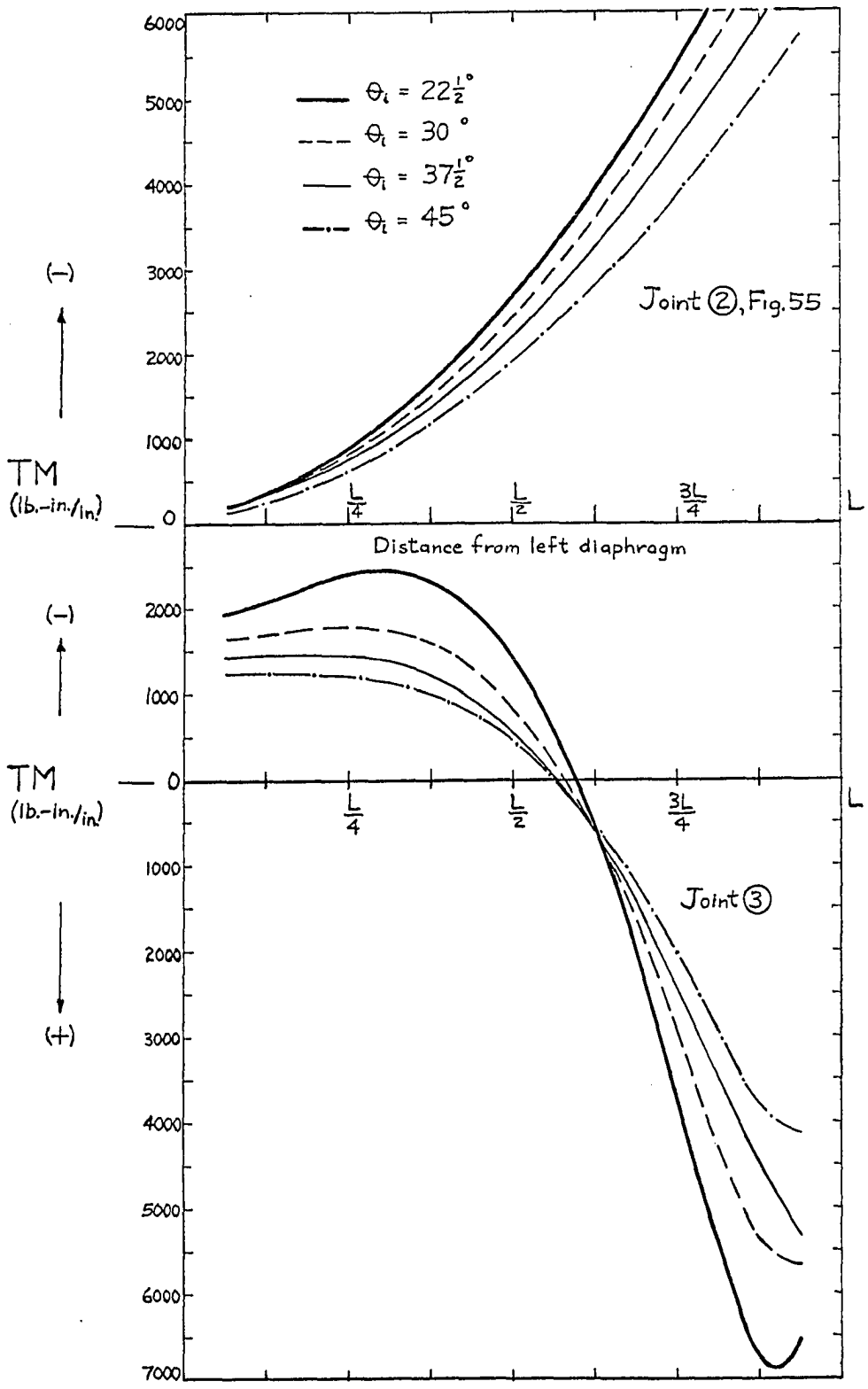

Fig. 64. Distributions of transverse moments in the study of the effects of slope

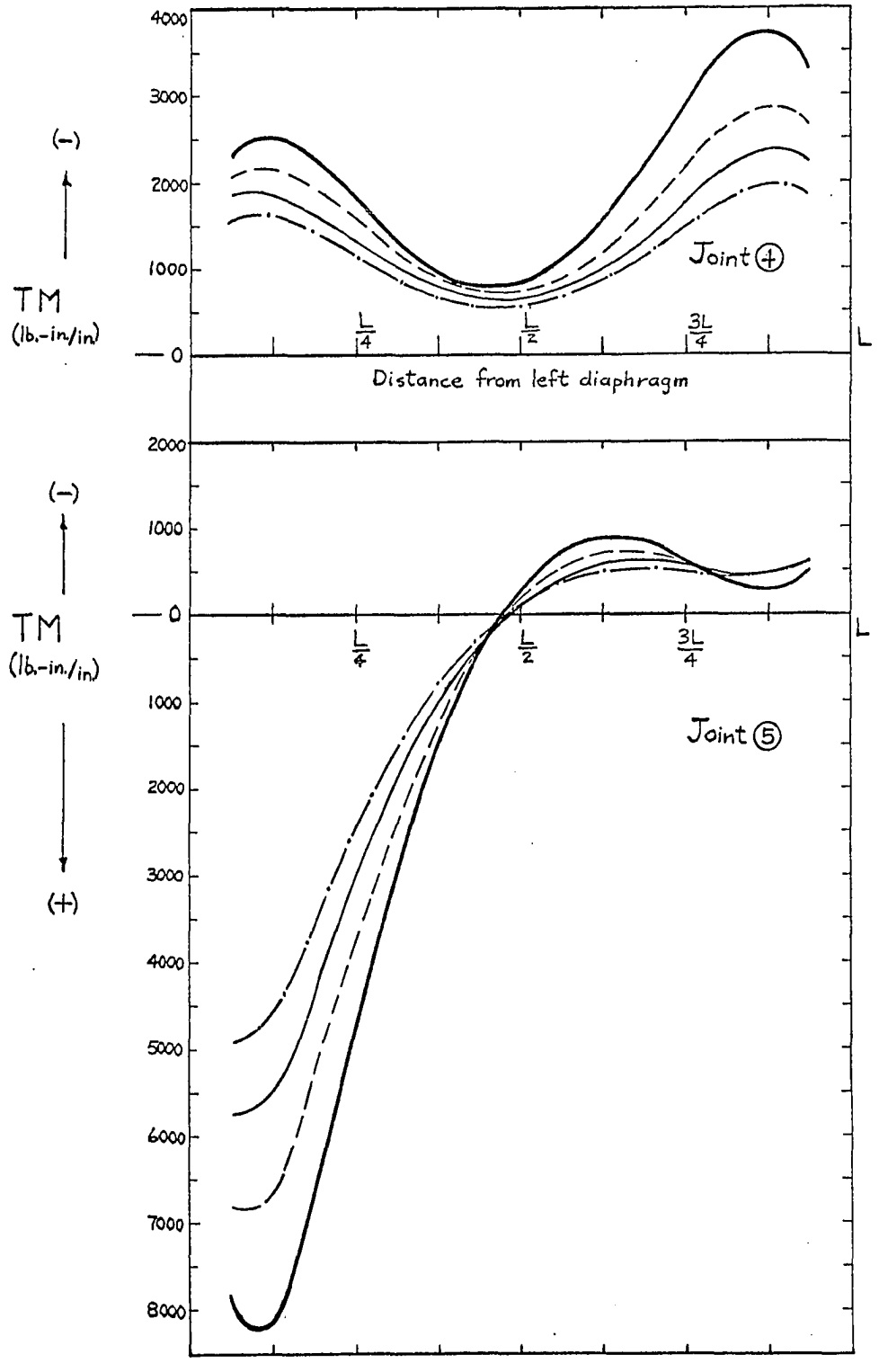

Fig. 64 (Continued)

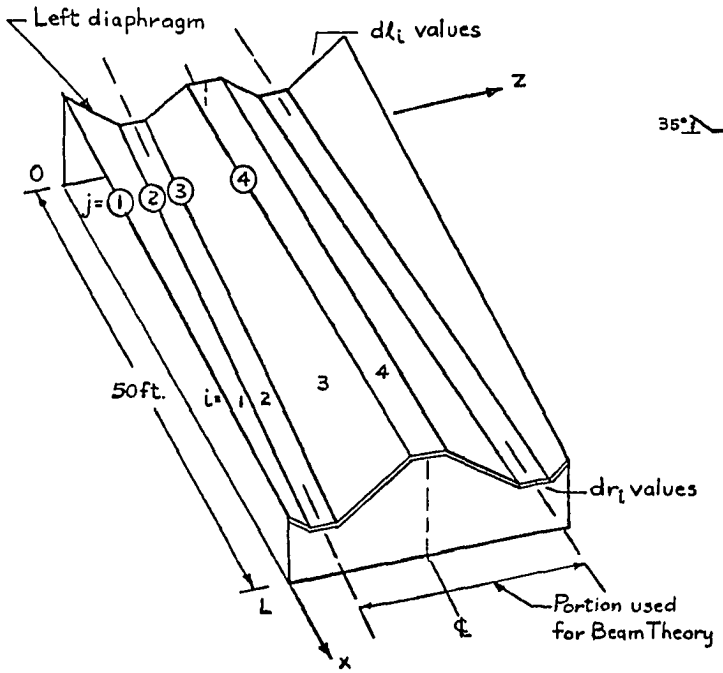

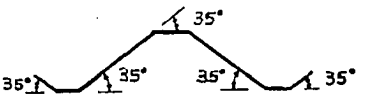

ω_{DL_i} = 56.3 lbs./ft.²
ω_{LL_i} = 20.0 lbs./ft.²
t_i = 4.5 in

Plate	$d\ell_i$ (ft.)	dr_i (ft.)	Lna_i (ft.)
1	7.5	2.5	50.06
2	3.0	3.0	50.17
3	5.0	10.0	50.06
4	4.0	4.0	50.08

Fig. 65. Structure No. 1 used in the study of cross-sectional form

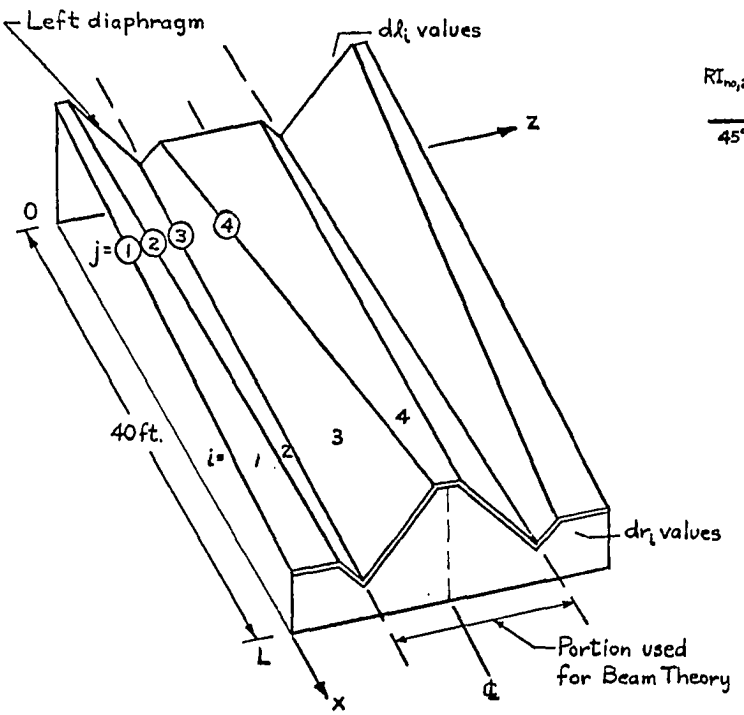

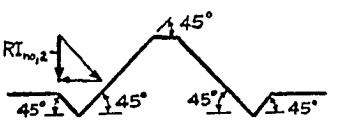

ω_{DL_i} = 50 lbs./ft.²
ω_{LL_i} = 20 lbs./ft.²
t_i = 4 in.

Plate	$d\ell_i$ (ft.)	dr_i (ft.)	Lna_i (ft.)
1	1.0	4.5	40.34
2	9.0	2.0	40.09
3	2.0	9.0	40.09
4	9.0	2.0	40.30

Fig. 66. Structure No. 2 used in the study of cross-sectional form

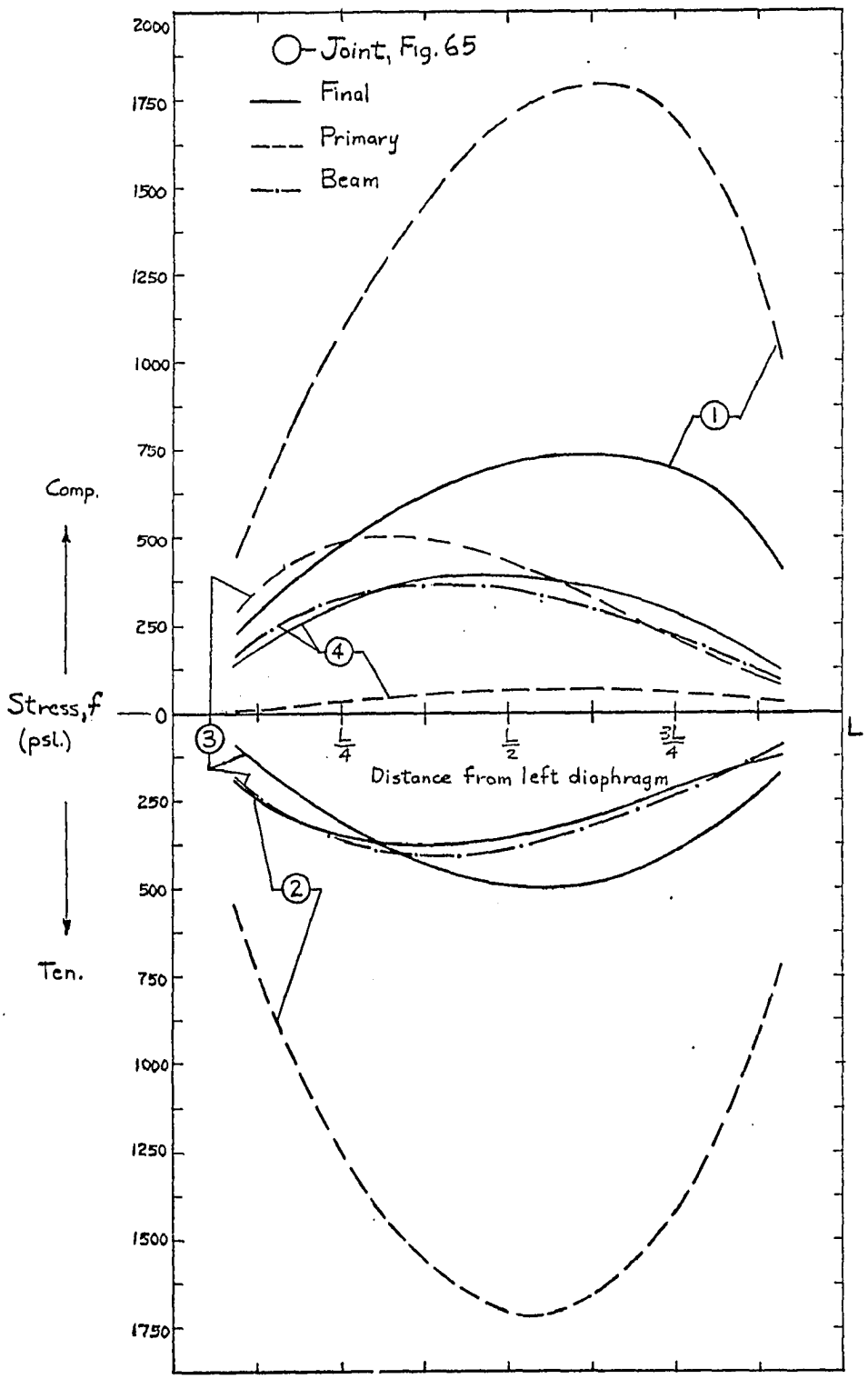

Fig. 67. Stress distributions in Structure No. 1 of the study of cross-sectional form

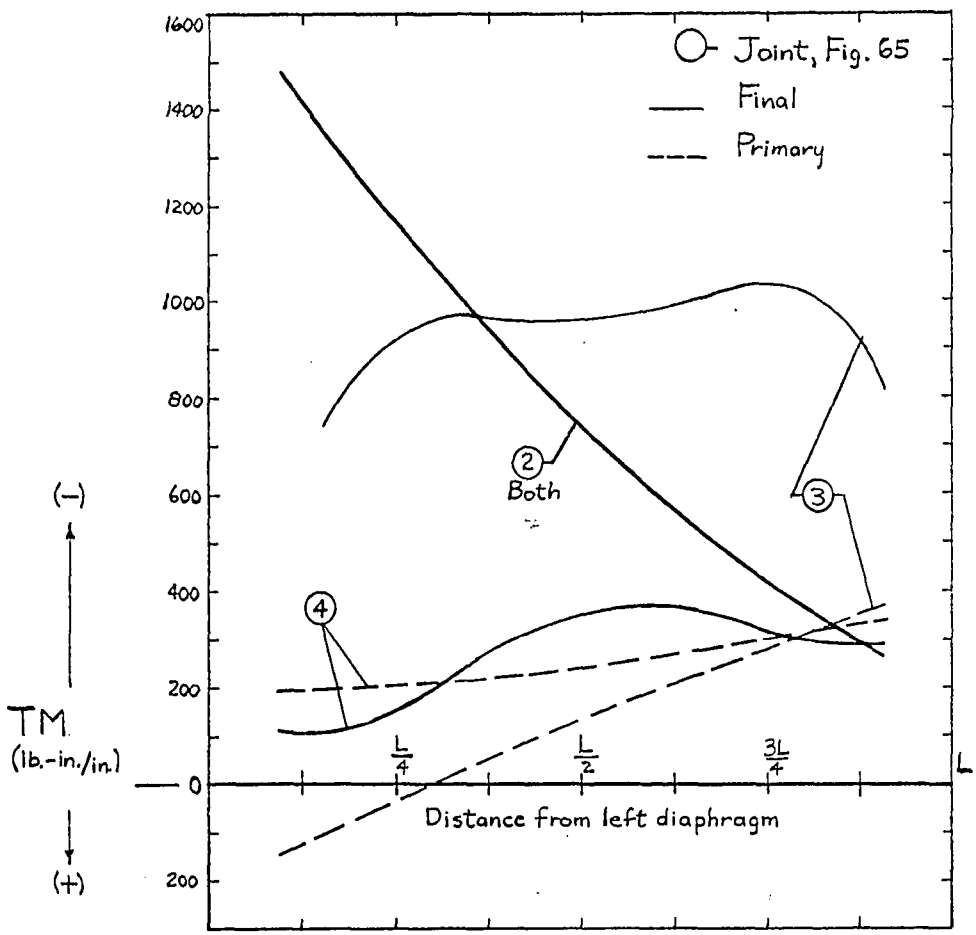

Fig. 68. Distributions of transverse moments in Structure No. 1 of the study of cross-sectional form

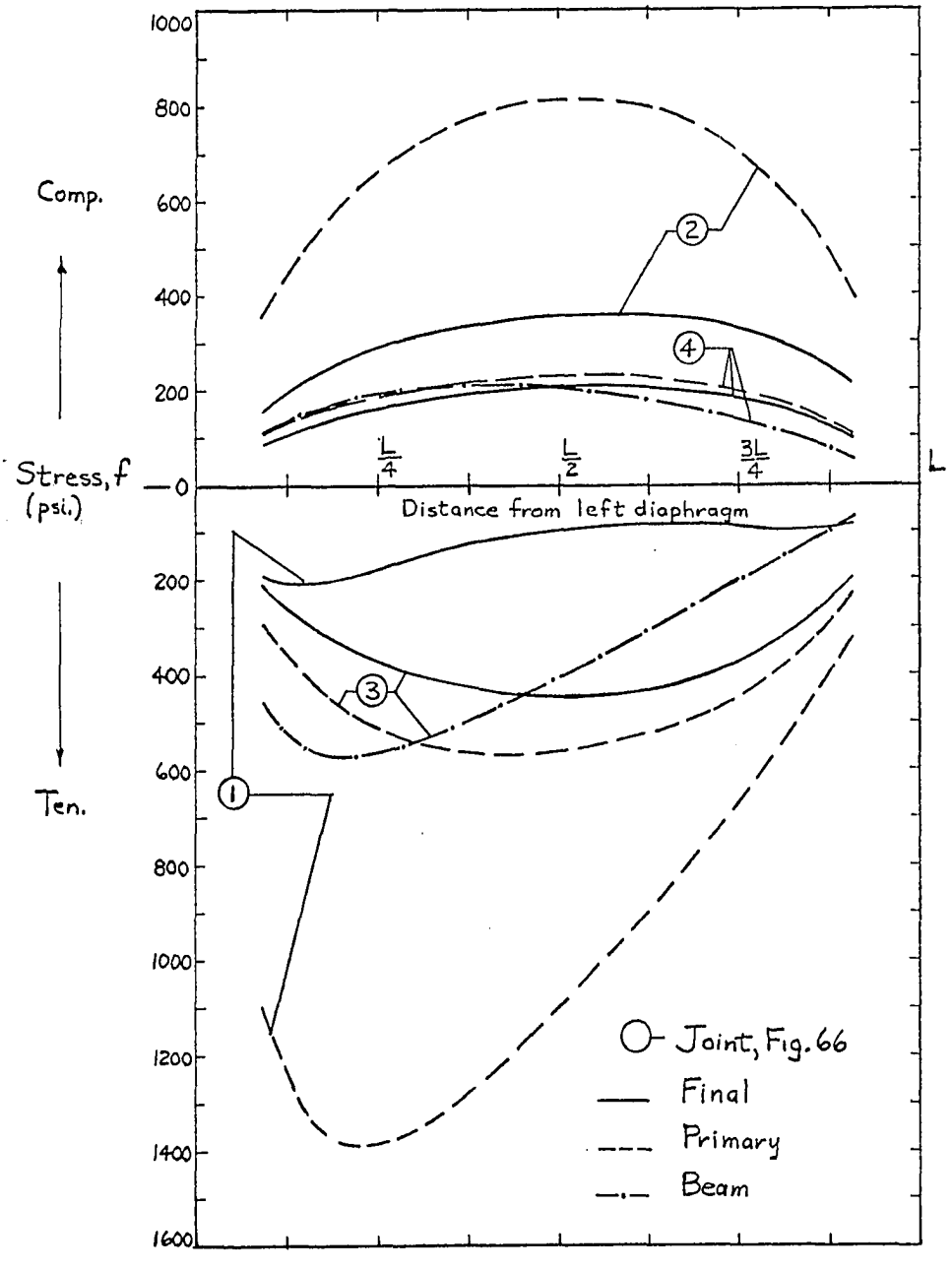

Fig. 69. Stress distributions in Structure No. 2 of the study of cross-sectional form

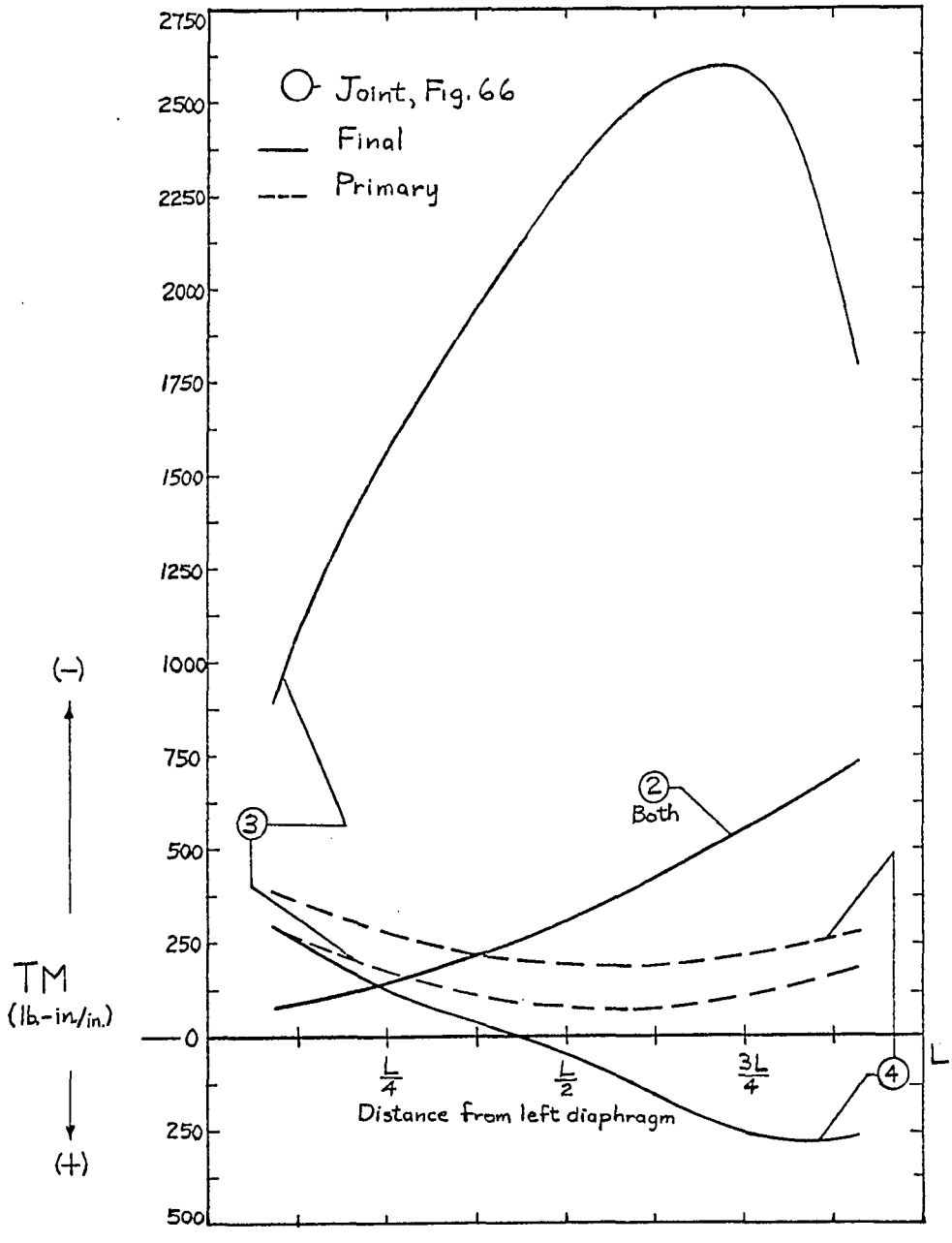

Fig. 70. Distributions of transverse moments in Structure No. 2 of the study of cross-sectional form

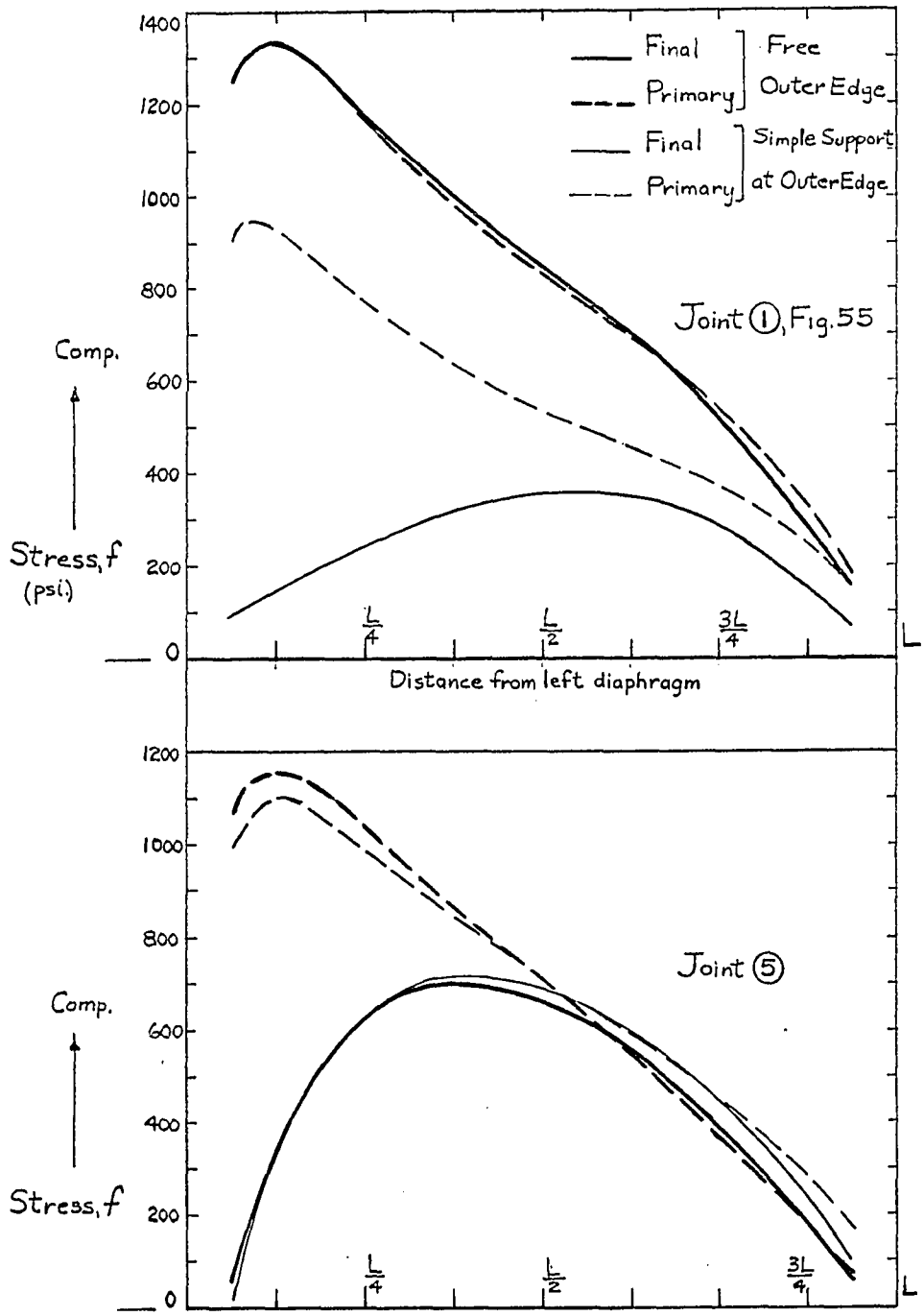

Fig. 71. Stress distributions as influenced by the boundary conditions along the outer longitudinal edges of a structure

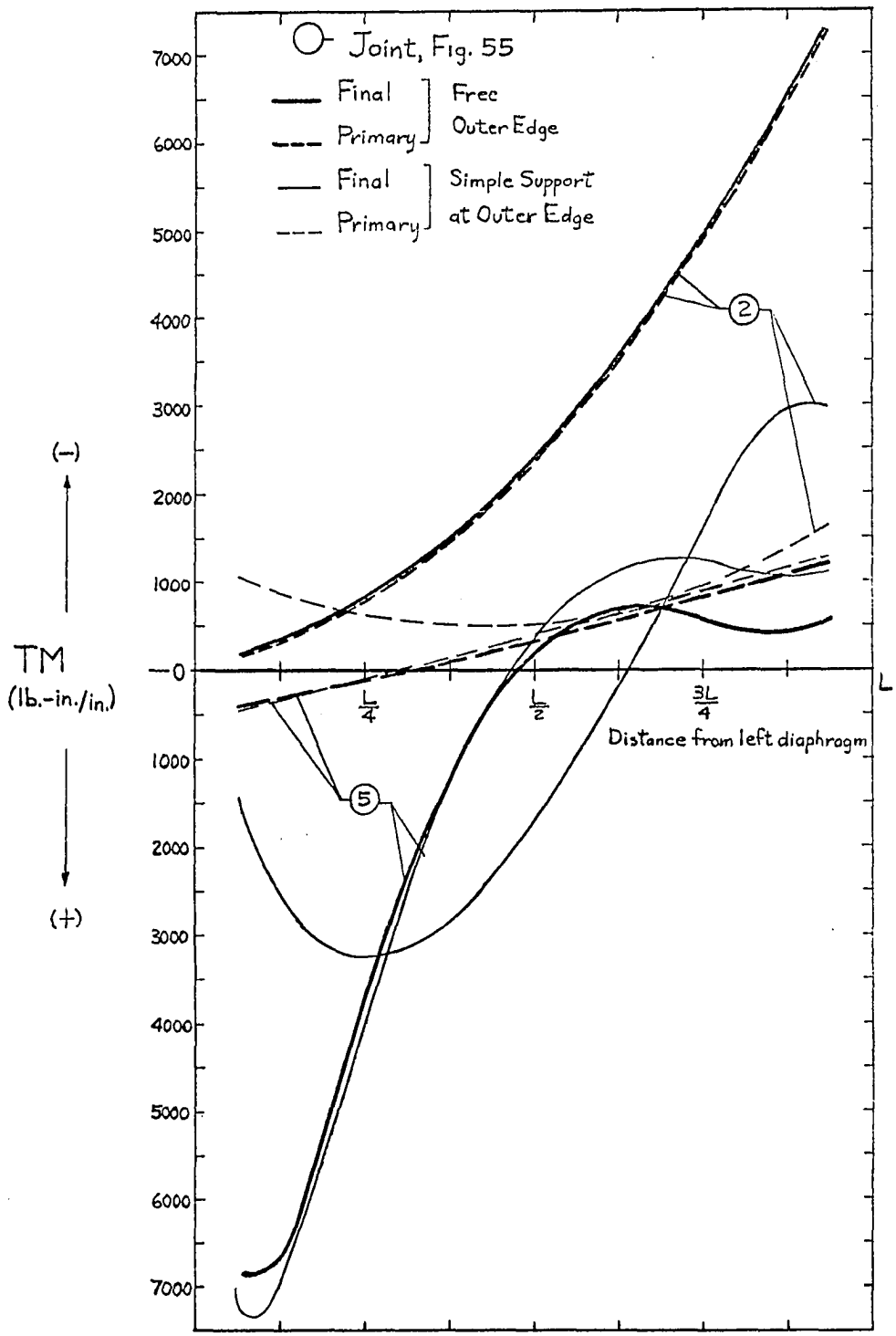

Fig. 72. Distributions of transverse moments as influenced by the boundary conditions along the outer longitudinal edges of a structure